Australian National University

Crawford School of Public Policy

CAMA

Centre for Applied Macroeconomic Analysis

Inflation and Professional Forecast Dynamics: An Evaluation of Stickiness, Persistence, and Volatility

CAMA Working Paper 60/2017
(Revised version of CAMA Working Paper 6/2015)
September 2017

Elmar Mertens
Bank for International Settlements, Switzerland

James M. Nason
Department of Economics, NC State University, and
Centre for Applied Macroeconomic Analysis, ANU

Abstract

This paper studies the joint dynamics of real time U.S. inflation and the mean inflation predictions of the Survey of Professional Forecasters (SPF) on a 1968Q4 to 2017Q2 sample. The joint data generating process (DGP) is an unobserved components (UC) model of inflation and a sticky information (SI) prediction mechanism for SPF inflation predictions. We add drifting gap inflation persistence to a UC model that already has stochastic volatility (SV) afflicting trend and gap inflation. Another innovation puts a time-varying frequency of inflation forecast updating into the SI-prediction mechanism. The joint DGP is a nonlinear state space model (SSM). We estimate the SSM using Bayesian tools grounded in a Rao-Blackwellized auxiliary particle filter, particle learning, and a particle smoother. The estimates show (i) longer horizon average SPF inflation predictions inform estimates of trend inflation, (ii) gap inflation persistence is pro-cyclical, and SI inflation updating is frequent before the Volcker disinflation, and (iii) subsequently, trend inflation and its SV fall, gap inflation persistence turns counter-cyclical, and SI inflation updating becomes infrequent.

Keywords

Inflation, unobserved components, professional forecasts, sticky information, stochastic volatility, time-varying parameters, Bayesian, particle filter

JEL Classification

E31, C11, C32

Address for correspondence:

(E) cama.admin@anu.edu.au

ISSN 2206-0332

Inflation and Professional Forecast Dynamics: An Evaluation of Stickiness, Persistence, and Volatility*

Elmar Mertens† AND **James M. Nason**‡

Current draft: September 12, 2017
First Draft: February 15, 2015

Abstract

This paper studies the joint dynamics of real time U.S. inflation and the mean inflation predictions of the Survey of Professional Forecasters (SPF) on a 1968$Q4$ to 2017$Q2$ sample. The joint data generating process (DGP) is an unobserved components (UC) model of inflation and a sticky information (SI) prediction mechanism for SPF inflation predictions. We add drifting gap inflation persistence to a UC model that already has stochastic volatility (SV) afflicting trend and gap inflation. Another innovation puts a time-varying frequency of inflation forecast updating into the SI-prediction mechanism. The joint DGP is a nonlinear state space model (SSM). We estimate the SSM using Bayesian tools grounded in a Rao-Blackwellized auxiliary particle filter, particle learning, and a particle smoother. The estimates show (*i*) longer horizon average SPF inflation predictions inform estimates of trend inflation, (*ii*) gap inflation persistence is pro-cyclical, and SI inflation updating is frequent before the Volcker disinflation, and (*iii*) subsequently, trend inflation and its SV fall, gap inflation persistence turns counter-cyclical, and SI inflation updating becomes infrequent.

JEL Classification Numbers: $E31$, $C11$, $C32$.

Key Words: inflation; unobserved components; professional forecasts; sticky information; stochastic volatility; time-varying parameters; Bayesian; particle filter.

†*email*: elmar.mertens@bis.org, *address*: Bank for International Settlements, Centralbahnplatz 2, CH 4051 Basel, Switzerland.

‡*email*: jmnason@ncsu.edu, *address*: Department of Economics, Campus Box 8110, NC State University, Raleigh, NC 27695–8110 and the Centre for Applied Macroeconomic Analysis.

*We thank Gregor Smith for several conversations that motivated this paper. We also received valuable comments from Todd Clark, Patrick Conway, Drew Creal, Bill Dupor, Monica Jain, Alejandro Justiniano, and Wolfgang Lemke, and suggestions from colleagues and participants at numerous seminars and conferences. Jim Nason thanks the Jenkins Family Economics Fund at North Carolina State University for financial support. The views herein are those of the authors and do not represent the views of the Bank for International Settlements.

1 Introduction

Central banks pay particular attention to inflation expectations. A good reason for this preoccupation is inflation expectations contain information about private agents' beliefs about the underlying factors driving observed inflation dynamics. We label these factors the inflation regime. For example, Bernanke (2007) argues that well anchored inflation expectations are necessary for a central bank to stabilize inflation. A problem is since monetary policy makers lack direct knowledge of inflation expectations, they must infer these expectations from estimates of the inflation regime. These estimates often rely on realized inflation and combinations of financial market data, statistical and economic models, and forecast surveys.

This paper estimates inflation regimes from the joint data generating process (DGP) of realized inflation and the inflation predictions of professional forecasters grounded in a nonlinear state space model (SSM). We tap a sample of inflation predictions from the Survey of Professional Forecasters (SPF) to extract beliefs its average respondent has about the (in)stability of the persistence, volatility, and stickiness of inflation. Average SPF inflation predictions are attractive for evaluating the SSM because, as Faust and Wright (2013) and Ang, Bekaert, and Wei (2007) observe, SPF inflation predictions often dominate model based out of sample forecasts. This forecasting performance suggests average SPF inflation predictions coupled with realized inflation harbor useful information to measure inflation expectations.

We study the joint DGP of realized inflation, π_t, and average SPF inflation predictions by linking a Stock and Watson (2007) unobserved components (SW-UC) model of inflation to a version of the Mankiw and Reis (2002) sticky information (SI) model. The SW-UC model is useful for evaluating the impact of different types of shocks on inflation and inflation expectations. First, it decomposes π_t into trend inflation, τ_t, and gap inflation, ε_t, which restricts the impact of permanent and transitory shocks on π_t. When permanent shocks dominate movements in π_t, the inference is inflationary expectations are not well anchored. The SW-UC model also inflicts stochastic volatility (SV) on the innovations of τ_t and ε_t. Trend and gap SV creates nonlinearities in inflation dynamics, which produce bursts of volatility in π_t. Persistence is not

often imposed on ε_t when estimating the SW-UC-SV model. We depart from this assumption by giving ε_t drifting persistence in the form of a time-varying parameter first-order autoregression, or a TVP-AR(1). Drifting gap persistence is another source of nonlinearity in a SW-UC model, which can exhibit pro- or counter-cyclical changes. We label the extended version of the DGP of π_t as the SW-UC-SV-TVP-AR(1) model.

Coibion and Gorodnichenko (2015) adapt a SI model to a setup in which forecasters update their rational expectations (RE) information set at a fixed probability $1-\lambda$. Averaging across forecasters defines the h-step ahead SI inflation prediction, $F_t\pi_{t+h}$, $h = 1, \ldots, \mathcal{H}$. The result is the SI inflation prediction evolves as a weighted average of the lagged SI forecast, $F_{t-1}\pi_{t+h}$, and a RE inflation forecast, $\mathbf{E}_t\pi_{t+h}$, where the weights are λ and $1-\lambda$. The result is the SI law of motion $F_t\pi_{t+h} = \lambda F_{t-1}\pi_{t+h} + (1-\lambda)\mathbf{E}_t\pi_{t+h}$, where $F_t\pi_{t+h}$ updates at the frequency $1/(1-\lambda)$ on average. In this reading, λ reflects the average forecaster's beliefs about the persistence or stickiness of the inflation regime.[1]

We innovate on the Coibion-Gorodnichenko static coefficient SI-law of motion by investing λ with drift. The result is a nonlinear SI-law of motion $F_t\pi_{t+h} = \lambda_t F_{t-1}\pi_{t+h} + (1-\lambda_t)\mathbf{E}_t\pi_{t+h}$, where the TVP-SI parameter, λ_t, evolves as an exogenous and bounded random walk (RW), $\lambda_{t+1} = \lambda_t + \sigma_\kappa\kappa_{t+1}$, and its innovation is drawn from a truncated normal distribution ($\mathcal{TN}$), $\kappa_{t+1} \sim \mathcal{TN}(0, 1; \lambda_{t+1} \in (0, 1))$. The SI forecaster's information set includes the innovation κ_t when $F_{t-1}\pi_{t+h}$ is updated to $F_t\pi_{t+h}$, which implies λ_t is also part of this information set.

A motivation for placing λ_t in the SI-law of motion is to uncover evidence about changes in the beliefs the average SPF participant holds about the inflation regime. Changes in these beliefs are embedded in observed movements of the average SPF participant's h-step ahead inflation prediction, $\pi^{SPF}_{t,t+h}$. We relate $\pi^{SPF}_{t,t+h}$ to $F_t\pi_{t,t+h}$ by adding a classical measurement error, $\zeta_{t,h}$, to set $\pi^{SPF}_{t,t+h} = F_t\pi_{t+h} + \sigma_{\zeta_h}\zeta_{h,t}$, where $\zeta_{h,t} \sim \mathcal{N}(0, 1)$, $h = 1, \ldots, \mathcal{H}$. The $\pi^{SPF}_{t,t+h}$ observation equation, SI-law of motion, and RW of λ_t form the SI-prediction mechanism.

The joint DGP of the SI-prediction mechanism and SW-UC-SV-TVP-AR(1) model maps shocks

[1] Sims (2003) constructs a dynamic optimizing model built on primitive form of information processing in which agents react to shifts in the true DGP of the economy by smoothing their forecasts.

to τ_t, ε_t, and SI state variables into movements in π_t and $\pi^{SPF}_{t,t+h}$.[2] Estimates of the joint DGP provide evidence about drift in λ_t and its co-movement with the SVs of τ_t and ε_t and drifting persistence in ε_t. If λ_t exhibits meaningful statistical and economic time variation and it moves with the SVs or drifting inflation gap persistence, we have evidence shifts in SI inflation updating are attuned to the hidden factors driving the inflation regime. A contribution of our paper is to report this evidence.

Another contribution is the sequential Monte Carlo (SMC) methods we use to estimate the joint DGP of the SI-prediction mechanism and SW-UC-SV-TVP-AR(1) model. These methods consist of the particle learning estimator (PLE) of Storvik (2002) and the particle smoother (PS) of Lindsten, Bunch, Särkkä, Schön, and Godsill (2016). The PLE and PS rely on a Rao-Blackwellized auxiliary particle filter (RB-APF). Our joint DGP is susceptible to Rao-Blackwellization because τ_t, ε_t, and the SI state variables form a linear SSM, given realizations of the nonlinear state variables, which are trend and gap inflation SVs, drifting inflation persistence, and λ_{t+1}, and estimates of the static coefficients of the SI-prediction mechanism and SW-UC-SV-TVP-AR(1) model. Applying the Kalman filter (KF) produces estimates of the distribution of the conditionally linear states that are integrated analytically, which increases the efficiency of the RB-APF. The RB-APF estimates the nonlinear states by simulation.

We estimate the joint DGP of the SI-prediction mechanism and SW-UC-SV-TVP-AR(1) model on a quarterly sample from $1968Q4$ to $2017Q2$. The sample matches π_t with the GNP or GDP deflator inflation available to the SPF in real time at date t. The average SPF inflation prediction is denoted $\pi^{SPF}_{t,t+h}$, where $\mathcal{H} = 5$ or $h = 1, \ldots,$ 1- to 5-quarter ahead forecast horizons.[3]

Given only a sample of $\left\{\pi_t,\ \pi^{SPF}_{t,t+1}, \ldots, \pi^{SPF}_{t,t+5}\right\}_{t=1}^{T}$ and our priors, the SSM yields posterior estimates of the beliefs the average SPF participant has about the hidden factors of the inflation

[2] Our approach to studying the joint dynamics of π_t and $\pi^{SPF}_{t,t+h}$ builds on Kozicki and Tinsley (2012), Mertens (2016), and Nason and Smith (2016a, b).

[3] The SPF contains average predictions of the GNP or GDP deflator for a nowcast and forecasts up to 4-quarters ahead. The surveys are collected at the middle of the quarter, which suggests $\pi^{SPF}_{t,t+h}$ is not based on full knowledge of π_t. We treat $\pi^{SPF}_{t,t+h}$ as conditional only on information available through the end of the previous quarter. This identifies the average SPF nowcast, 1-quarter, ..., 4-quarter ahead predictions with $\pi^{SPF}_{t,t+h}$, $h = 1, 2, \ldots, 5$. We discuss these timing issues in section 4.1.

regime. Our estimates of trend inflation are aligned with average SPF inflation predictions, especially at longer horizons. Gap inflation is more volatile before the Volcker disinflation than afterwards. There is a spike in gap inflation SV during the 1973–1975 recession while trend inflation SV displays peaks during the 1981–1982 and 2007–2009 recessions. The drift in gap inflation persistence is procyclical before the Volcker disinflation, turns counter cyclical afterwards, disappears by the 2007–2009 recession, and returns to pre-2000 rates by 2014. The average SPF participant updates SI inflation forecasts frequently from the late 1960s to 1988. The frequency of SI inflation updating falls from 1990 to 1995 and then steadies until 2007. During the 2007–2009 recession, SI inflation updating occurs more frequently and drops slowly afterwards. Thus, movements in the frequency of SI inflation updating displays co-movement with trend inflation, its SV, and drifting inflation persistence. We conclude the beliefs of the average member of the SPF are sensitive to the impact of permanent shocks on the conditional mean of inflation and the Volcker disinflation marks the moment at which the behavior of trend inflation, its SV, and the cyclicality of the drift in inflation gap persistence changed.

The structure of the paper is as follows. In section 2, we build a SSM of the joint DGP of π_t and $\pi^{SPF}_{t,t+h}$, $h = 1, \ldots, \mathcal{H}$. Section 3 discusses the SMC methods we engage to estimate the SSM. Results appear in section 4. Section 5 offers our conclusions.

2 Statistical and Econometric Models

This section describes the statistical and economic models used to estimate the joint dynamics of π_t and $\pi^{SPF}_{t,t+h}$, $h = 1, \ldots, \mathcal{H}$. Stock and Watson (2007) is the source of the statistical model to which we add drifting persistence to ε_t. The economic model is a SI-prediction mechanism that has a SI-TVP parameter. Drift in inflation persistence and the frequency of SI inflation updating create nonlinearities in the state transition dynamics of the SSM. The SI-TVP also interacts with trend and gap inflation SVs to produce nonlinearites in the impulse structure of the SSM.[4]

[4]We relegate to an online appendix construction of a SSM in which persistence in ε_t is a AR(1) with a static slope coefficient. The online appendix is available at `http://www.elmarmertens.com/`.

2.1 The SW-UC Model

The SW-UC model generates π_t. Stock and Watson (2010), Creal (2012), Shephard (2013), Cogley and Sargent (2015), and Mertens (2016) have estimated versions of the model in which SV in innovations to τ_t and ε_t is the source of nonlinearity in π_t. We add an additional nonlinearity to the SW-UC-SV model in the form of drift in the persistence of ε_t created by a TVP-AR(1). We collect these features into the SW-UC-SV-TVP-AR(1) model

$$\pi_t = \tau_t + \varepsilon_t + \sigma_{\zeta,\pi}\zeta_{\pi,t}, \quad \zeta_{\pi,t} \sim \mathcal{N}(0,1), \tag{1.1}$$

$$\tau_{t+1} = \tau_t + \varsigma_{\eta,t+1}\eta_t, \quad \eta_t \sim \mathcal{N}(0,1), \tag{1.2}$$

$$\varepsilon_{t+1} = \theta_{t+1}\varepsilon_t + \varsigma_{\upsilon,t+1}\upsilon_t, \quad \upsilon_t \sim \mathcal{N}(0,1), \tag{1.3}$$

$$\ln \varsigma^2_{\ell,t+1} = \ln \varsigma^2_{\ell,t} + \sigma_\ell \xi_{\ell,t+1}, \quad \xi_{\ell,t+1} \sim \mathcal{N}(0,1), \ \ell = \eta, \upsilon, \tag{1.4}$$

$$\theta_{t+1} = \theta_t + \sigma_\phi \phi_{t+1}, \quad \phi_{t+1} \sim \mathcal{N}(0,1), \tag{1.5}$$

where measurement error on π_t, $\zeta_{\pi,t}$, is uncorrelated with τ_t and ε_t and the innovations, η_t and υ_t, these innovations are afflicted by SV, which evolve as RWs in $\ln \varsigma^2_{\eta,t+1}$ and $\ln \varsigma^2_{\upsilon,t+1}$, drifting persistence in ε_{t+1} is tied to θ_{t+1}, restricting the RW of $\theta_{t+1} \in (-1, 1)$ ensures stationarity of ε_{t+1} at each date $t+1$, and innovations to the linear state variables, η_t and υ_t, and innovations to nonlinear state variables, $\xi_{\eta,t+1}$, $\xi_{\upsilon,t+1}$, and ϕ_{t+1}, are uncorrelated.

A special case of the SW-UC-SV-TVP-AR(1) model gives a result about forecasting traced to Muth (1960). Shut down SV, $\sigma_\eta = \varsigma_{\eta,t}$ and $\sigma_\upsilon = \varsigma_{\upsilon,t}$, and eliminate gap inflation persistence, $\theta_t = 0$, for all dates t. The result is a fixed coefficient SW-UC model with an IMA$(1,1)$ reduced form, $(1-\mathbf{L})\pi_t = (1-\varpi\mathbf{L})\nu_t$, where the MA1 coefficient $\varpi \in (-1,1)$, $\mathbf{L}$ is the lag operator, $\pi_{t-1} = \mathbf{L}\pi_t$, and the one-step ahead forecast error $\nu_t = \eta_t + \varepsilon_t + \tau_t - \tau_{t-1|t-1}$.[5] The IMA$(1,1)$ implies a RE inflation updating equation, $\mathbf{E}\{\pi_{t+1} \,|\, \pi^t, \sigma_\eta, \sigma_\upsilon\} = (1-\varpi)\pi_t + \varpi\mathbf{E}\{\pi_t \,|\, \pi^{t-1}, \sigma_\eta, \sigma_\upsilon\}$, where π^t is the date t history of inflation, $\pi_t, \ldots, \pi_1$.

[5] Stock and Watson (2007), Grassi and Proietti (2010), and Shephard (2013) tie ϖ to the autocovariance functions (ACFs) of the IMA$(1,1)$ and fixed coefficient SW-UC model. At lags zero and one, the ACFs set $(1+\varpi^2)\sigma^2_\nu = \sigma^2_\eta + 2\sigma^2_\varepsilon$ and $-\varpi\sigma^2_\nu = -\sigma^2_\varepsilon$. Substitute for σ^2_ν to find $\varpi^2 - \left(2 + \sigma^2_\eta \big/ \sigma^2_\varepsilon\right)\varpi + 1 = 0$. The solution is $\varpi = \left[1 + 0.5\sigma^2_\eta \big/ \sigma^2_\varepsilon\right] - \dfrac{\sigma_\eta}{\sigma_\varepsilon}\sqrt{1 + 0.25\sigma^2_\eta \big/ \sigma^2_\varepsilon}$, given $\varpi \in (-1,1)$ and $\sigma_\eta, \sigma_\varepsilon > 0$.

Stock and Watson (2007), Grassi and Prioietti (2010) and Shephard (2013) note the SW-UC-SV model replaces ϖ with the time-varying local weight ϖ_t in the reduced form IMA$(1,1)$. The result is a exponentially weighted moving average (EWMA) updating recursion or smoother

$$\mathbf{E}\left\{\pi_{t+1}\,|\,\boldsymbol{\pi}^t,\,\varsigma_{\eta,t},\,\varsigma_{\upsilon,t}\right\} \;=\; \sum_{j=0}^{\infty}\mu_{\varpi,t-j}\left(\prod_{\ell=0}^{j}\varpi_{t-\ell}\right)\pi_{t-j}, \tag{2}$$

in which the discount ϖ_t adjusts to changes in the latest data, where $\mu_{\varpi,t}=(1-\varpi_t)/\varpi_t$.

2.2 The SI-Prediction Mechanism

This section begins by reproducing the SPF observation equation, the nonlinear SI-law of motion, and the random walk law of motion of λ_t. These elements form the system of equations

$$\pi^{SPF}_{t,t+h} \;=\; F_t\pi_{t+h} \;+\; \sigma_{\zeta,h}\zeta_{h,t}, \qquad \zeta_{h,t}\;\sim\;\mathcal{N}(0,\,1), \tag{3.1}$$

$$F_t\pi_{t+h} \;=\; \lambda_t F_{t-1}\pi_{t+h} \;+\; (1-\lambda_t)\mathbf{E}_t\pi_{t+h}, \qquad h\;=\;1,\,\ldots,\,\mathcal{H}, \tag{3.2}$$

$$\lambda_{t+1} \;=\; \lambda_t \;+\; \sigma_\kappa\kappa_{t+1}, \qquad \kappa_{t+1}\;\sim\;\mathcal{N}(0,\,1), \tag{3.3}$$

where $\mathbf{E}_t\pi_{t+h}$ is conditional on the average SPF participant's statistical model of inflation and $\lambda_t\in(0,\,1)$ for all dates t. Equations (3.1)–(3.3) define the SI-prediction mechanism through which shocks to λ_t and movements in other state variables generate fluctuations in $\pi^{SPF}_{t,t+h}$.

The SI-law of motion (3.2) implies a EWMA smoother. Iterate (3.2) backwards, substitute the result into (3.2), and repeat the process many times to produce the SI-EWMA smoother

$$F_t\pi_{t+h} \;=\; \sum_{j=0}^{\infty}\mu_{\lambda,t-j}\left(\prod_{\ell=0}^{j}\lambda_{t-\ell}\right)\mathbf{E}_{t-j}\pi_{t+h}, \tag{4}$$

where the discount rate is the SI-TVP, λ_t, and $\mu_{\lambda,t}=(1-\lambda_t)/\lambda_t$. The SI-EWMA smoother (4) nests the RE forecast, $\lim_{\lambda_t\longrightarrow 0}F_t\pi_{t+h}=\mathbf{E}_t\pi_{t+h}$, and the pure SI update, $\lim_{\lambda_t\longrightarrow 1}F_t\pi_{t+h}=\sum_{j=1}^{\infty}\mu_{\lambda,t-j}\left(\prod_{\ell=1}^{j}\lambda_{t-\ell}\right)\mathbf{E}_{t-j}\pi_{t+h}$. The former limit shuts down SI as λ_t falls to zero because the discount on $\mathbf{E}_{t-j}\pi_{t+h}$ increases with j. In this case, SI inflation forecast updates rely only on $\mathbf{E}_t\pi_{t+h}$ period by period. At the other extreme, less weight is placed on $\mathbf{E}_t\pi_{t+h}$ and more on $\mathbf{E}_{t-j}\pi_{t+h}$, $j>1$, as λ_t rises to one. Thus, $F_{t-1}\pi_{t+h}$ summarizes the SI inflation forecast.

Between these polar cases, shocks to λ_t alter the discount applied to the history of $\mathbf{E}_t\pi_{t+h}$ in the SI-EWMA smoother (4). This information aids in identifying movements in $\pi^{SPF}_{t,t+h}$ with respect to innovations in λ_t. The EWMA smoother (2) shows a similar relationship exists between $\mathbf{E}_t\pi_{t+h}$, π_t, and the time-varying discount generated by $\varsigma_{\eta,t}$, $\varsigma_{\upsilon,t}$, and θ_t. This gives us several sources of information to identify movements in π_t and $\pi^{SPF}_{t,t+h}$ within the joint DGP of the SI-prediction mechanism and the SW-UC-SV-TVP-AR(1) model.[6]

2.3 The State Space Model of the Joint DGP

Drift in inflation gap persistence complicates building a SSM for the joint DGP of the SI-prediction mechanism and SW-UC-SV-TVP-AR(1) model. The SSM rests on the RE and SI term structures of inflation forecasts for which the latent factors are the RE state variables $\mathcal{X}_t = [\tau_t \ \ \varepsilon_t]'$ and SI analogues $F_t\mathcal{X}_t = [F_t\tau_t \ \ F_t\varepsilon_t]'$. The problem is the law of iterated expectation (LIE) cannot be employed to create predictions of $\mathcal{X}_{t+h}$ or $F_t\mathcal{X}_{t+h}$ because forecasts of θ_t are needed. Instead, we construct RE and SI term structures of inflation forecasts in the presence of drifting gap inflation persistence by invoking the anticipated utility model (AUM).

The RE term structure of inflation forecasts is based on the observation and state equations of the SW-UC-SV-TVP-AR(1) model. The observation equation (1.1) of the SW-UC-SV-TVP-AR(1) model links π_t to τ_t, ε_t, and $\zeta_{\pi,t}$, which can be rewritten as

$$\pi_t \ = \ \delta_{\mathcal{X}}\mathcal{X}_t \ + \ \sigma_{\zeta,\pi}\zeta_{\pi,t}, \tag{5.1}$$

where $\delta_{\mathcal{X}} = [1 \ 1]$. The state equations of the SW-UC-SV-TVP-AR(1) model are created by placing the random walk (1.3) below the TVP-AR(1) (1.3)

$$\mathcal{X}_{t+1} \ = \ \mathbf{\Theta}_{t+1}\mathcal{X}_t \ + \ \mathbf{\Upsilon}_{t+1}\mathcal{W}_t, \tag{5.2}$$

where $\mathbf{\Theta}_{t+1} = \begin{bmatrix} 1 & 0 \\ 0 & \theta_{t+1} \end{bmatrix}$, $\mathbf{\Upsilon}_{t+1} = \begin{bmatrix} \varsigma_{\eta,t+1} & 0 \\ 0 & \varsigma_{\upsilon,t+1} \end{bmatrix}$, and $\mathcal{W}_t = \begin{bmatrix} \eta_t \\ \upsilon_t \end{bmatrix}$. The transition dy-

[6] Krane (2011), Coibion and Gorodnichenko (2012), and Jain (2013) engage forecast revisions to identify the responses of professional forecasters to disparate shocks, which is an alternative to our approach.

namics of the state equations (5.2) are nonlinear in $\mathbf{\Theta}_{t+1}$. These nonlinearities rule out applying the LIE to construct the RE term structure of inflation forecasts.

We appeal to two aspects of the AUM to solve the problem. The AUM resurrects the LIE by (i) assuming agents are ignorant of the true DGP and (ii) treating the TVPs of the joint DGP as fixed (locally) at each date t.[7] These assumptions are instructions to hold TVPs at their date t values within RE and SI forecasts that condition on date t information.[8]

The RE term structure of inflation forecasts is easy to construct under the AUM. First, generate h-step ahead RE forecasts of $\mathcal{X}_t$ by iterating the state equations (5.2) forward, apply the expectations operator, and invoke the AUM to find $\mathbf{E}_t\mathbf{\Theta}_{t+h}\mathcal{X}_{t+h} = \mathbf{\Theta}_{t|t}^h\mathcal{X}_t$. Next, push the observation equation (5.1) h-steps ahead and take expectations to obtain the RE term structure of inflation forecasts under the SW-UC-SV-TVP-AR(1) model and AUM

$$\mathbf{E}_t\pi_{t+h} = \delta_{\mathcal{X}}\mathbf{\Theta}_{t|t}^h\mathcal{X}_t. \tag{6}$$

The AUM restricts the impact of drifting inflation gap persistence on these RE forecasts by conditioning θ_t on date t information.

Next, we show the SI term structure of inflation forecasts is built on the SI-EWMA formula (4), RE term structure of inflation forecasts (6), and a conjecture about the law of motion of the SI vector $F_{t+1}\mathcal{X}_{t+1}$. The SI-EWMA formula (4) depends on the RE inflation forecasts $\mathbf{E}_{t-j}\pi_{t+h}$. Since these RE forecasts are $\mathbf{E}_{t-j}\pi_{t+h} = \delta_{\mathcal{X}}\mathbf{\Theta}_{t|t}^{h+j}\mathcal{X}_{t-j}$ under the AUM, other RE forecasts are needed to replace $\mathbf{E}_{t-j}\pi_{t+h}$ in the SI-EWMA smoother (4). Our solution assumes the average member of the SPF fixes drift in inflation gap persistence at its current value when iterating SI recursions backwards. Under this assumption, $\mathbf{E}_{t-j}\pi_{t+h} = \delta_{\mathcal{X}}\mathbf{\Theta}_{t|t}^{h+j}\mathcal{X}_{t-j}$ in the SI-EWMA smoother (4). The result is $F_t\pi_{t+h} = \delta_{\mathcal{X}}\mathbf{\Theta}_{t|t}^h\sum_{j=0}^{\infty}\mu_{\lambda,t-j}\left(\prod_{\ell=0}^{j}\lambda_{t-\ell}\right)\mathbf{\Theta}_{t|t}^j\mathcal{X}_{t-j}$. Next, we conjecture the law of motion of the SI state vector is $F_t\mathcal{X}_{t+h} = (1-\lambda_t)\mathbf{E}_t\mathcal{X}_{t+h} + \lambda_t F_{t-1}\mathcal{X}_{t+h}$. An implication is the SI-EWMA smoother $F_t\mathcal{X}_{t+h} = \sum_{j=0}^{\infty}\mu_{\lambda,t-j}\left(\prod_{\ell=0}^{j}\lambda_{t-\ell}\right)\mathbf{E}_{t-j}\mathcal{X}_{t+h}$. Condition on the date t drift in inflation

[7] For example, Cogley and Sbordone (2008) employ the AUM model to study the dynamics of trend and gap inflation within a TVP-new Keynesian Phillips curve.

[8] The AUM assumptions result in decision making that is consistent with Bayesian forecasting, according to Cogley and Sargent (2008). They also note Kreps (1998) argues agents engaging in AUM-like behavior are acting rationally when seeing through to the true model is costly.

gap persistence on date t information, $\theta_{t|t}$, to find $F_t\mathcal{X}_{t+h} = \sum_{j=0}^{\infty}\mu_{\lambda,t-j}\left(\prod_{\ell=0}^{j}\lambda_{t-\ell}\right)\boldsymbol{\Theta}_{t|t}^{h+j}\mathcal{X}_{t-j}$. When $h = 0$, we have $F_t\mathcal{X}_t = \sum_{j=0}^{\infty}\mu_{\lambda,t-j}\left(\prod_{\ell=0}^{j}\lambda_{t-\ell}\right)\boldsymbol{\Theta}_{t|t}^{j}\mathcal{X}_{t-j}$. By combining the SI-EWMA smoothers of $F_t\pi_{t+h}$ and $F_t\mathcal{X}_t$, the SI term structure of inflation forecasts is the result

$$F_t\pi_{t+h} \;=\; \delta_{\mathcal{X}}\boldsymbol{\Theta}_{t|t}^{h}F_t\mathcal{X}_t. \tag{7}$$

The online appendix has details about the SI term structure of inflation forecasts (7).

The online appendix also develops state equations for $F_{t+1}\mathcal{X}_{t+1}$. Remember the SI-EWMA smoother of $F_t\mathcal{X}_t$ is $\sum_{j=0}^{\infty}\mu_{\lambda,t-j}\left(\prod_{\ell=0}^{j}\lambda_{t-\ell}\right)\boldsymbol{\Theta}_{t|t}^{j}\mathcal{X}_{t-j}$, which by induction gives a law of motion, $F_t\mathcal{X}_t = (1-\lambda_t)\mathcal{X}_t + \lambda_t\boldsymbol{\Theta}_{t|t}F_{t-1}\mathcal{X}_{t-1}$. We create state equations for $F_{t+1}\mathcal{X}_{t+1}$ by pushing this law of motion forward a period and substituting for $\mathcal{X}_{t+1}$ with the state equations (5.2) of the SW-UC-SV-TVP-AR(1) model. Stack the latter equations on top of the former to obtain the state equations of the SSM of the joint DGP

$$\mathcal{S}_{t+1} \;=\; \boldsymbol{\mathcal{A}}_{t+1}\mathcal{S}_t \;+\; \boldsymbol{\mathcal{B}}_{t+1}\mathcal{W}_t, \tag{8.1}$$

where $\mathcal{S}_t = \begin{bmatrix}\mathcal{X}_t' \\ F_t\mathcal{X}_t'\end{bmatrix}$, $\boldsymbol{\mathcal{A}}_{t+1} = \begin{bmatrix}\boldsymbol{\Theta}_{t+1} & \mathbf{0}_{2\times 2} \\ \left(1-\lambda_{t+1}\right)\boldsymbol{\Theta}_{t+1} & \lambda_{t+1}\boldsymbol{\Theta}_{t+1}\end{bmatrix}$, $\boldsymbol{\mathcal{B}}_{t+1} = \begin{bmatrix}\boldsymbol{\Upsilon}_{t+1} \\ \left(1-\lambda_{t+1}\right)\boldsymbol{\Upsilon}_{t+1}\end{bmatrix}$, and the conditioning time subscript on $\boldsymbol{\Theta}_{t+1}$ is dropped. The state equations (8.1) show shocks to λ_t alter the transition and impulse dynamics only of $F_t\tau_t$ and $F_t\varepsilon_t$. Changes in θ_t shift the transition dynamics of all elements of $\mathcal{S}_t$ while its impulse dynamics react to $\varsigma_{\eta,t}$, and $\varsigma_{\upsilon,t}$.

We complete the SSM by constructing its observation equations. First, replace $F_t\pi_{t+h}$ in the SPF measurement equation (3.1) with the SI term structure of inflation forecasts (7) for $h = 1, \ldots, \mathcal{H}$. Place the results below the observation equation (5.1) of the SW-UC-SV-TVP-AR(1) model to form the SSM's observation equations

$$\mathcal{Y}_t \;=\; \boldsymbol{\mathcal{C}}_t\mathcal{S}_t \;+\; \boldsymbol{\mathcal{D}}\mathcal{U}_t, \tag{8.2}$$

where $\mathcal{Y}_t = \begin{bmatrix}\pi_t \\ \pi_{1,t}^{SPF} \\ \vdots \\ \pi_{\mathcal{H},t}^{SPF}\end{bmatrix}$, $\boldsymbol{\mathcal{C}}_t = \begin{bmatrix}\delta_{\mathcal{X}} & \mathbf{0}_{1\times 2} \\ \mathbf{0}_{1\times 2} & \delta_{\mathcal{X}}\boldsymbol{\Theta}_t \\ \vdots & \vdots \\ \mathbf{0}_{1\times 2} & \delta_{\mathcal{X}}\boldsymbol{\Theta}_t^{\mathcal{H}}\end{bmatrix}$, $\boldsymbol{\mathcal{D}} = \begin{bmatrix}\sigma_{\zeta,\pi} & 0 & \ldots & 0 \\ 0 & \sigma_{\zeta,1} & \ldots & 0 \\ 0 & 0 & \ddots & 0 \\ 0 & 0 & \ldots & \sigma_{\zeta,\mathcal{H}}\end{bmatrix}$, $\mathcal{U}_t =$

$\left[\zeta_{\pi,t} \;\; \zeta_{1,t} \;\; \ldots \;\; \zeta_{\mathcal{H},t}\right]'$, and $\mathbf{\Omega}_{\mathcal{U}} = \mathcal{D}\mathcal{D}'$. The SSM integrates $F_t\pi_{t+h}$ out of the observation equations (8.2) using the SI term structure of inflation forecasts (7). As a result, $F_t\varepsilon_t$ produces mean reversion in $\pi^{SPF}_{t,t+h}$ while permanent movements are tied directly to $F_t\tau_t$ and $\mathbf{\Theta}_t$ and indirectly to $\varsigma_{\eta,t}$, $\varsigma_{\upsilon,t}$, λ_t, and $\mathbf{\Theta}_t$. The direct response of $\pi^{SPF}_{t,t+h}$ to $\mathbf{\Theta}_t$ is produced by the observation equations (8.2). Drift in $\mathbf{\Theta}_t$ also alters transition dynamics in the state equations (8.1), which generates movements in $F_t\tau_t$ and $F_t\varepsilon_t$, and hence, $\pi^{SPF}_{t,t+h}$.

3 Econometric Methods

We combine a RB-APF algorithm adapted from Lopes and Tsay (2011) with the PLE of Storvik (2002) to estimate the SSM (8.1) and (8.2); also see Carvalho, Johannes, Lopes, and Polson (2010), Creal (2012), and Herbst and Schorfheide (2016). The RB-APF and PLE produce filtered estimates of τ_t, ε_t, $F_t\tau_t$, $F_t\varepsilon_t$, $\varsigma_{\eta,t}$, $\varsigma_{\upsilon,t}$, λ_t, and θ_t. Lindsten, Bunch, Särkkä, Schön, and Godsill (2016) give instructions for a PS that generates smoothed estimates of these state variables.

3.1 Rao-Blackwellization of a Nonlinear State Space Model

Lopes and Tsay (2011, p. 173) and Creal (2012, section 2.5.7) outline APF algorithms that rely on the Rao-Blackwellization procedure of Chen and Liu (2000). The first step in Rao-Blackwellizing the SSM (8.1) and (8.2) gathers the nonlinear state variables in $\mathcal{V}_t = \left[\ln\varsigma^2_{\eta,t} \;\; \ln\varsigma^2_{\upsilon,t} \;\; \theta_t \;\; \lambda_t\right]'$. We generate updates of the nonlinear states by simulating the multivariate RW process

$$\mathcal{V}_{t+1} \;=\; \mathcal{V}_t \;+\; \mathbf{\Omega}^{0.5}_{\mathcal{E}}\mathcal{E}_{t+1}, \tag{9}$$

where $\mathcal{D}_{\mathcal{E}} = \left[\sigma^2_\eta \;\; \sigma^2_\upsilon \;\; \sigma^2_\phi \;\; \sigma^2_\kappa\right]$ is the vector of non-zero elements of the diagonal covariance matrix $\mathbf{\Omega}_{\mathcal{E}}$ and $\mathcal{E}_{t+1} = \left[\xi_{\eta,t+1} \;\; \xi_{\upsilon,t+1} \;\; \phi_{t+1} \;\; \kappa_{t+1}\right]'$.[9] The RB-APF uses the KF to create an analytic distribution of $\mathcal{S}_t$ using the SSM (8.1) and (8.2), given simulated values of $\mathcal{V}_t$. Analytic integration endows the RB-APF estimator of the linear state variables with greater numerical efficiency.

[9]The innovations vector $\mathcal{E}_{t+1} \sim \mathcal{N}(\mathbf{0}_{4\times1}, \mathbf{I}_4)$ conditions on $\theta_{t+1} \in (-1, 1)$ and $\lambda_{t+1} \in (0, 1)$.

3.2 Priors and Initial Conditions

We posit priors for the static volatility parameters and initial conditions to generate synthetic samples of linear and nonlinear states using the SSM (8.1) and (8.2) and multivariate RW (9). The static scale volatility parameters are collected in $\Psi = \left[\sigma_\eta^2 \;\; \sigma_\upsilon^2 \;\; \sigma_\phi^2 \;\; \sigma_\kappa^2 \;\; \sigma_{\zeta,\pi}^2 \;\; \sigma_{\zeta,1}^2 \;\ldots\; \sigma_{\zeta,5}^2\right]'$. Priors on Ψ are grounded in restrictions of the joint DGP of the SI-prediction mechanism and SW-UC-SV-TVP-AR(1) model while remaining consistent with the PLE of Storvik (2002). The PLE requires priors for Ψ to have analytic posterior distributions. The posterior distributions serve as transition equations to update or "learn" about the joint distribution of $\mathcal{S}_t$ and Ψ.

Table 1 lists our priors for the static volatility parameters found in Ψ. We endow these parameters with inverse gamma ($\mathcal{IG}$) priors. Columns labeled α_ℓ and β_ℓ denote the scale and shape parameters of the $\mathcal{IG}$ priors of the elements of Ψ, the mean is $0.5\beta_\ell/(0.5\alpha_\ell - 1)$, and the two right most columns display the associated 2.5 and 97.5 percent quantiles, where $\ell = \eta$, υ, ϕ, κ, ζ_π, ζ_h, and $h = 1, \ldots, 5$.

Table 1. Inverse Gamma Priors on the Static Coefficients

$$\Psi = \left[\sigma_\eta^2 \;\; \sigma_\upsilon^2 \;\; \sigma_\phi^2 \;\; \sigma_\kappa^2 \;\; \sigma_{\zeta,\pi}^2 \;\; \sigma_{\zeta,1}^2 \;\ldots\; \sigma_{\zeta,5}^2\right]'$$

					Quantiles	
Scale Volatility on Innovation to		α_ℓ	β_ℓ	Mean	2.5%	97.5%
Trend Inflation SV, $\ln \varsigma_{\eta,t+1}$:	σ_η^2	3.0	0.04	0.04	[0.004,	0.186]
Gap Inflation SV, $\ln \varsigma_{\upsilon,t+1}$:	σ_υ^2	3.0	0.04	0.04	[0.004,	0.186]
TVP-AR1 Coefficient, θ_{t+1}:	σ_ϕ^2	3.0	0.01	0.01	[0.001,	0.046]
SI Coefficient, λ_{t+1}:	σ_κ^2	3.0	0.01	0.01	[0.001,	0.046]
Measurement Error on π_t:	$\sigma_{\zeta,\pi}^2$	20.0	2.88	0.16	[0.084,	0.300]
Measurement Error on $\pi_{t,t+h}^{SPF}$:	$\sigma_{\zeta,h}^2$	20.0	2.88	0.16	[0.084,	0.300]

Priors on the static volatility coefficients are $\sigma_\ell^2 \sim \mathcal{IG}\left(\frac{\alpha_\ell}{2}, \frac{\beta_\ell}{2}\right)$, where α_ℓ and β_ℓ are scale and shape parameters, $\ell = \eta,\ \upsilon,\ \phi,\ \kappa,\ \zeta_\pi,\ \zeta_h$, and $h = 1, \ldots, 5$

Two features are worth discussing about our priors on the scale volatility coefficients of $\mathcal{D}_{\mathcal{E}}$. First, we give σ_{η}^2 and σ_{υ}^2 prior means equal to 0.04. These prior means are larger than the prior mean of 0.01 placed on σ_{ϕ}^2 and σ_{κ}^2. Second, our priors on $\sigma_{\eta}^2,\ \sigma_{\upsilon}^2,\ \sigma_{\phi}^2$, and σ_{κ}^2 deliver 2.5 and 97.5 percent quantiles that exhibit greater variation in innovations to $\ln \varsigma_{\eta,t+1}^2$ and $\ln \varsigma_{\upsilon,t+1}^2$ compared with variation in innovations to θ_{t+1} and λ_{t+1}. Nonetheless, the 2.5 and 97.5 percent quantiles of $\sigma_{\zeta,\pi}^2,\ \sigma_{\zeta,1}^2, \ldots, \sigma_{\zeta,5}^2$ reveal our belief that volatility in the measurement errors of π_t and $\pi_{t,t+h}^{SPF}$ dominate shock volatility in the joint DGP of the SI-prediction mechanism and SW-UC-SV-TVP-AR(1) model.

Priors on initial conditions of the linear state variables appear in the left two columns of table 2. We draw τ_0 and $F_0\tau_0$ from normal priors with a mean of two percent, which is about the mean of GNP deflator inflation on a $1958Q1$ to $1967Q4$ training sample. A variance of 100^2 indicates a flat prior over a wide range of values for τ_0 and $F_0\tau_0$. The joint prior of ε_0 and $F_0\varepsilon_0$ is drawn from $\mathcal{N}(\mathbf{0}_{2\times 1}, \mathbf{\Sigma}_0)$, which equates the prior means to zero (*i.e.*, unconditional means). Prior variances are produced by the ergodic bivariate normal distribution of particle draws of $\varsigma_{\upsilon,0}$, θ_0, and λ_0; see the notes to table 2. We also restrict priors on $\tau_0,\ \varepsilon_0,\ F_0\tau_0$, and $F_0\varepsilon_0$ by splitting the training sample variance of the first difference of GNP deflator inflation between trend (one-third) and gap (two-thirds) shocks.

The last two columns of table 2 lists priors on initial conditions of the nonlinear state variables. We endow priors of $\ln \varsigma_{\upsilon,0}^2$ and $\ln \varsigma_{\eta,0}^2$ with normal distributions. Prior means are calibrated to pre-1968 inflation data similar to Stock and Watson (2007). Uncertainty about $\ln \varsigma_{\upsilon,0}^2$ and $\ln \varsigma_{\eta,0}^2$ is reflected in prior variances of ten. Table 2 shows that θ_0 is drawn from a standard normal, subject to truncation at $(-1, 1)$, and another truncated normal bounds $\lambda_0 \in (0, 1)$ with (untruncated) mean of 0.5 and a unit variance. These priors are in essence uninformative about values inside the bounds.

Table 2. Priors on Initial Conditions of the Linear and Nonlinear States

$$\mathcal{S}_0 = \begin{bmatrix} \tau_0 & \varepsilon_0 & F_0\tau_0 & F_0\varepsilon_0 \end{bmatrix}' \text{ and } \mathcal{V}_0 = \begin{bmatrix} \ln \varsigma^2_{\eta,0} & \ln \varsigma^2_{\upsilon,0} & \theta_0 & \lambda_0 \end{bmatrix}'$$

Initial State	Prior Distribution	Initial State	Prior Distribution
τ_0:	$\mathcal{N}\left(2.0,\ 100.0^2\right)$	$\ln \varsigma^2_{\eta,0}$:	$\ln \mathcal{N}\left(\ln 0.2 - 5.0,\ 10.0\right)$
$F_0\tau_0$:	$\mathcal{N}\left(2.0,\ 100.0^2\right)$	$\ln \varsigma^2_{\upsilon,0}$:	$\ln \mathcal{N}\left(\ln 0.4 - 5.0,\ 10.0\right)$
ε_0:	$\mathcal{N}\left(0.0,\ \sigma^2_{\varepsilon_0}\right)$	θ_0:	$\mathcal{TN}\left(0.0,\ 1.0,\ -1.0,\ 1.0\right)$
$F_0\varepsilon_0$:	$\mathcal{N}\left(0.0,\ \sigma^2_{F_0\varepsilon_0}\right)$	λ_0:	$\mathcal{TN}\left(0.5,\ 1.0,\ 0.0,\ 1.0\right)$

The truncated normal distribution is denoted $\mathcal{TN}$, where the first two entries are the mean and variance of the prior and the last two entries restrict the range of the prior. The priors on ε_0 and $F_0\varepsilon_0$ are drawn jointly from $\mathcal{N}\left(\mathbf{0}_{2\times 1},\ \mathbf{\Sigma}_0^{(i)}\right)$, where $\sigma^2_{\varepsilon_0}$ and $\sigma^2_{F_0\varepsilon_0}$ are diagonal elements of

$$\mathbf{\Sigma}_0^{(i)} = \sum_{j=0}^{\infty} \begin{bmatrix} \theta_0^{(i)} & 0 \\ (1-\lambda_0^{(i)})\theta_0^{(i)} & \lambda_0^{(i)}\theta_0^{(i)} \end{bmatrix}^j \begin{bmatrix} \varsigma^{2,(i)}_{\upsilon,0} & \lambda_0^{(i)}\varsigma^{2,(i)}_{\upsilon,0} \\ \lambda_0^{(i)}\varsigma^{2,(i)}_{\upsilon,0} & \lambda_0^{2,(i)}\varsigma^{2,(i)}_{\upsilon,0} \end{bmatrix} \begin{bmatrix} \theta_0^{(i)} & (1-\lambda_0^{(i)})\theta_0^{(i)} \\ 0 & \lambda_0^{(i)}\theta_0^{(i)} \end{bmatrix}^j,$$

and $\lambda_0^{(i)}$, $\theta_0^{(i)}$, and $\varsigma^{2,(i)}_{\upsilon,0}$ are the ith particle draws from priors on the associated initial conditions. If $\theta_0^{(i)} = 0$, the formula computing $\mathbf{\Sigma}_0^{(i)}$ remains valid.

3.3 The Auxiliary Particle Filter

Section 3.1 applies the RB process to the SSM (8.1) and (8.2). This process increases the numerical efficiency of the estimator of the linear states, $\mathcal{S}_t$, by shrinking Monte Carlo error. Another method to improve the efficiency of this estimator is the APF of Pitt and Shephard (1999, 2001). In this section, we sketch a RB-APF to estimate the linear and nonlinear states that begins from algorithm 2 of Lopes and Tsay (2011, p.173); also see Creal (2012, section 2.5.7).[10] The online appendix provides a complete exposition of our implementation of the RB-APF.

[10]We sketch a RB-APF separate from the PLE for clarity, but recognize the RB-APF is integral to the PLE.

A RB-APF obtains estimates of the likelihood by running the prediction step of the KF on the SSM (8.1) and (8.2) particle by particle. At date t, the KF predictive step produces the log likelihood, $\ell_t^{(i)}$, and particle weights, $\widehat{\omega}_t^{(i)} = \exp\left\{\ell_t^{(i)}\right\} \Big/ \sum_i^M \exp\left\{\ell_t^{(i)}\right\}$, $i = 1, \ldots, M$. Stratified resampling of $\left\{\widehat{\omega}_t^{(i)}\right\}_{i=1}^M$ yields indexes that are used to regroup $\mathcal{S}_{t-1|t-1}^{(i)}$, its mean square error (MSE), $\boldsymbol{\Sigma}_{t-1|t-1}^{(i)}$, and $\mathcal{V}_t^{(i)}$; see steps 3(a) and 3(b) of section A3.1 of the online appendix and Hol, Schön, and Gustafsson (2006). This step aims to prevent a particle from receiving all the probability mass as M becomes large. The ensemble of weights $\left\{\widehat{\omega}_t^{(i)}\right\}_{i=1}^M$ are also resampled generating $\left\{\widetilde{\omega}_t^{(i)}\right\}_{i=1}^M$; see step 3(d) of section A3.1 of the online appendix. The resampled particles $\mathcal{S}_{t-1|t-1}^{(i)}$, $\boldsymbol{\Sigma}_{t-1|t-1}^{(i)}$, and $\mathcal{V}_t^{(i)}$ are employed in the entire KF to update $\left\{\mathcal{S}_{t|t}^{(i)}, \boldsymbol{\Sigma}_{t|t}^{(i)}, \ell_t^{(i)}\right\}_{i=1}^M$ and produce new weights $\omega_t^{(i)} = \exp\left\{\ell_t^{(i)}\right\} \Big/ \sum_i^M \exp\left\{\ell_t^{(i)}\right\}$, $i = 1, \ldots, M$; see step 3(e) of section A3.1 of the online appendix. By simulating the multivariate RW (9), the nonlinear states are updated to $\mathcal{V}_{t+1}^{(i)}$ across the M particles. Estimates of $\mathcal{S}_{t|t}$, $\boldsymbol{\Sigma}_{t|t}$, and $\mathcal{V}_{t|t}$ rely on the weights $\omega_t^{(i)} = \omega_t^{(i)} \Big/ \widetilde{\omega}_t^{(i)}$; see step 4 of section A3.1 of the online appendix.

As already noted, a useful product of the RB-APF is the likelihood of the conditionally linear SSM (8.1) and (8.2). Since the M particles have been reweighted at every step using information contained in the likelihood of the KF, the estimate of the date t data density is

$$\mathcal{P}\left(\mathcal{Y}_t \,\middle|\, \mathcal{Y}_{1:t-1};\, \Psi\right) \;\propto\; \frac{1}{M} \sum_{i=1}^{M} \exp\left\{\ell_t^{(i)}\right\}, \quad t = 1, \ldots, T. \tag{10}$$

Sum the data density (10) over the $t = 1, \ldots, T$ observations to compute the log likelihood of the SSM

$$\mathcal{L}\left(\Psi \,\middle|\, \mathcal{Y}_{1:T}\right) \;=\; \sum_{t=1}^{T} \ln\left(\mathcal{P}\left(\mathcal{Y}_t \,\middle|\, \mathcal{Y}_{1:t-1};\, \Psi\right)\right). \tag{11}$$

Section 4 reports estimates of the joint DGP of the SI-prediction mechanism and SW-UC-SV-TVP-AR(1) model. Its estimated log likelihood is compared with the log likelihood of a joint DGP estimated conditional on setting $\theta_t = 0$ or estimating a constant SI parameter, $\lambda_t = \lambda$. Thus, we use log likelihood (11) to evaluate competing joint DGPs, but only after marginalizing Ψ. The next section discusses the PLE used to estimate Ψ.

3.4 The Particle Learning Estimator

We estimate the joint posterior distribution of $\mathcal{S}_t$, $\boldsymbol{\Sigma}_t$, $\mathcal{V}_t$, and Ψ by embedding the RB-APF in the PLE of Storvik (2002), given priors on the joint DGP of the SI-prediction mechanism and SW-UC-SV-TVP-AR(1) model.[11] The PLE rests on two insights. First, choosing conjugate priors for Ψ yields an analytic solution of its posterior distributions. The posterior distribution is recovered conditional on the states and sample data. The idea is to draw Ψ from particle streams of a vector of sufficient statistics, $\Gamma_t^{(i)}$ that depend on $\mathcal{V}_t^{(i)}$, given $\mathcal{Y}_{1:t}$. Since the sufficient statistics are grounded on the $\mathcal{IG}$ priors of Ψ, the mapping to the analytic posterior distributions is a system of transition equations that simulate M particles to learn about or update from $\Gamma_{t-1}^{(i)}$ to $\Gamma_t^{(i)}$. The transition equations are appended to the process that draws $\mathcal{V}_t^{(i)}$ to sample $\Psi^{(i)} \sim \mathcal{P}\left(\Psi \middle| \Gamma_t^{(i)}\right)$, which in essence equates $\mathcal{P}\left(\Psi \middle| \mathcal{Y}_{1:t}, \mathcal{V}_t^{(i)}\right)$ to $\mathcal{P}\left(\Psi \middle| \Gamma_t^{(i)}\right)$. We denote the system of transition equations $\Gamma_t^{(i)} = \oint\left(\Gamma_{t-1}^{(i)}, \mathcal{Y}_{1:t}, \mathcal{V}_t^{(i)}, \mathcal{V}_{t-1}^{(i)}\right),\ i = 1, \ldots, M$.

Second, the PLE marginalizes Ψ out of the posterior of the states produced by the RB-APF. The idea is to update $\Gamma_t^{(i)}$ at the same time the RB-APF generates $\mathcal{S}_t^{(i)}$, $\boldsymbol{\Sigma}_t^{(i)}$, and $\mathcal{V}_t^{(i)}$. Thus, Ψ is estimated by the PLE jointly with $\mathcal{S}_{t|t}$, $\boldsymbol{\Sigma}_{t|t}$, and $\mathcal{V}_{t|t}$.

As noted, we place $\mathcal{IG}$ priors on Ψ to expedite Storvik's PLE. The priors, which are reviewed in section 3.2 and table 1, are $\sigma_\ell^2 \sim \mathcal{IG}\left(\frac{\alpha_\ell}{2}, \frac{\beta_\ell}{2}\right)$, where ℓ indexes the elements of Ψ. The $\mathcal{IG}$ priors are useful because the associated posterior distributions are solved analytically. For example, the posterior distribution of the static volatility coefficient of the RW of θ_{t+1} is $\sigma_\phi^{2(i)} \sim \mathcal{IG}\left(\frac{\alpha_t}{2}, \frac{\beta_{\phi,t}^{(i)}}{2}\right)$, where $\alpha_t = \alpha_{t-1} + t - 1$ and $\beta_{\phi,t}^{(i)} = \sum_{\ell=1}^{t}\left[\theta_\ell^{(i)} - \theta_{\ell-1}^{(i)}\right]^2$. The process generating $\beta_{\phi,t}^{(i)}$ suggests conditioning the posterior $\sigma_\phi^{2(i)} \middle| \mathcal{V}_t^{(i)}, \mathcal{V}_{t-1}^{(i)} \sim \mathcal{IG}\left(\frac{\alpha_t}{2}, \frac{\beta_{\phi,t}^{(i)}}{2}\right)$, where the shape parameter $\beta_{\phi,t}^{(i)}$ is a sufficient statistic for σ_ϕ^2.[12] We extend the idea of identifying $\beta_{\ell,t}^{(i)}$ as sufficient statistics to the entire collection of static volatility parameters in Ψ.

[11] Another method to estimate Ψ is to wrap a Metropolis-Hasting Markov chain Monte Carlo (MCMC) simulator around a PF. Andrieu, Doucet, and Holenstein (2010) prove the distribution of a MCMC simulator is independent of the error created by a particle in a SMC algorithm. Hence, a PF gives an unbiased estimate of the likelihood (11).

[12] The shape parameter is the numerator of the standard deviation of a random variable distributed $\mathcal{IG}$.

The online appendix gives procedures to simulate and update $\beta_{\eta,t}^{(i)}$, $\beta_{\upsilon,t}^{(i)}$, $\beta_{\phi,t}^{(i)}$, and $\beta_{\kappa,t}^{(i)}$ in steps 2 and 3.(a) of the RB-APF algorithm. The algorithm samples $\sigma_{\eta,t}^{2(i)}$, $\sigma_{\upsilon,t}^{2(i)}$, $\sigma_{\phi,t}^{2(i)}$, and $\sigma_{\kappa,t}^{2(i)}$ from particle streams of sufficient statistics. The law of motion of sufficient statistic $\beta_{\ell,t}^{(i)}$ matches the transition equation $\beta_{\ell,t}^{(i)} = \mathfrak{f}\left(\beta_{\ell,t-1}^{(i)}, y_{1:t}, v_t^{(i)}, v_{t-1}^{(i)}\right)$, for $\ell = \eta, \upsilon, \phi$, and κ.

This leaves us to describe the routines that sample the measurement error scale volatility parameters, $\sigma_{\zeta,\pi}^2$ and $\sigma_{\zeta,h}^2$, $h = 1, \ldots, 5$. Since these variances lack laws of motion that can be employed to build transition equations, the relevant shape parameters are updated on information obtained from KF operations of the RB-APF. For example, we sample $\sigma_{\zeta,h}^{2(i)} \left| y_{1:t} \sim \mathcal{IG}\left(\frac{\alpha_t}{2}, \frac{\beta_{\zeta,h,t}^{(i)}}{2}\right)\right.$, where updates of $\beta_{\zeta,h,t}^{(i)}$ are calculated using information from step 3.(b) of the RB-APF; see the online appendix. Thus, updates of the shape parameters of the posterior distributions of $\sigma_{\zeta,\pi}^2$ and $\sigma_{\zeta,h}^2$, which are the sufficient statistics $\beta_{\zeta,\pi,t}^{(i)}$ and $\beta_{\zeta,h,t}^{(i)}$, are driven by the KF prediction error of y_t weighted by the "gain" of these innovations.

We summarize the PLE and the way it interacts with RB-APF with the following algorithm.

1. Before initializing the RB-APF at date 0, draw $\Psi^{(i)} = \mathcal{P}\left(\Gamma_0^{(i)}\right)$.

2. Next, carry out steps 1, 2, and 3.(a)–3.(c) of the RB-APF algorithm (that appear in the online appendix) to obtain the KF predictive likelihood $\ell_t^{(i)} \propto \mathcal{P}\left(y_t \left| s_{t-1|t-1}^{(i)}, \mathbf{\Sigma}_{t-1|t-1}^{(i)}, v_t^{(i)}, \Psi^{(i)}\right.\right)$ and calculate the particle weights, $\widehat{\omega}_t^{(i)}$.

3. Update the particles $\Psi^{(i)}$, $i = 1, \ldots, M$, using the system of transition equations $\Gamma_t^{(i)} = \mathfrak{f}\left(\Gamma_{t-1}^{(i)}, y_{1:t}, v_t^{(i)}, v_{t-1}^{(i)}\right)$, which guide the evolution of this vector of sufficient statistics.

4. Engage $\left\{\widehat{\omega}_t^{(i)}\right\}_{i=1}^M$ to resample $\left\{\Gamma_t^{(i)}\right\}_{i=1}^M$ and perform steps 3.(d)–3.(f), 4, and 5 of the RB-APF (that are listed in the online appendix).

5. Resample $\Delta_{\ell,t}^{(i)}$, which are changes to $\beta_{\ell,t}^{(i)}$, $\ell = \eta, \upsilon, \phi$, and κ, as described in step 3.(d) of the RB-APF discussed in the online appendix, but "innovations" to $\beta_{\zeta,\pi,t-1}^{(i)}$ and $\beta_{\zeta,h,t-1}^{(i)}$, $\Delta_{\zeta,\pi,t}^{(i)}$ and $\Delta_{\zeta,h,t}^{(i)}$, are not resampled.

6. Repeat steps 1 to 5 of the PLE starting at date $t = 1$ and stopping at date T.

7. Full sample estimates of the static volatility parameters are computed according to $\hat{\Psi} = \sum_{i=1}^{M} \omega_T^{(i)} \Psi_T^{(i)} = \sum_{i=1}^{M} \omega_T^{(i)} \mathcal{P}\left(\Gamma_T^{(i)}\right)$.

By repeating step 5 at dates $t = 1, \ldots, T-1$, the PLE produces information about the content of $\mathcal{Y}_t$ for the way the RB-APF "learns" about Ψ.

3.5 A Rao-Blackwellized Particle Smoother

Lindsten, Bunch, Särkkä, Schön, and Godsill (2016) develop an algorithm to compute smoothed estimates of $\mathcal{S}_t$ and $\mathcal{V}_t$, given $\mathcal{Y}_{1:T}$ and $\hat{\Psi}$. The algorithm is a forward filter-backward smoother (FFBS) for SSMs amenable to Rao-Blackwellization. The forward filter is the RB-APF described in section 3.3 and online appendix. The FFBS applies Rao-Blackwellization methods moving from date T to date 1 to generate smoothed estimates of $\mathcal{V}_t$ conditional on forward filtered particles. Forward filtering operations are conducted using the SSM (8.1) and (8.2) to produce smoothed estimates of $\mathcal{S}_t$, given smoothed estimates of $\mathcal{V}_t$.[13] Lindsten, Bunch, Särkkä, Schön, and Godsill (LBSSG) refer to the entire process as a forward-backward-forward smoother.

The RB-PS operates only on the nonlinear states of the joint DGP of the SI-prediction mechanism and SW-UC-SV-TVP-AR(1) model. The problem is, when moving backwards from date t to date $t-1$, smoothing $\mathcal{V}_t$ can cause its Markov structure to be lost. A reason is marginalizing the linear states produces a likelihood that depends on $\mathcal{V}_{1:t}$ rather than $\mathcal{V}_t$.

LBSSG solve this sampling problem by decomposing the target density $\mathcal{P}\left(\mathcal{V}_{1:T} \middle| \mathcal{Y}_{1:T};\, \hat{\Psi}\right)$ into $\mathcal{P}\left(\mathcal{V}_{1:t} \middle| \mathcal{V}_{1:t+1},\, \mathcal{Y}_{1:T};\, \hat{\Psi}\right) \mathcal{P}\left(\mathcal{V}_{t+1:T} \middle| \mathcal{Y}_{1:T};\, \hat{\Psi}\right)$. Drawing from $\mathcal{P}\left(\mathcal{V}_{t+1:T} \middle| \mathcal{Y}_{1:T};\, \hat{\Psi}\right)$ yields an incomplete path of the approximate smoothed nonlinear states from date $t+1$ to date T, which is denoted $\tilde{\mathcal{V}}_{t+1:T}$. Since these draws are initialized at date T by sampling from the date T filtered nonlinear states, $\left\{\mathcal{V}_T^{(i)}\right\}_{(i)=1}^{M}$, backward extension to $\tilde{\mathcal{V}}_{T-1:T}$ is drawn probabilistically from the cloud $\left\{\mathcal{V}_{1:T-1}^{(i)}\right\}_{(i)=1}^{M}$. The Rao-Blackwellized particle smoother is repeated for $t = T-2, \ldots, 1$.

[13] Alternative PS are found in Lopes and Tsay (2011) and Carvalho, Johannes, Lopes, and Polson (2010). These approaches to smoothing, which build on the PS of Godsill, Doucet, and West (2004), are applicable to APFs, but not to the RB-APF we employ.

The aforesaid factorization of $\mathcal{P}\left(\mathcal{V}_{1:T}\middle|\mathcal{Y}_{1:T};\,\hat{\Psi}\right)$ is also useful because there is information in $\mathcal{P}\left(\mathcal{V}_{1:t}\middle|\mathcal{V}_{1:t+1},\,\mathcal{Y}_{1:T};\,\hat{\Psi}\right)$ about the probabilities (*i.e.*, normalized weights) needed to draw smoothed nonlinear states. Gaining access to this information is difficult because the conditional density of $\mathcal{V}_{1:t}$ is not easy to evaluate.[14] LBSSG's propose simulation methods to perform the backward filtering implicit in $\mathcal{P}\left(\mathcal{V}_{1:t}\middle|\mathcal{V}_{1:t+1},\,\mathcal{Y}_{1:T};\,\hat{\Psi}\right)$. This density can be decomposed into

$$\mathcal{P}\left(\mathcal{V}_{1:t}\middle|\mathcal{V}_{1:t+1},\,\mathcal{Y}_{1:T};\,\hat{\Psi}\right)\;\propto\;\mathcal{P}\left(\mathcal{Y}_{t+1:T},\,\mathcal{V}_{t+1:T}\middle|\mathcal{V}_{1:t},\,\mathcal{Y}_{1:t};\,\hat{\Psi}\right)\mathcal{P}\left(\mathcal{V}_{1:t}\middle|\mathcal{Y}_{1:t};\,\hat{\Psi}\right),$$

where the object of interest is the predictive density $\mathcal{P}\left(\mathcal{Y}_{t+1:T},\,\mathcal{V}_{t+1:T}\middle|\mathcal{V}_{1:t},\,\mathcal{Y}_{1:t};\,\hat{\Psi}\right)$. LBSSG show this density equals $\int\mathcal{P}\left(\mathcal{Y}_{t+1:T},\,\mathcal{V}_{t+1:T}\middle|\mathcal{S}_t,\,\mathcal{V}_t;\,\hat{\Psi}\right)\mathcal{P}\left(\mathcal{S}_t\middle|\mathcal{Y}_{1:t},\,\mathcal{V}_{1:t};\,\hat{\Psi}\right)d\mathcal{S}_t$. Hence, run the KF forward to obtain estimates of $\mathcal{S}_t$ and $\boldsymbol{\Sigma}_t$ by drawing from $\mathcal{P}\left(\mathcal{S}_t\middle|\mathcal{Y}_{1:t},\,\mathcal{V}_{1:t};\,\hat{\Psi}\right)$. The mean and MSE of $\mathcal{S}_t$ are employed in simulations to generate sufficient statistics that approximate the density of the SSM (8.1) and (8.2), which when normalized are the probabilities of drawing a path of $\widetilde{\mathcal{V}}_{1:T}$. In a final step that is conditional on the path of $\widetilde{\mathcal{V}}_{1:t}$, the linear states are smoothed by iterating the KF forward. The upshot is, although $\mathcal{S}_t$ does not enter $\mathcal{P}\left(\mathcal{V}_{1:t}\middle|\mathcal{V}_{1:t+1},\,\mathcal{Y}_{1:T};\,\hat{\Psi}\right)$, the conditionally linear states are relevant for estimating the probability of sampling $\widetilde{\mathcal{V}}_{1:T}$.

Our implementation of LBSSG's RB-PS is described in the next algorithm.

1. Retrieve a stored ensemble of M particles, $\left\{\left\{\mathcal{S}_{t|t}^{(i)},\;\boldsymbol{\Sigma}_{t|t}^{(i)},\;\mathcal{V}_t^{(i)},\;\omega_t^{(i)}\right\}_{t=1}^{T}\right\}_{i=1}^{M}$, created by running the RB-APF on the SSM (8.1) and (8.2), given the PLE of Ψ, $\hat{\Psi}$.

2. Initialize the PS at date T

   (a) by drawing $\widetilde{\mathcal{V}}_T^{(i)}$ for each i from the filtered particle draws $\left\{\mathcal{V}_T^{(i)}\right\}_{i=1}^{M}$ that have been resampled using the weights $\omega_T^{(i)}$, and

   (b) compute $\widetilde{\mathfrak{O}}_T^{(i)}=\left(\mathfrak{C}_T^{(i)}\right)'\hat{\Omega}_{\mathcal{U}}^{-1}\mathfrak{C}_T^{(i)}$, $\widetilde{\mathbb{S}}_T^{(i)}=\left(\mathfrak{C}_T^{(i)}\right)'\hat{\Omega}_{\mathcal{U}}^{-1}\mathcal{Y}_T$, and $\mathfrak{V}_T^{(i)}=\mathbf{I}+\left(\mathfrak{B}_T^{(i)}\right)'\widetilde{\mathfrak{O}}_T^{(i)}\mathfrak{B}_T^{(i)}$ across M resampled particles, which are used to build sufficient statistics of $\mathcal{S}_T$.

[14] The KF creates an exact predictive density (up to a normalizing constant). However, computing the density involves iterating the filter forward from dates $t=1,\ldots,T-1$ to date T across M particle streams. These calculations are computationally costly, which motivate LBSSG to approximate the predictive density with simulated sufficient statistics.

3. For each particle $i = 1, \ldots, M$, iterate from date $t = T-1$ to date $t = 1$ to calculate the unnormalized weights, $\mathbb{W}_t^{(i)} = \omega_t^{(i)} \jmath_t^{(i)} \left| \boldsymbol{\upsilon}_t^{(i)} \right|^{-0.5} \exp\left\{ \frac{1}{2} \vartheta_t^{(i)} \right\}$, which generate smoothed normalized weights, $\widetilde{\omega}_{t|T}^{(i)} = \mathbb{W}_t^{(i)} \Big/ \sum_{m=1}^{M} \mathbb{W}_t^{(m)}$, where

   (a) $\Pr\left(\jmath = i \right) = \widetilde{\omega}_{t|T}^{(i)}$ counts the number of instances $\mathfrak{u} > \sum_{j=1}^{m} \widetilde{\omega}_{t|T}^{(j)}$, $\mathfrak{u} \sim \mathcal{U}(0, 1)$, and $m = 1, \ldots, M$,

   (b) $\jmath_t^{(i)} \sim \mathcal{P}\left(\widetilde{\mathcal{V}}_{t+1} \middle| \mathcal{V}_t^{(i)}; \hat{\Psi} \right)$, which is implemented by $\jmath_t^{(i)} = \exp\left\{ \mathfrak{v}_{\eta,t}^{(i)} + \mathfrak{v}_{\upsilon,t}^{(i)} \right\} \times \mathfrak{v}_{\theta,t}^{(i)} \times \mathfrak{v}_{\lambda,t}^{(i)}$,

$$
\begin{aligned}
\mathfrak{v}_{\ell,t}^{(i)} &= -\frac{1}{2} \left[\frac{\ln \tilde{\varsigma}_{\ell,t+1}^{2\,(i)} - \ln \varsigma_{\ell,t}^{2\,(i)}}{\hat{\sigma}_\ell} \right]^2, \quad \ell = \eta, \upsilon, \\
\mathfrak{v}_{\theta,t}^{(i)} &= \frac{\mathcal{N}\left(\tilde{\theta}_{t+1}, \theta_t^{(i)}, \hat{\sigma}_\phi \right)}{\mathcal{N}_{\Delta,\theta,t}}, \quad \mathfrak{v}_{\lambda,t}^{(i)} = \frac{\mathcal{N}\left(\tilde{\lambda}_{t+1}, \lambda_t^{(i)}, \hat{\sigma}_\phi \right)}{\mathcal{N}_{\Delta,\lambda,t}}, \\
\mathcal{N}_{\Delta,\theta,t} &= \Phi\left(\frac{1 - \theta_t^{(i)}}{\hat{\sigma}_\phi} \right) - \Phi\left(\frac{-1 - \theta_t^{(i)}}{\hat{\sigma}_\phi} \right), \; \mathcal{N}_{\Delta,\lambda,t} = \Phi\left(\frac{1 - \lambda_t^{(i)}}{\hat{\sigma}_\kappa} \right) - \Phi\left(\frac{-\lambda_t^{(i)}}{\hat{\sigma}_\kappa} \right),
\end{aligned}
$$

   $\Phi(\cdot)$ is the CDF of the normal distribution,

   (c) $\boldsymbol{\upsilon}_t^{(i)} = \mathbf{I} + \left(\boldsymbol{\Sigma}_t^{(i)} \right)' \tilde{\mathbf{O}}_t^{(i)} \boldsymbol{\Sigma}_t^{(i)}$, which depends on the backwards transition equations [15]

$$
\begin{aligned}
\overline{\mathbf{O}}_t^{(i)} &= \left(\boldsymbol{\mathcal{A}}_{t+1}^{(i)} \right)' \left[\mathbf{I} - \tilde{\mathbf{O}}_{t+1}^{(i)} \boldsymbol{\Sigma}_{t+1}^{(i)} \left(\boldsymbol{\upsilon}_{t+1}^{(i)} \right)^{-1} \left(\boldsymbol{\Sigma}_{t+1}^{(i)} \right)' \right] \tilde{\mathbf{O}}_{t+1}^{(i)} \boldsymbol{\mathcal{A}}_{t+1}^{(i)}, \\
\tilde{\mathbf{O}}_t^{(i)} &= \overline{\mathbf{O}}_t^{(i)} + \left(\mathfrak{C}_t^{(i)} \right)' \hat{\Omega}_{\mathcal{U}}^{-1} \mathfrak{C}_t^{(i)},
\end{aligned}
$$

   and

   (d) $\vartheta_t^{(i)} = \left(\tilde{\mathbb{S}}_t^{(i)} \right)' \left(\tilde{\mathbf{O}}_t^{(i)} \right)^{\frac{1}{2}} \left(\tilde{\mathbf{O}}_t^{(i)} \right)^{\frac{1}{2}\prime} \tilde{\mathbb{S}}_t^{(i)} - 2 \left(\tilde{\mathbb{S}}_t^{(i)} \right)' \mathbb{S}_t^{(i)} - \left[\boldsymbol{\Sigma}_t^{(i)} \left(\tilde{\mathbb{S}}_t^{(i)} - \tilde{\mathbf{O}}_t^{(i)} \mathbb{S}_t^{(i)} \right) \left(\tilde{\mathbf{O}}_t^{(i)} \right)^{-1} \right]^2$, where the backwards laws of motion consist of $\tilde{\mathbb{S}}_t^{(i)} = \overline{\mathbb{S}}_t^{(i)} + \left(\mathfrak{C}_t^{(i)} \right)' \hat{\Omega}_{\mathcal{U}}^{-1} \mathcal{Y}_t$ and $\overline{\mathbb{S}}_t^{(i)} = \left(\boldsymbol{\mathcal{A}}_{t+1}^{(i)} \right)' \left[\mathbf{I} - \tilde{\mathbf{O}}_{t+1}^{(i)} \boldsymbol{\Sigma}_{t+1}^{(i)} \left(\boldsymbol{\upsilon}_{t+1}^{(i)} \right)^{-1} \left(\boldsymbol{\Sigma}_{t+1}^{(i)} \right)' \right] \tilde{\mathbb{S}}_{t+1}^{(i)}$.

4. Given the draw $\jmath$ in step 3.(a), add $\mathcal{V}_t^{\jmath}$ to $\tilde{\mathcal{V}}_{t+1:T}$ to produce the approximate (partially) smoothed trajectory $\tilde{\mathcal{V}}_{t:T} = \left\{ \mathcal{V}_t^{\jmath} \quad \tilde{\mathcal{V}}_{t+1:T} \right\}$.

[15] LBSSG propose a square root KF to ensure numerical stability of the backward filtering operations.

5. Subsequent to iterating backwards from date T to date 1 for each of the M particle paths, calculate the distribution of $\widetilde{\mathcal{S}}_t$ by running the KF on the SSM (8.1) and (8.2) to produce

$$\mathcal{P}\left(\mathcal{S}_{1:T}\middle|\mathcal{Y}_{1:T};\widehat{\Psi}\right)=\int_{\widetilde{\mathcal{V}}_{1:T}}\mathcal{P}\left(\mathcal{S}_{1:T}\middle|\widetilde{\mathcal{V}}_{1:T}^{(i)},\mathcal{Y}_{1:T};\widehat{\Psi}\right)dF\left(\widetilde{\mathcal{V}}_{1:T}\right)\approx\sum_{i=1}^{M}\mathcal{P}\left(\mathcal{S}_{1:T}\middle|\widetilde{\mathcal{V}}_{1:T}^{(i)},\mathcal{Y}_{1:T};\widehat{\Psi}\right),\quad(12)$$

which is conditional on the backward filtered smoothed approximate paths of $\widetilde{\mathcal{V}}_{1:T}$.

The density $\mathcal{P}\left(\mathcal{S}_{1:T}\middle|\widetilde{\mathcal{V}}_{1:T}^{(i)},\mathcal{Y}_{1:T};\widehat{\Psi}\right)$ is the multivariate normal distribution that results from running the Kalman smoother (KS) on the SSM (8.1) and (8.2), where the approximation on the right side of (12) conditions on the M trajectories of $\widetilde{\mathcal{V}}_{1:T}^{(i)}$. We use the disturbance smoothing algorithm of Durbin and Koopman (2002) to draw $\widetilde{\mathcal{S}}_{1:T}$ from the distribution created by the KS, given a $\widetilde{\mathcal{V}}_t^{(i)}$ generated by the PS.

4 The Data and Estimates

We present estimates of the joint DGP of the SI-prediction mechanism and SW-UC-SV-TVP-AR(1) model in this section. These estimates are compared with ones gleaned from joint DGPs that lack inflation gap persistence, $\theta_t = 0$ or drift in SI updating $\lambda_t = \lambda$.[16] The goal is to evaluate the impact of inflation gap persistence or SI on the dynamics of π_t and $\pi_{t,t+h}^{SPF}$, $h = 1, \ldots, 5$. The joint DGPs are estimated using a RB-APF, PLE, and PS that engage $M = 100{,}000$ particles. These estimates are used to study (*i*) comovement of τ_t and $F_t\tau_t$ with π_t, and $\pi_{t,t+h}^{SPF}$, (*ii*) fluctuations in ε_t and $F_t\varepsilon_t$, (*iii*) the history of $\varsigma_{\eta,t}$ and $\varsigma_{\upsilon,t}$ since the start of the sample, (*iv*) movements in θ_t and λ_t over the business cycle, and (*v*) the contributions of $\mathcal{Y}_t$, π_t, and $\pi_{t,t+h}^{SPF}$ to variation in τ_t and $F_t\tau_t$.

4.1 The Data

Our estimates rest on a sample of real time realized inflation, π_t, and h-step ahead average SPF inflation prediction, $\pi_{t,t+h}^{SPF}$. We obtain the data from the Real-Time Data Set for Macroe-

[16] When $\theta_t = 0$ ($\lambda_t = \lambda$), σ_ϕ^2 (σ_κ^2) is deleted from Ψ. Fixing the frequency of SI updating also adds λ to Ψ, where the prior on $\lambda \sim \text{Beta}(1, 1)$.

conomists (RTDSM), which is compiled by the Federal Reserve Bank (FRB) of Philadelphia.[17] The data consist of observations from $1968Q4$ through $2017Q2$ for real time realized inflation and average SPF inflation predictions.

Realized inflation is the RTDSM's quarterly real-time vintages of the GNP and GDP deflator.[18] These vintages reflect data releases that were publicly available around the middle of quarter t and most often the publicly available information contains observations through quarter $t-1$. We employ these vintages to compute the quarterly difference in the log levels of real time observations on the GNP or GDP deflator, P_t. The quarterly price level data are transformed into inflation measured at an annualized rate using $\pi_t = 400[\ln P_t - \ln P_{t-1}]$.

Average SPF inflation predictions include a nowcast of the GNP or GDP deflator's level and forecasts of these price levels 1-, 2-, 3-, and 4-quarters ahead. These surveys are collected at quarter t without full knowledge of π_t. We comply with this timing protocol by assuming the average nowcast, 1-quarter, ..., and 4-quarter ahead predictions, which are denoted $\pi^{SPF}_{t,t+1}$, $\pi^{SPF}_{t,t+2}$, ..., and $\pi^{SPF}_{t,t+5}$, are conditional on data available at the end of quarter $t-1$. These inflation predictions are the annualized log difference of the average SPF prediction of the deflator's level and one lag of the real time realized price level supplied by the RTDSM.

Figure 1 plots π_t and four different average SPF inflation predictions. Plots of π_t and the average SPF inflation nowcast, $\pi^{SPF}_{t,t+1}$, appear in figure 1(a). Realized inflation is also found in figure 1(b), but the 1-quarter ahead average SPF inflation prediction, $\pi^{SPF}_{t,t+2}$, replaces $\pi^{SPF}_{t,t+1}$. Figure 1(c) displays π_t and the 3-quarter ahead average SPF inflation prediction, $\pi^{SPF}_{t,t+4}$, and figure 1(d) has π_t and the 4-quarter ahead average SPF inflation prediction, $\pi^{SPF}_{t,t+5}$. The panels depict π_t with a dot-dash (red) line and average SPF inflation predictions with a solid (blue) line. Vertical gray shaded bars denote NBER recession dates.

[17] The data are available at `http://www.philadelphiafed.org/research-and-data/real-time-center/survey-of-professional-forecasters/`.

[18] The SPF measured the output price level with the implicit GNP deflator before $1992Q1$. From $1992Q1$ to $1996Q4$, the implicit GDP deflator played this role. It was replaced by the chain weighted GDP deflator from $1997Q1$ to the end of the sample.

Figure 1: Realized Inflation and SPF Inflation Predictions, 1968$Q4$ to 2017$Q2$

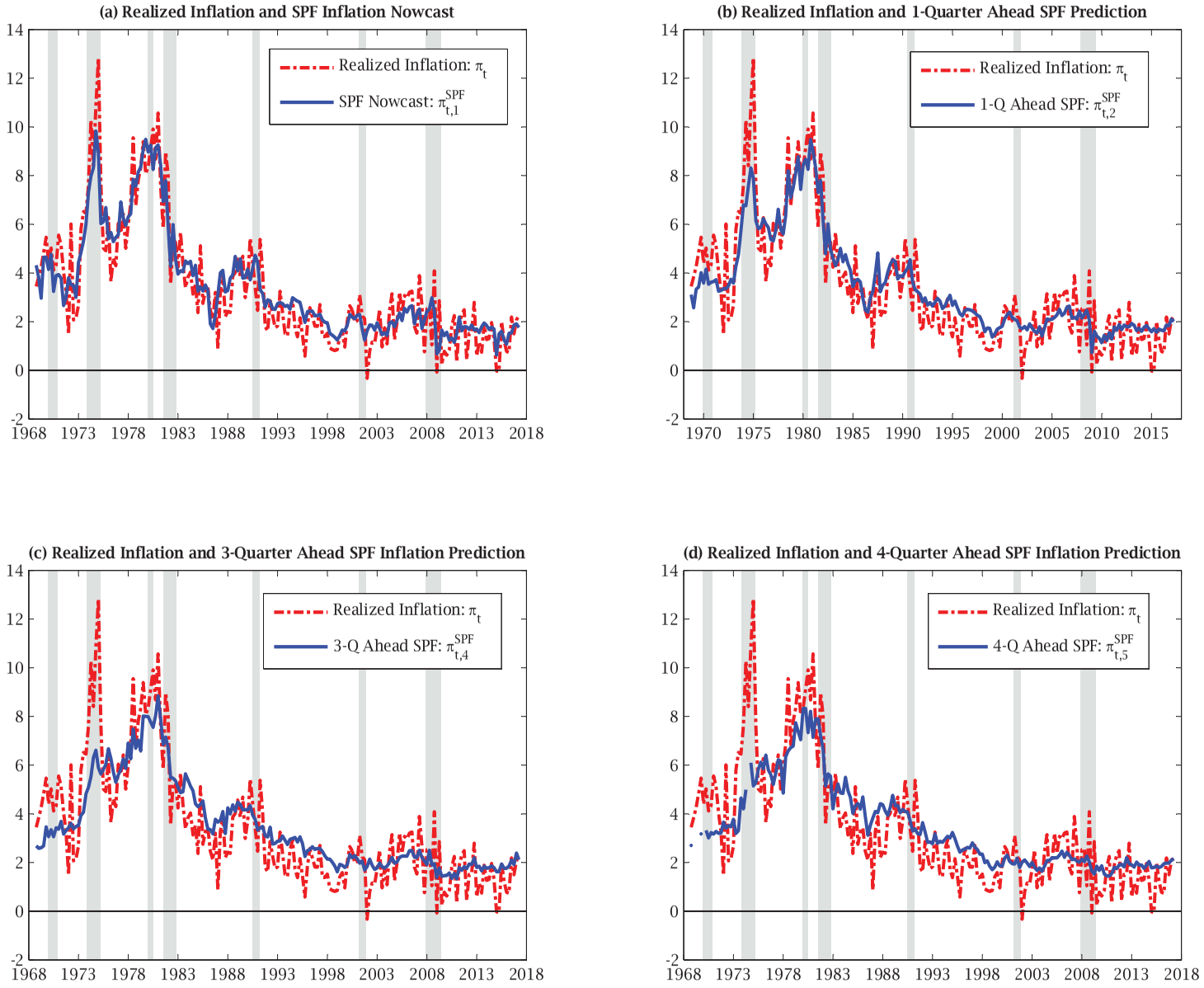

Note: The four plots contain vertical gray bands that denote NBER dated recessions.

The plots reveal several features of π_t and the average SPF inflation predictions. First, average SPF inflation predictions exhibit less variation than π_t throughout the sample. Next, as h increases, average SPF inflation predictions become smoother and are centered on π_t. All this suggests the average SPF surveys provide useful forecasts of inflation, which is a point made by Ang, Bekaert, and Wei (2007), Faust and Wright (2013), Mertens (2016), and Nason and Smith (2016a), among others.

Disparities in the average SPF nowcast to 4-quarter ahead prediction contain information to identify τ_t, ε_t, $F_t\tau_t$, and $F_t\varepsilon_t$. For example, the average SPF inflation nowcast peaks close to 10 percent during the 1973–1975 recession and around the double dip recessions of the early 1980s as Figure 1(a) shows. The former peak in inflation falls moving from $\pi^{SPF}_{t,t+2}$ to $\pi^{SPF}_{t,t+5}$ in figures 1(b), 1(c), and 1(d). At a 4-quarter ahead horizon, the average SPF inflation prediction rises steadily from about three percent in the early 1970s to a peak greater than eight percent around the 1980 recession.[19] Our estimates rely on this information, which is a function of the SPF inflation prediction horizon, to identify persistence, stickiness, and volatility in RE and SI trend and gap inflation.

4.2 Posterior Estimates of Ψ and Fit of the Joint DGPs

Table 3 lists full sample estimates of Ψ, $\hat{\Psi}$, for three joint DGPs. The DGPs combine the SI-prediction mechanism and SW-UC-SV-TVP-AR(1) model, SI-prediction mechanism and a SW-UC model in which no persistence, $\theta_t = 0$, only SV drives gap inflation, and a fixed parameter, $\lambda_t = \lambda$, SI-prediction mechanism and the SW-UC-SV-TVP-AR(1) model.

The restrictions on inflation gap persistence and the frequency of SI inflation updating affect $\hat{\Psi}$ in several ways. First, innovations to the RW of trend inflation SV are more volatile than innovations to the RW of gap inflation SV in the DGPs with drifting gap persistence because $\hat{\sigma}^2_\eta > \hat{\sigma}^2_\upsilon$. However, $\hat{\sigma}^2_\eta$ is larger while $\hat{\sigma}^2_\upsilon$ is smaller in the DGP that estimates θ_t and λ_t. In

[19] Figure 1(d) shows $\pi^{SPF}_{t,t+5}$ is missing observations in 1969, 1970, and 1974. The KF is modified to accommodate the missing observations.

contrast, $\hat{\sigma}_{\eta}^2$ and $\hat{\sigma}_{\upsilon}^2$ are about equal in the DGP with $\theta_t = 0$ and close to the calibrated values Stock and Watson (2007) and Creal (2012) use to estimate the state of the SW-UC-SV model. Next, there is little variation in estimates of the scale volatility on innovations to the RWs of θ_t and λ_t, $\hat{\sigma}_{\phi}^2$ and $\hat{\sigma}_{\kappa}^2$, across the DGPs in which these parameters appear. The DGPs with drifting gap persistence produce estimates of the scale volatility on the measurement errors of SPF inflation predictions, $\hat{\sigma}_{\zeta,h}^2$, $h = 1, \ldots, 5$, that are quantitatively similar. The converse is true for estimates of the scale volatility on the measurement errors of π_t, $\hat{\sigma}_{\zeta,\pi}^2$, because it is nearly twice as large in the DGP that estimates θ_t and λ_t compared with the other two DGPs.

Estimates of log marginal data densities (MDDs) appear at the bottom of table 3 for the three joint DGPs. Equation (11) is used to calculate $\mathcal{L}\left(\Psi \middle| y_{1:T}\right)$, which is the log MDD for a joint DGP tied to Ψ. Standard errors of the log MDDs are beneath estimates of $\mathcal{L}\left(\Psi \middle| y_{1:T}\right)$.[20] The estimates of $\mathcal{L}\left(\Psi \middle| y_{1:T}\right)$, indicate the data have, at a minimum, a very strong preference for the joint DGP of the SI prediction mechanism and SW-UC-SV-TVP-AR(1) model. Hence, the rest of the paper reports evidence this joint DGP has for the stickiness, persistence, and volatility of τ_t, $F_{t|t}\tau_t$, ε_t, and $F_{t|t}\varepsilon_t$.

Figure 2 plots the PLE paths of $\hat{\sigma}_{\eta}^2$, $\hat{\sigma}_{\upsilon}^2$, $\hat{\sigma}_{\phi}^2$, and $\hat{\sigma}_{\kappa}^2$ consistent with the joint DGP favored by the data. The scale volatility parameters are plotted with solid (navy blue) lines and 68 and 90 percent uncertainty bands appear as dark and light shading in figures 2(a)–2(d). These figures show $\hat{\sigma}_{\eta}^2$ more than doubles, $\hat{\sigma}_{\upsilon}^2$ falls by about a third, σ_{ϕ}^2 rises by about a quarter, and σ_{κ}^2 changes little from the start to the end of sample. The PLE path of $\hat{\sigma}_{\eta}^2$ drifts up for much of the sample as seen in figure 2(a). However, the PLE paths of these parameters are smooth from the 2001 recession to the end of the sample. Also, the 68 percent uncertainty bands are tight for the most part in figure 2, but the 90 percent uncertainty bands are wider and on occasion display substantial variation.

[20] The standard errors are standard deviations of estimates of the log MDDs obtained from rerunning the PF using different random seeds across the three DGPs. Hence, the approximation error of the PF is measured by the standard errors of $\mathcal{L}\left(\Psi \middle| y_{1:T}\right)$ and not the sampling uncertainty of a joint DGP.

Table 3: Posterior Estimates of the Joint DGPs of the SI Prediction Mechanism and SW-UC-SV Models

Parameter	TVP-SI: λ_t TVP-AR(1): θ_t	TVP-SI: λ_t Gap-SV: $\theta_t = 0$	Fixed SI: $\lambda_t = \lambda$ TVP-AR(1): θ_t
σ_η^2	0.423 [0.372, 0.481]	0.194 [0.167, 0.226]	0.336 [0.294, 0.385]
σ_υ^2	0.103 [0.090, 0.118]	0.193 [0.163, 0.302]	0.191 [0.168, 0.218]
σ_ϕ^2	0.101 [0.089, 0.114]	–	0.107 [0.095, 0.121]
σ_κ^2	0.081 [0.071, 0.093]	0.084 [0.038, 0.099]	–
$\sigma_{\zeta,\pi}^2$	0.213 [0.171, 0.263]	0.115 [0.085, 0.148]	0.115 [0.090, 0.146]
$\sigma_{\zeta,1}^2$	0.148 [0.126, 0.173]	0.314 [0.266, 0.371]	0.148 [0.126, 0.175]
$\sigma_{\zeta,2}^2$	0.070 [0.059, 0.082]	0.093 [0.079, 0.110]	0.068 [0.057, 0.080]
$\sigma_{\zeta,3}^2$	0.052 [0.044, 0.061]	0.053 [0.044, 0.062]	0.052 [0.044, 0.061]
$\sigma_{\zeta,4}^2$	0.046 [0.039, 0.055]	0.068 [0.058, 0.080]	0.047 [0.040, 0.55]
$\sigma_{\zeta,5}^2$	0.048 [0.040, 0.056]	0.098 [0.083, 0.116]	0.048 [0.041, 0.056]
$\mathfrak{L}\left(\Psi \middle\vert y_{1:T}\right)$	−473.132 (7.068)	−669.150 (5.823)	−483.996 (6.691)

The table presents posterior means of the elements of Ψ, which are calculated using the full sample at date $T = 2017Q2$. The values in brackets below the posterior means are 5 and 95 percent quantiles. The model in which the SI parameter is fixed yields the posterior mean $\widehat{\lambda} = 0.304$ with 5 and 95 percent quantiles of 0.250 and 0.360 conditional on the data and priors. The log MDDs are computed using the formula for $\mathfrak{L}\left(\Psi \middle\vert y_{1:T}\right)$ described by equation (11) in section 3.3. Volatility over the log MDDs are measured by standard errors that appear in parentheses. The estimates of the static scale volatility parameters and log marginal data densities are created using $M = 100{,}000$ particles.

Figure 2: Estimates of Static Volatility Parameters, 1968$Q4$ to 2017$Q2$

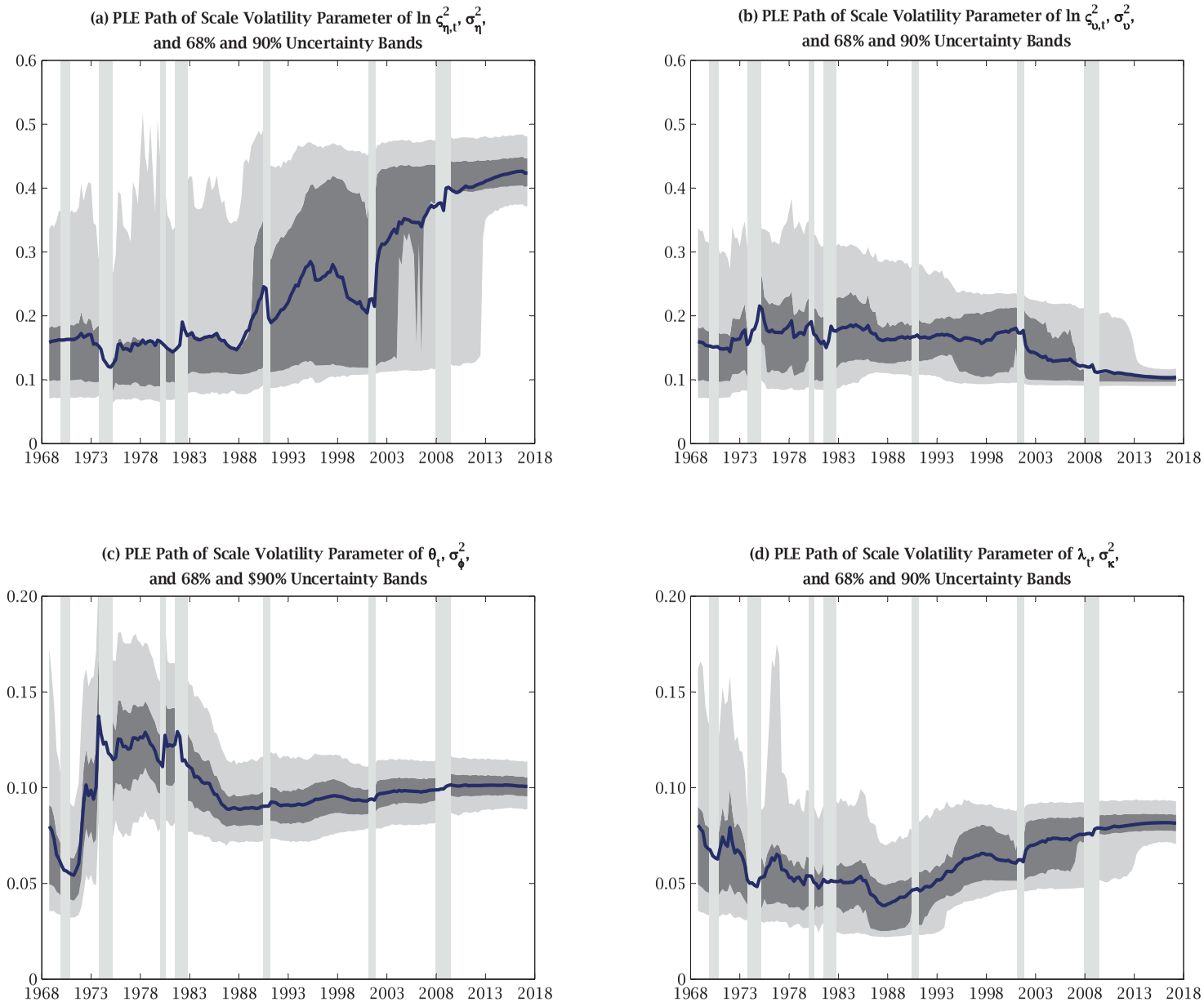

Note: The dark (light) gray areas surrounding estimates of the static scale volatility parameters, σ^2_η, σ^2_υ, σ^2_ϕ, and σ^2_κ cover 68 (90) percent uncertainty bands. The four plots contain vertical gray bands that denote NBER dated recessions.

4.3 Trend and Gap Inflation

Figure 3 contains π_t, the average SPF inflation nowcast and 4-quarter ahead inflation prediction, $\pi^{SPF}_{t,t+1}$ and $\pi^{SPF}_{t,t+5}$, filtered RE trend inflation, $\tau_{t|t}$, filtered SI trend inflation, $F_{t|t}\tau_t$, filtered RE gap inflation, $\varepsilon_{t|t}$, and filtered SI gap inflation, $F_{t|t}\varepsilon_t$, on the $1968Q4$ to $2017Q2$ sample. Plots of $\pi^{SPF}_{t,t+1}$, $F_{t|t}\tau_t$, and its 68 percent uncertainty bands are in figure 3(a). Figure 3(b) is similar, but replaces $\pi^{SPF}_{t,t+1}$ with $\pi^{SPF}_{t,t+5}$. In these figures, solid (blue) lines are average SPF inflation predictions and $F_{t|t}\tau_t$ is the dotted (black) lines. Figure 3(c) displays $\tau_{t|t}$ with a dash (green) line, $F_{t|t}\tau_t$ with a dotted (black) line, and π_t with a dot-dash (red) line. Estimates of RE and SI gap inflation appear in figure 3(d) as a dashed (green) line, $\varepsilon_{t|t}$, and dotted (black) line, $F_{t|t}\varepsilon_t$.

Estimates of SI trend inflation are informed by the 1973–1975 recession, inflation surge of the late 1970s and early 1980s, and Volcker disinflation.[21] In $1974Q4$, figure 3(a) displays a spike in $\pi^{SPF}_{t,t+1}$ of nearly 10 percent, but $F_{t|t}\tau_t$ is only 3.8 percent. At the same time, $\pi^{SPF}_{t,t+5}$ is 6.1 percent. The peaks in $\pi^{SPF}_{t,t+5}$ and $F_{t|t}\tau_t$, which occur a year and a half later, are close to 6.5 percent. The next peaks in $\pi^{SPF}_{t,t+1}$ and $\pi^{SPF}_{t,t+5}$ are 9.5 in $1979Q4$ and 8.3 percent in $1980Q1$. However, only in $1981Q2$ does $F_{t|t}\tau_t$ peak at 7.5 percent. After 1983, $\pi^{SPF}_{t,t+1}$, $\pi^{SPF}_{t,t+5}$, and $F_{t|t}\tau_t$ fall steadily before leveling off in the late 1990s as figures 3(a) and 3(b) show. However, $F_{t|t}\tau_t$ often deviates from $\pi^{SPF}_{t,t+1}$ between 1983 and 2000. As a result, $\pi^{SPF}_{t,t+1}$ often is outside the 68 percent uncertainty bands of $F_{t|t}\tau_t$ during this period while $\pi^{SPF}_{t,t+5}$ falls within the 68 percent uncertainty bands of $F_{t|t}\tau_t$ after the Volcker disinflation in figure 3(b).

Figure 3(c) has several interesting features. First, π_t is volatile compared with $\tau_{t|t}$ and $F_{t|t}\tau_t$. Another striking aspect of figure 3(c) is $\tau_{t|t}$ and $F_{t|t}\tau_t$ are nearly identical for much of the sample. This is not true for π_t and $F_{t|t}\tau_t$ (or $\tau_{t|T}$) from $1968Q4$ to 2000. For example, $\tau_{t|t}$ and $F_{t|t}\tau_t$ are less than a third of π_t during the first oil price shock. However, $F_{t|t}\tau_t$ explains much of the increases in π_t and $\pi^{SPF}_{t,t+1}$ by the late 1970s and early 1980s. Hence, $\tau_{t|t}$ and $F_{t|t}\tau_t$ respond slowly to the first oil price shock, but the inflation shock of the late 1970s and early 1980s produces quicker responses in $\tau_{t|t}$ and $F_{t|t}\tau_t$. Subsequently, π_t is often less than $\tau_{t|t}$

[21] Meltzer (2014, p. 1209) establishes 1986 as the end of the Volcker disinflation.

and $F_{t|t}\tau_t$ from 1983 to 2000. Beginning in 2003, $\tau_{t|t}$ and $F_{t|t}\tau_t$ are often centered on π_t.

The estimates RE and SI trend inflation are a counterpoint to studies in which gap inflation dominates movements in inflation; see Cogley and Sbordone (2008) among others. For example, only after the 1973–1975 recession does $\tau_{t|t}$ and $F_{t|t}\tau_t$ become important for explaining movements in π_t. Moreover, our results of trend inflation differ Grassi and Prioietti (2010), Creal (2012), and Shephard (2013) because our estimates condition on $\pi^{SPF}_{t,t+h}$, $h = 1, \ldots, 5$.

We plot $\varepsilon_{t|t}$ and $F_{t|t}\varepsilon_{t|t}$ in figure 3(d). These plots show $\varepsilon_{t|t}$ and $F_{t|t}\varepsilon_t$ are nearly inseparable for the $1968Q4$–$2017Q2$ sample. These estimates of gap inflation rise from less than one percent in $1968Q4$ to about 3.5 percent in 1970. Thereafter, $\varepsilon_{t|t}$ and $F_{t|t}\varepsilon_t$ turn negative before the 1973–1975 recession, which coincides with the largest spikes in $\varepsilon_{t|t}$ and $F_{t|t}\varepsilon_t$ of nearly nine percent. These spikes are followed by $\varepsilon_{t|t}$ and $F_{t|t}\varepsilon_t$ falling to about -2.5 percent by 1976. From the late 1970s to 1981, $\varepsilon_{t|t}$ and $F_{t|t}\varepsilon_t$ range from about zero to 3.7 percent.

There are two more aspects of figure 3(d) worth discussing. First, $\varepsilon_{t|t}$ and $F_{t|t}\varepsilon_t$ are less volatile subsequent to the Volcker disinflation compared with the 1970s. After 1983, (the absolute values of) $\varepsilon_{t|t}$ and $F_{t|t}\varepsilon_t$ are never larger than three percent. Second, $\varepsilon_{t|t}$ and $F_{t|t}\varepsilon_t$ are often negative from 1983 to 2000, which leads the average SPF participant to expect an increase in future growth in realized inflation. Nelson (2008) explains this prediction is an implication of the Beveridge and Nelson (1981) decomposition, which is built into the SW-UC-SV-TVP-AR(1) model of the joint DGP. Hence, the average SPF participant believes the Volcker disinflation produced only a transitory drop in realized inflation.

Movements in $F_{t|t}\varepsilon_t$ have parallels in monetary policy. Remember the average SPF participant expects mean reversion in π_t during the 1973–1975 recession. However, in the late 1970s the average SPF participant believes unit root dynamics dominates π_t. An explanation for this shift in the average SPF participant's beliefs about the inflation regime is discussed by Meltzer (2014, pp. 1006–1007). He notes that in the 1970s U.S. monetary policy makers would not distinguish permanent from transitory shocks. As a result, their responses to the first oil price shock contributed to unanchored inflation expectations by the late 1970s.

Figure 3: Realized Inflation, SPF Inflation Predictions, and Estimates of Trend and Gap Inflation, 1968$Q4$ to 2017$Q2$

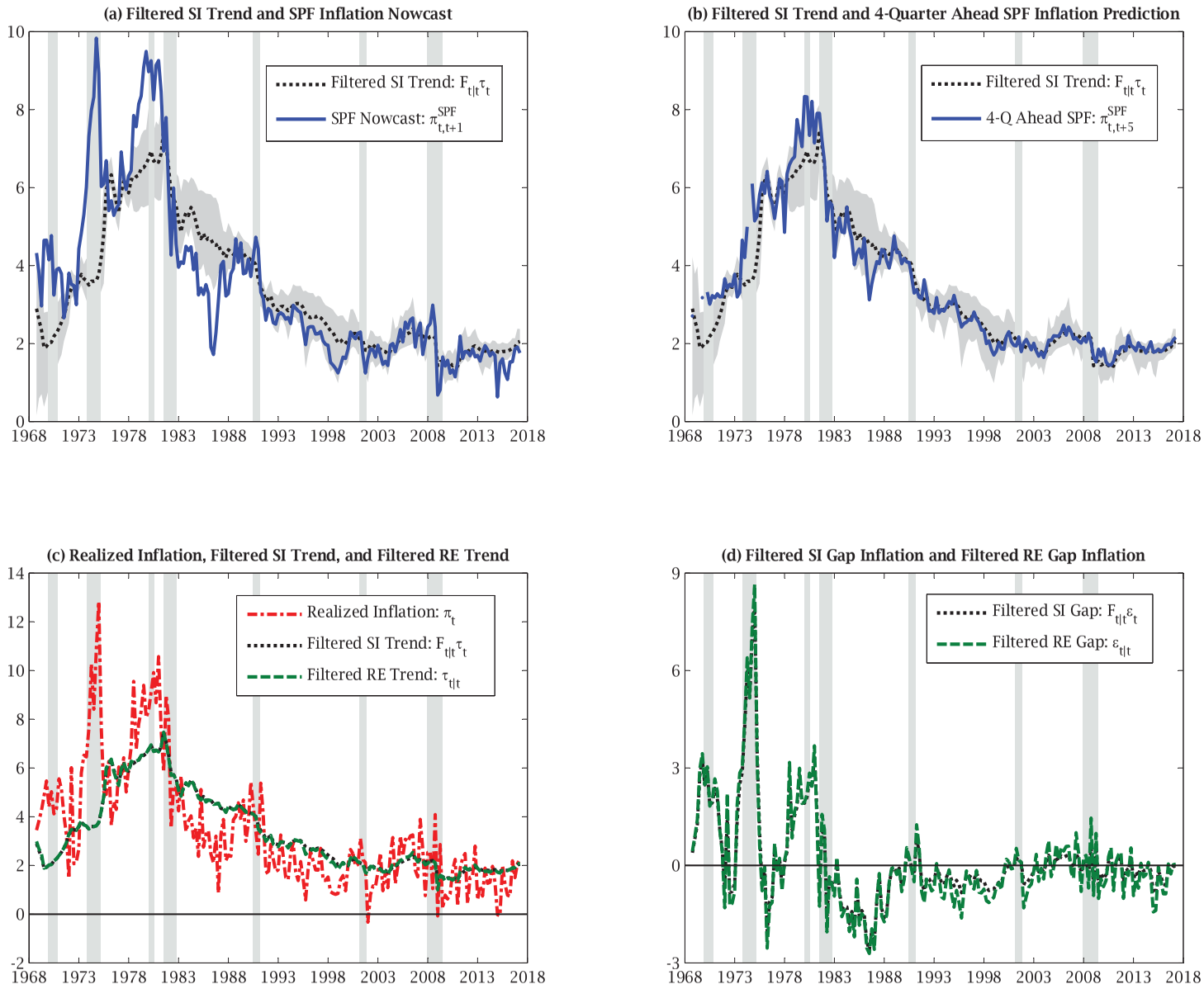

Note: The top row of charts contains light gray shaded areas that represent 68 percent uncertain bands around estimates of filtered SI trend inflation, $F_{t|t}\tau_t$. The vertical gray bands denote NBER dated recessions in the four charts.

The Volcker disinflation is another example. After 1983, π_t and $F_{t|t}\tau_t$ begin to fall, but the drop in π_t is steeper as figure 3(c) shows. These plots are consistent with mostly negative realizations for $F_{t|t}\varepsilon_t$ from 1983 to 2000 as in figure 3(d). As discussed previously, we assign these movements in $F_{t|t}\tau_t$ and $F_{t|t}\varepsilon_t$ to the average SPF participant expecting a temporary fall in π_t during and after the Volcker disinflation. The assessment agrees with Goodfriend and King (2005) and Meltzer (2014, p. 1131). They argue households, firms, and investors expected only a transitory drop in inflation after 1983.

4.4 Trend and Gap Inflation Volatilities

Estimates of filtered and smoothed trend and gap inflation SV appear in figure 4. Figures 4(a) and 4(c) contain dotted lines, which are $\varsigma_{\eta,t|t}$ (purple) and $\varsigma_{\upsilon,t|t}$ (teal). Dot-dashed (purple and teal) lines are $\varsigma_{\eta,t|T}$ and $\varsigma_{\upsilon,t|T}$ in figures 4(b) and 4(d). These figures also include 90 percent uncertainty bands, which are thinner solid (black) lines.

Figure 4 makes several points about $\varsigma_{\eta,t|t}$, $\varsigma_{\upsilon,t|t}$, $\varsigma_{\eta,t|T}$, and $\varsigma_{\upsilon,t|T}$. Figures 4(a) shows the largest peaks in $\varsigma_{\eta,t|t}$ occur in 1977, 1983, and 2009 while $\varsigma_{\upsilon,t|t}$ is dominated by a spike in 1975 in figure 4(c). Figures 4(b) and 4(d) display peaks in $\varsigma_{\eta,t|T}$ and $\varsigma_{\upsilon,t|T}$ during the 1981–1982 recession and in 1975, respectively. Hence, these plots are more evidence shocks to gap inflation dominate movements in π_t and $\pi^{SPF}_{t,t+h}$ during the 1973–1975 recession, but in the inflation surge of the late 1970s and early 1980s permanent shocks are more important.

Another revealing feature of figures 4(a) and 4(c) is the behavior of SV around NBER dated recessions. The filtered SVs, $\varsigma_{\eta,t|t}$ and $\varsigma_{\upsilon,t|t}$, often rise during or after a NBER recessions as depicted in figures 4(a) and 4(c). There are peaks $\varsigma_{\eta,t|T}$ ($\varsigma_{\upsilon,t|T}$) during the 1990–1991 and 2007–2009 (1981–1982, 1990–1991, 2001, and 2007–2009) recessions.

Figure 4(b) and 4(d) are also informative about the long run behavior of $\varsigma_{\eta,t|T}$ and $\varsigma_{\upsilon,t|T}$. These SVs display steady declines for extended periods during the sample. The descent starts in 1983 for $\varsigma_{\eta,t|T}$ while this process starts in 1975 for $\varsigma_{\upsilon,t|T}$.

Figure 4: Estimates of the Stochastic Volatility of Trend and Gap Inflation, 1968$Q4$ to 2017$Q2$

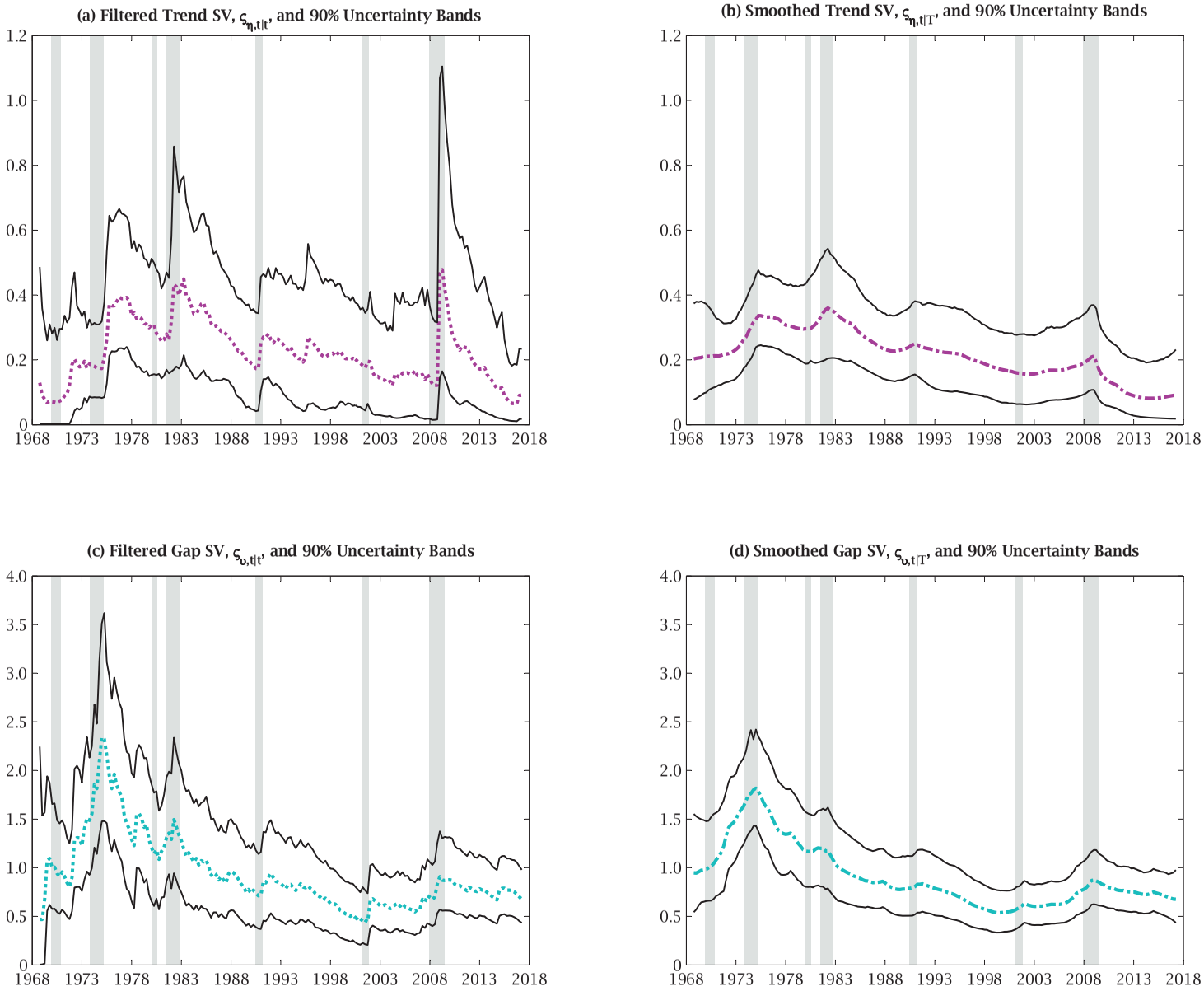

Note: The solid thin (black) lines around estimates of filtered and smoothed trend and gap inflation SV are lower and upper bounds on 90 percent uncertainty bands. The four plots contain vertical gray bands that denote NBER dated recessions.

Finally, our estimates show $\varsigma_{\eta,t|T}$ is smaller than $\varsigma_{\upsilon,t|T}$ for the entire sample. These estimates differ from Grassi and Prioietti (2010), Stock and Watson (2010), Creal (2012), and Shephard (2013). These authors report trend SV dominates inflation gap SV from the 1970s well into the late 1990s. However, Creal and Shephard find that gap inflation SV is greater than trend SV after 2000.

4.5 Drifting Inflation Gap Persistence

Figures 5(a) and 5(b) display filtered and smoothed estimates of drifting inflation gap persistence, $\theta_{t|t}$ and $\theta_{t|T}$. Dotted and dot-dash (orange) lines denote $\theta_{t|t}$ and $\theta_{t|T}$. Surrounding $\theta_{t|t}$ and $\theta_{t|T}$ are 68 and 90 percent uncertainty bands in the dark and light gray shaded areas. Figures 5(c) and 5(d) plot the absolute value of smoothed inflation gap persistence, $|\theta_{t|T}|$, and accumulated changes of this absolute value, $|\theta_{t|T}| - |\theta_{1|T}|$. These plots depict $|\theta_{t|T}|$ and $|\theta_{t|T}| - |\theta_{1|T}|$ with dot-dashed (orange) lines, where the dark and light gray shaded areas are 68 and 90 percent uncertainty bands.

There is co-movement between $\theta_{t|t}$ and $\theta_{t|T}$ with NBER dated cycles in figures 5(a) and 5(b). The co-movement is pro-cyclical during the 1969–1970, 1973–1975, and 1980 recessions. These recessions see peaks in $\theta_{t|t}$ and $\theta_{t|T}$ while there are troughs between these recession. Post-1981, $\theta_{t|t}$ and $\theta_{t|T}$ turn counter-cyclical. Filtered and smoothed estimates of drifting inflation gap persistence peak between the recessions of 1981–1982, 1990–1991, 2001, and 2007–2009 while these recessions see troughs in $\theta_{t|t}$ and $\theta_{t|T}$.

Uncertainty bands of $\theta_{t|t}$ and $\theta_{t|T}$ also appear in figures 5(a) and 5(b). The 90 percent quantiles of $\theta_{t|T}$ ($\theta_{t|t}$) cover zero in 1971–1972, 1990–1991, and 2006–2014 (1968–1969, 1972–1973, 1975, 1976–1978, 1983, 1990–1993, and 2003–2014). Hence, we infer there are episodes in which inflation gap persistence is zero. These results are similar to evidence presented by Cogley, Primiceri, and Sargent (2010). They find inflation gap persistence drops after 1983. However, our evidence is tied to pro-cyclical troughs in $\theta_{t|T}$ before 1983 and to the 2007–2009 recession and its aftermath, which occurs more than 20 years after the Volcker disinflation.

Figure 5: Estimates of Time-Varying Inflation Gap Persistence, 1968$Q4$ to 2017$Q2$

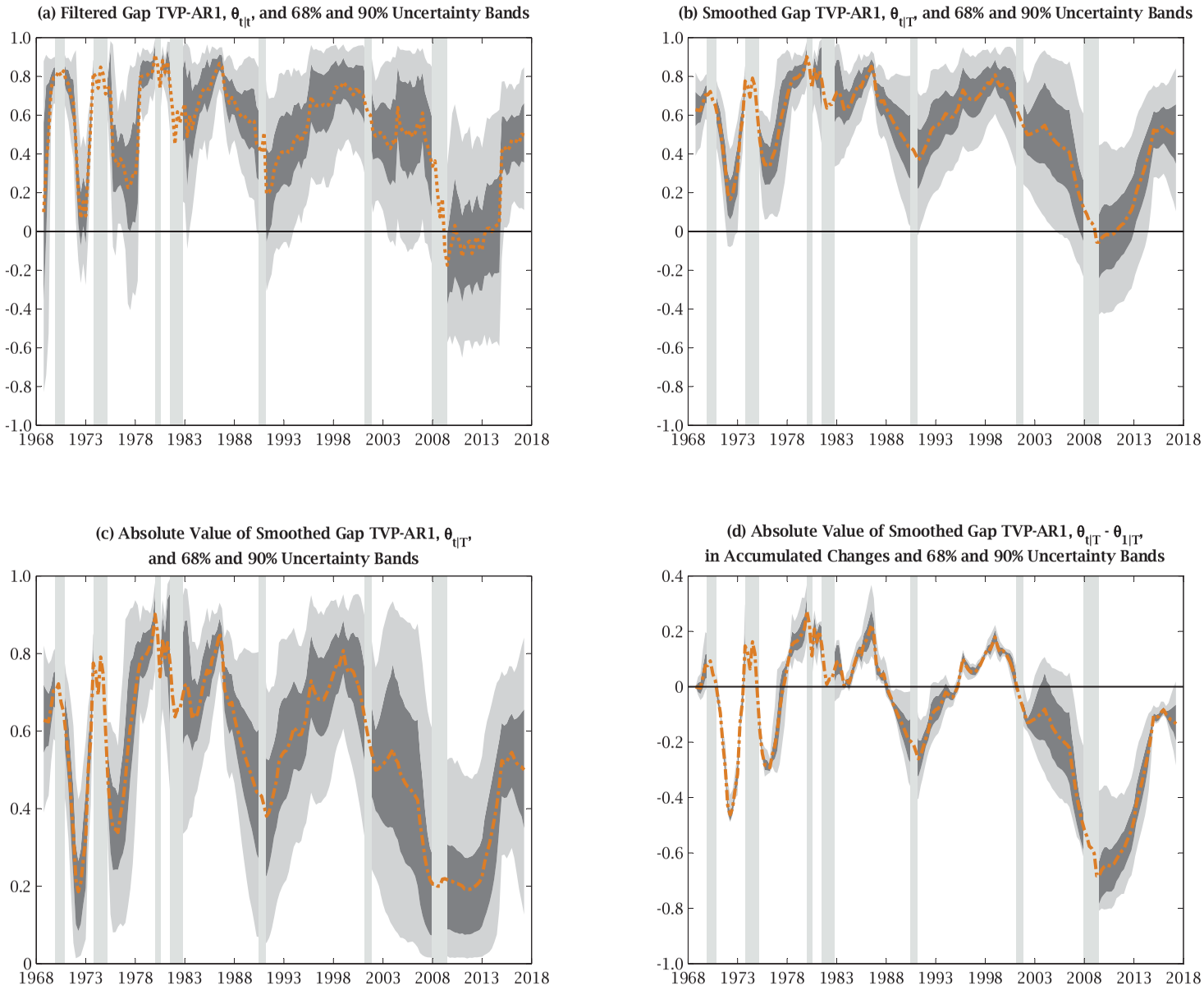

Note: The dark (light) gray areas surrounding estimates of the TVP-AR1 of gap inflation cover 68 (90) percent uncertainty bands. The four plots contain vertical gray bands that denote NBER dated recessions.

Another take on the statistical and economic significance of drifting gap inflation persistence appears in figure 5(c). This figure displays the absolute value of $\theta_{t|T}$, $|\theta_{t|T}|$. The plot of $|\theta_{t|T}|$ gives evidence similar to that found in figure 5(b). There is evidence of a shift in business cycle behavior of $|\theta_{t|T}|$ around the Volcker disinflation. Drift in the absolute value of inflation gap persistence also declines steadily from the late 1990s to 2013.

There remains the inference problem that $\theta_{t|t}$, $\theta_{t|T}$, and $|\theta_{t|T}|$ are not necessarily informative about the statistical and economic content of changes in drifting inflation gap persistence during the sample. We rectify this problem by plotting accumulating changes in $|\theta_{t|T}|$, $|\theta_{t|T}| - |\theta_{1|T}|$, in figure 5(d). Figure 5(d) shows these changes have tighter uncertainty bands compared with the plots in figures 5(a), 5(b), and 5(c). Nonetheless, the path of $|\theta_{t|T}| - |\theta_{1|T}|$ continues to show peaks coincide with recessions pre-1981 and troughs occur between these recessions but the opposite is observed post-1981. Hence, we have evidence that dates a shift from pro-cyclical to counter-cyclical drifting inflation gap persistence to 1981. This break is consistent with an argument made by Meltzer (2014, p. 1006 and p. 1207). He contends there was a shift in U.S. inflation persistence because the Fed changed the way it operated monetary policy in the 1980s and 1990s compared with the 1970s.

4.6 Time Variation in the Frequency of SI Updating

Figure 6 presents filtered and smoothed estimates of the time variation in the frequency of SI updating, $\lambda_{t|t}$ and $\lambda_{t|T}$. These panels plot $\lambda_{t|t}$ and $\lambda_{t|T}$ as dotted (light green) and dot-dashed (brick) lines. The thin solid (brick) lines denote 90 percent uncertainty bands of $\lambda_{t|T}$ and 90 percent uncertainty bands of $\lambda_{t|t}$ are depicted with light gray areas. Figures 6(b) and 6(d) plot accumulated changes in $\lambda_{t|T}$, $\lambda_{t|T} - \lambda_{1|T}$. In these panels, dark and light gray areas are 68 and 90 percent uncertainty bands of $\lambda_{t|T} - \lambda_{1|T}$. The top row of figure 6 has $\lambda_{t|t}$, $\lambda_{t|T}$, and $\lambda_{t|T} - \lambda_{1|T}$ estimated using the joint DGP of the SI-prediction mechanism and the SW-UC-SV-TVP-AR(1) model. Figures 6(c) and 6(d) report similar estimates, but the SW-UC-SV model lacks persistence in gap inflation, or $\theta_t = 0$ for all dates t.

Plots of $\lambda_{t|t}$ and $\lambda_{t|T}$ display a decade long swing from more frequent to less frequent updating beginning in the late 1980s in figure 6(a). From the late 1960s to the 1988, the average SPF inflation respondent is estimated to update almost every quarter to changes in $\mathbf{E}_t\pi_{t+h}$ because $\lambda_{t|T}$ varies between 0.01 and 0.35. However, there is uncertainty about these estimates because the 90 percent confidence bands of $\lambda_{t|T}$ range from 0.01 to 0.60.

Figures 6(a) also shows $\lambda_{t|t}$ and $\lambda_{t|T}$ reach a plateau from 1994 to 2007 before falling during the 2007–2009 recession. From 1995 to 2008, $\lambda_{t|t}$ and $\lambda_{t|T}$ range between 0.50 and 0.70. The recession of 2007-2009 sees $\lambda_{t|T}$ $(\lambda_{t|t})$ dropping to 0.25 (0.35). Subsequently, $\lambda_{t|T}$ $(\lambda_{t|t})$ recovers to 0.47 (0.60) before $2017Q2$. The filtered and smoothed estimates of λ_t are also associated with substantial uncertainty. For example, when $\lambda_{t|T}$ plateaus in the late 1990s, the five percent quantile is as low as 0.20 and the 95 percent quantile is as high as 0.95. Furthermore, the 90 percent uncertainty bands of $\lambda_{t|t}$ and $\lambda_{t|T}$ remain wide in figure 6(a) as the sample moves past the recession of 2001, the "considerable" and "extended" period policy regimes of the Greenspan and Bernanke Feds, the 2007–2009 recession, and unconventional policy regimes of the Bernanke and Yellen Feds.

There are useful inferences to draw from $\lambda_{t|t}$ and $\lambda_{t|T}$, even with the uncertainty surrounding these estimates. For example, a low frequency of SI inflation updating by the average member of the SPF is consistent with the Fed engaging in a policy of "opportunistic disinflation" during the 1990s as described by Meyer (1996) and Orphanides and Wilcox (2002). Orphanides and Wilcox quote Vice Chairman Blinder and President Boehne of the FRB-Philadelphia as advocating the Fed of the mid 1990s should wait for a state of the world in which there is little cost to monetary policy lowering inflationary expectations rather than to take actions during periods when the potential for a costly disinflation are large. However, since the joint DGP of the SI-prediction mechanism and SW-UC-SV-TVP-AR(1) model is the source of estimates of $\lambda_{t|t}$ and $\lambda_{t|T}$, these estimates are about the average SPF respondent's beliefs about changes in the inflation regime and not evidence about shifts in the monetary policy regime.[22]

[22] Information about monetary policy interventions is needed to conduct a monetary policy evaluation of this kind as studied, for example, by Leeper and Zha (2003).

Figure 6: Estimates of the Time-Varying SI Parameter, 1968$Q4$ to 2017$Q2$

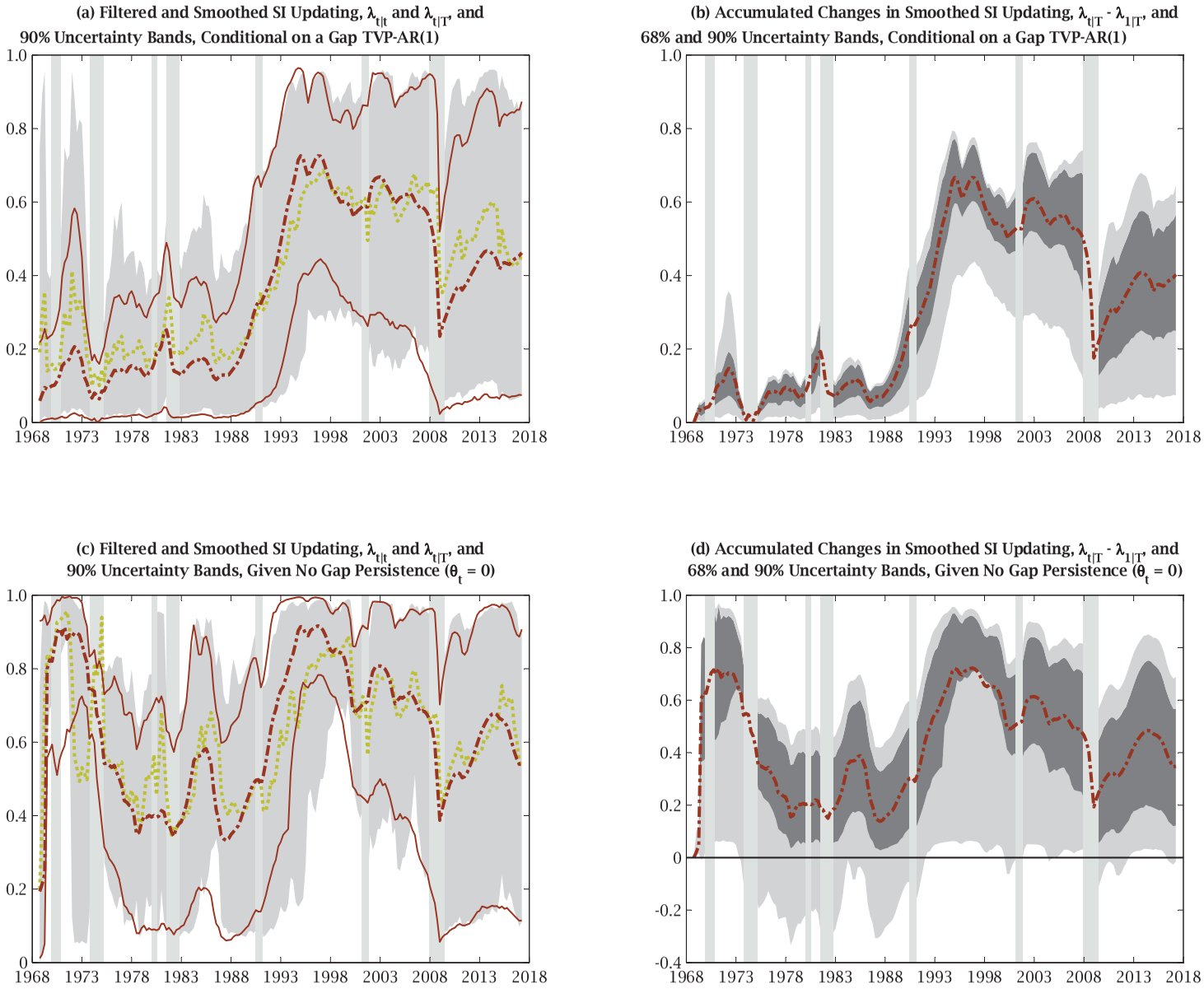

Note: The dark (light) gray areas surrounding estimates of the SI-TVP cover 68 (90) percent uncertainty bands. The left column of charts also displays solid thin (red) lines around smoothed estimates of the SI-TVP, $\lambda_{t|T}$, that are lower and upper bounds on 90 percent uncertainty bands. The four plots contain vertical gray bands that denote NBER dated recessions.

There is greater support for statistically and economically important time variation in the frequency of SI inflation updating in figure 6(b). This figure plots $\lambda_{t|T} - \lambda_{1|T}$ for the joint DGP in which there is drift in inflation gap persistence. In this case, the path of $\lambda_{t|T} - \lambda_{1|T}$ in figure 6(b) is similar to $\lambda_{t|T}$ displayed in figure 6(a) with respect to level and slope. Another interesting feature of figure 6(b) is the uncertainty bands surrounding $\lambda_{t|T} - \lambda_{1|T}$. Figure 6(b) displays 90 percent uncertainty bands of $\lambda_{t|T} - \lambda_{1|T}$ that are narrower for the entire sample compared with the analogous confidence bands of $\lambda_{t|T}$ in figure 6(a). These estimates strengthen the case that changes in the frequency of SI inflation updating by the average member of the SPF are statistical and economic important.

This message is reinforced by figure 6(d). This figure present estimates of $\lambda_{t|T} - \lambda_{1|T}$ conditional on a joint DGP in which there is no persistence in the inflation gap. Given θ_t is zero, SI inflation updating is less frequent quarter by quarter as depicted by $\lambda_{t|t}$ and $\lambda_{t|T}$ in figure 6(c) compared with the estimates found in figure 6(a). Although figure 6(c) suggests there is useful information about the frequency of SI inflation updating conditional on $\theta_t = 0$, the plot of $\lambda_{t|T} - \lambda_{1|T}$ in figure 6(d) indicates otherwise. Figure 6(d) depicts $\lambda_{t|T} - \lambda_{1|T}$ as fluctuating around zero with 90 percent uncertainty bands that often contain zero under the joint DGP in which inflation gap has no persistence.

This section reports estimates of $\lambda_{t|t}$, $\lambda_{t|T}$, and $\lambda_{t|T} - \lambda_{1|T}$ that show SI inflation updating by the average SPF respondent is statistically and economically significant for the last 48 years. These results agree with Coibion and Gorodnichenko (2015). Nonetheless, our estimates also reveal shifts in SI inflation updating during the sample. From the 1969 to 1988, the frequency of SI inflation updating occurred almost every quarter. The frequency declines to about once every two to three quarter until 2007, followed by a sharp increase during the 2007–2009 recession. Afterwards, the frequency drops by $2017Q2$. These shifts in estimates of SI inflation updating indicate the average SPF participant's beliefs about the inflation regime changed within a few years of the end of the Volcker disinflation. The average SPF participant's beliefs about the inflation regime also appear to have been altered by the recession of 2007–2009.

4.7 SPF Inflation Predictions and Trend Inflation Uncertainty

Figure 7 displays conditional volatilities of RE trend inflation, τ_t, and SI trend inflation, $F_t\tau_t$. The plots quantify uncertainty over time in τ_t and $F_t\tau_t$ conditional on the history of y_t, or histories of subsets of its elements, smoothed estimates of the nonlinear states, $\widetilde{\mathcal{V}}_{t|T}$, and estimates of the static scale volatility coefficients, $\hat{\Psi}$. The measure of the volatility of τ_t is $\text{Var}(\tau_t \,|\, y_{1:t},\, \widetilde{\mathcal{V}}_{t|T},\, \hat{\Psi})$, where the entire information set runs from the first observation to quarter t, the smoothed nonlinear states begin at quarter t and end with quarter T, and estimates of the static scale volatility parameters are full sample. Similar computations are used to produce the conditional volatility of $F_t\tau_t$. Thus, the paths of the nonlinear states and parameter estimates are held fixed across changes in the sample data fed into the KF to produce estimates of the conditional volatilities of τ_t and $F_t\tau_t$.

Figure 7(a) plots the conditional volatilities of τ_t. The conditional volatilities of $F_t\tau_t$ are found in figure 7(b). In these figures, the solid (black) line, dashed (blue) line, dotted (red) line, and dot-dashed (green) line are $\text{Var}(x \,|\, y_{1:t},\, \widetilde{\mathcal{V}}_{t|T},\, \hat{\Psi})$, $\text{Var}(x \,|\, \pi_{1:t},\, \widetilde{\mathcal{V}}_{t|T},\, \hat{\Psi})$, $\text{Var}(x \,|\, \pi^{SPF}_{1:t},\, \widetilde{\mathcal{V}}_{t|T},\, \hat{\Psi})$, and $\text{Var}(x \,|\, \pi_{1:t},\, \pi^{SPF}_{1:t},\, \widetilde{\mathcal{V}}_{t|T},\, \hat{\Psi})$, respectively, where $x = \tau_t,\, F_t\tau_t$.

Figures 7(a) and 7(b) reveal π_t and $\pi^{SPF}_{t,t+5}$ jointly contribute the bulk of the information pertinent to estimate τ_t and $F_t\tau_t$. The reason is the dot-dashed (green) lines of figures 7(a) and 7(b) are always near the solid (black) lines. Hence, given only π_t and $\pi^{SPF}_{t,t+5}$, $\text{Var}(\tau_t \,|\, \pi_t,\, \pi^{SPF}_{1:t,t+5},\, \widetilde{\mathcal{V}}_{t|T},\, \hat{\Psi})$ and $\text{Var}(F_t\tau_t \,|\, \pi_t,\, \pi^{SPF}_{1:t,t+5},\, \widetilde{\mathcal{V}}_{t|T},\, \hat{\Psi})$ are close to the estimates conditioned on the entire information set, $\text{Var}(\tau_t \,|\, y_t,\, \widetilde{\mathcal{V}}_{t|T},\, \hat{\Psi})$ and $\text{Var}(F_t\tau_t \,|\, y_t,\, \widetilde{\mathcal{V}}_{t|T},\, \hat{\Psi})$. In contrast, the dotted (blue) lines are far from the solid (black) and large dot-dashed (green) lines in the first half of the sample. Hence, prior to the Volcker disinflation, there is insufficient information in π_t alone to estimate τ_t and $F_t\tau_t$ without also generating more variation in these estimates compared with estimates conditioning on either y_t or π_t and $\pi^{SPF}_{t,t+5}$. However, conditioning only on $\pi^{SPF}_{t,t+5}$ produces substantial variation around $F_t\tau_t$ that is manifested by large differences between plots of $\text{Var}(F_t\tau_t \,|\, \pi^{SPF}_{1:t,t+5},\, \widetilde{\mathcal{V}}_{t|T},\, \hat{\Psi})$ and $\text{Var}(F_t\tau_t \,|\, y_t,\, \widetilde{\mathcal{V}}_{t|T},\, \hat{\Psi})$ or $\text{Var}(F_t\tau_t \,|\, \pi_t,\, \pi^{SPF}_{1:t,t+5},\, \widetilde{\mathcal{V}}_{t|T},\, \hat{\Psi})$ in figure 7(b).

Figure 7: Uncertainty Measure of Trend Inflation Conditional on Different Information Sets, 1968$Q4$ to 2017$Q2$

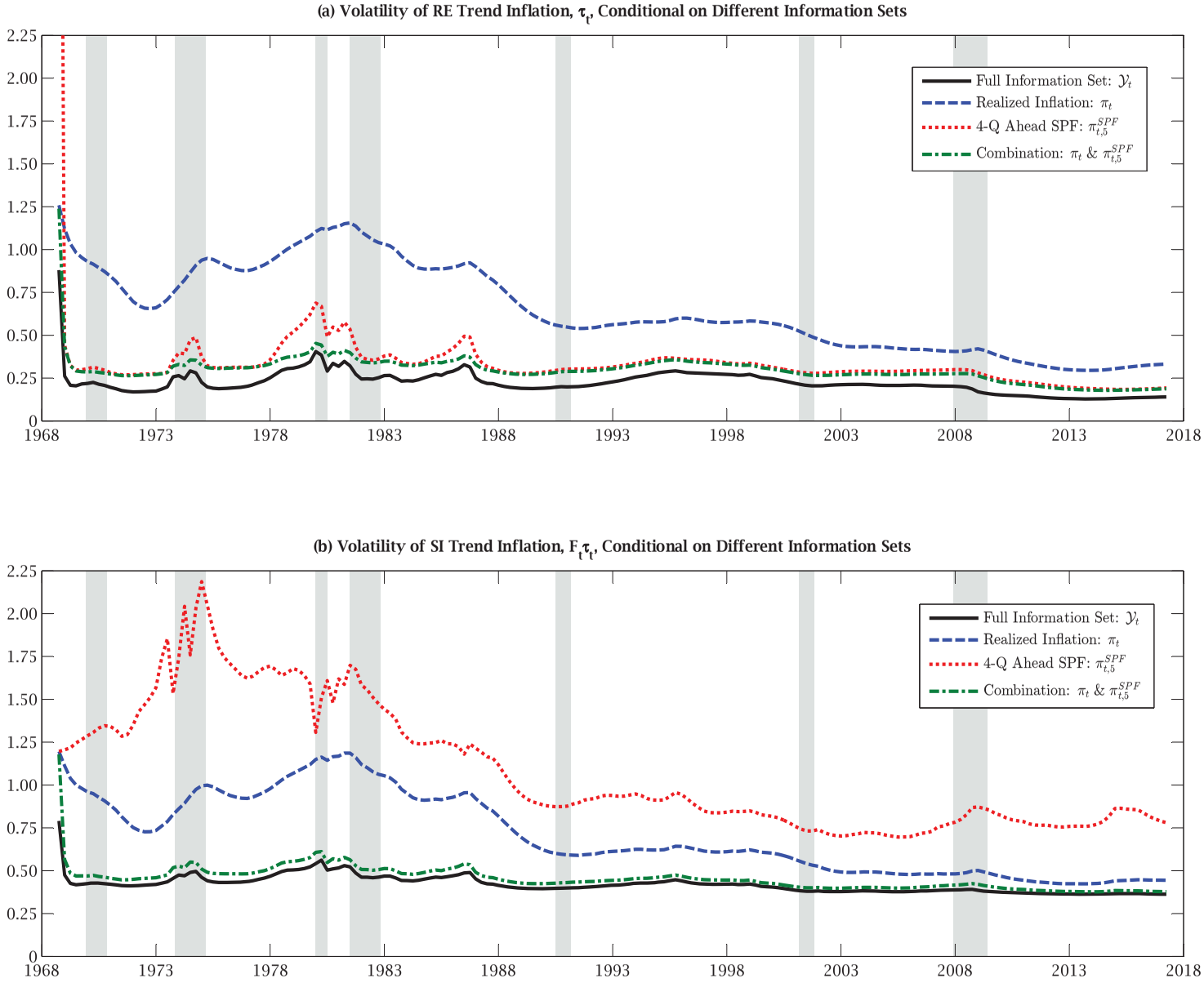

Note: The two plots contain vertical gray bands that denote NBER dated recessions.

In summary, figure 7 shows realized inflation and the 4-quarter ahead average SPF inflation prediction contain much of the information useful for reducing uncertainty surrounding τ_t and $F_t\tau_t$ and, hence, efficiently estimating these measures of trend inflation.

5 Conclusions

This paper studies the joint dynamics of realized inflation and inflation predictions of the Survey of Professional Forecasters (SPF). The joint data generating process (DGP) mixes a Stock and Watson (2007) unobserved-components (SW-UC) model with the Coibion and Gorodnichenko (2015) version of the Mankiw and Reis (2002) sticky information (SI) model. The SW-UC model with stochastic volatility (SV) in trend and gap inflation is extended to include drift in inflation gap persistence. The SI law of motion is endowed with drift in the SI inflation updating parameter. We estimate the joint DGP on a sample of real time realized inflation and averages of SPF inflation predictions from $1968Q4$ to $2017Q2$. The estimator embeds a Rao-Blackwellized auxiliary particle filter into the particle learning estimator of Storvik (2002). Smoothed estimates of the state variables are constructed using an algorithm developed by Lindsten, Bunch, Särkkä, Schön, and Godsill (2016).

Estimates of the joint DGP are summarized as follows. First, longer horizon average SPF inflation predictions provide useful information for estimating rational expectations (RE) and SI trend inflation and reducing uncertainty around these estimates. Second, RE and SI gap inflation dominate inflation fluctuations during the first oil price shock. This is reversed during the late 1970s and early 1980s. Third, trend (gap) inflation SV falls steadily after 1983 (1975). We also find that inflation gap persistence is pro-cyclical before 1981 and turns counter-cyclical afterwards. Fifth, changes in the frequency of SI inflation updating are statistically and economically important. The average SPF participant is often updating SI inflation predictions from the late 1960s through the late 1980s. Subsequently, the frequency of SI inflation updating falls to levels associated with estimates reported by Coibion and Gorodnichenko (2015), among others,

and remains low until the 2007–2009 recession.

Our results fit into a literature represented by, among others, Krane (2011), Mertens (2016), and Nason and Smith (2016a, b). These authors find the responses of professional forecasters to permanent shocks are greater than to transitory shocks when revising their predictions, say, of inflation. In the same way that this research inspired us, we hope this paper stimulates further research into the ways in which professional forecasters and other economic agents process information to form beliefs and predictions about future economic outcomes and events.

References

Andrieu, C., A. Doucet, R. Holenstein (2010). Particle Markov chain Monte Carlo methods. *Journal of the Royal Statistical Society, Series B* 72, 269–342.

Ang, A., G. Bekaert, M. Wei (2007). Do macro variables, asset markets, or surveys forecast inflation better? *Journal of Monetary Economics* 54, 1163–1212.

Bernanke, B.S. (2007). Inflation Expectations and Inflation Forecasting. Remarks given at the Monetary Economics Workshop of the National Bureau of Economic Research Summer Institute, Cambridge, Massachusetts (July 10). Available at `http://www.federalreserve.gov/newsevents/speech/Bernanke20070710a.htm`.

Beveridge, S., C.R. Nelson. (1981). A New Approach to Decomposition of Economic Time Series into Permanent and Transitory Components with Particular Attention to Measurement of the Business Cycle. *Journal of Monetary Economics* 7, 151–174.

Carvalho, C.M., M.S. Johannes, H.F. Lopes, and N.G. Polson (2010). Particle learning and smoothing. *Statistical Science* 25, 88–106.

Chen, R., J.S. Liu (2000). Mixture Kalman filters. *Journal of the Royal Statistical Society, Series B* 62, 493–508.

Cogley, T., G. Primiceri, T.J. Sargent (2010). Inflation-gap persistence in the US. *American Economic Journal: Macroeconomics* 2, 43–69.

Cogley, T., T.J. Sargent (2015). Measuring price-pevel uncertainty and instability in the U.S., 1850–2012. *Review of Economics and Statistics* 97, 827–838.

Cogley, T., T.J. Sargent (2008). Anticipated utility and rational expectations as approximations of Bayesian decision making. *International Economic Review* 49, 185–221.

Cogley, T., A. Sbordone (2008). Trend inflation, indexation, and inflation persistence in the new Keynesian Phillips curve inflation-gap persistence in the US. *American Economic Review* 98, 2101–2126.

Coibion, O., Y. Gorodnichenko (2015). Information rigidity and the expectations formation process: A simple framework and new facts. *American Economic Review* 105, 2644–2678.

Coibion, O., Y. Gorodnichenko (2012) What can survey forecasts tell us about informational rigidities? *Journal of Political Economy* 120, 116–159.

Creal, D. (2012). A survey of sequential Monte Carlo methods for economics and finance. *Econometric Reviews* 31, 245–296.

Durbin, J., S.J. Koopman 2002. A simple and efficient simulation smoother for state space time series analysis. *Biometrika* 89, 603–615.

Faust, J., J.H. Wright (2013). Forecasting inflation. In Elliot, G., A. Timmermann (eds.), HANDBOOK OF ECONOMIC FORECASTING, VOL. 2, pp. 2–56. New York, NY: Elsevier.

Godsill, S.J., A. Doucet, M. West (2004). Monte Carlo smoothing for nonlinear time series. *Journal of the American Statistical Association* 99, 156–168.

Goodfriend, M., R.G. King (2005). The incredible Volcker disinflation. *Journal of Monetary Economics* 52, 981–1015.

Grassi, S., T. Proietti (2010). Has the volatility of U.S. inflation changed and how? *Journal of Time Series Econometrics* 2:1, article 6.

Herbst, E., F. Schorfheide (2016). BAYESIAN INFERENCE FOR DSGE MODELS. Princeton, NJ: Princeton University Press.

Hol, J.D., T.B. Schön, F. Gustafsson (2006). On resampling algorithms for particle filters. In 2006 IEEE NONLINEAR STATISTICAL SIGNAL PROCESSING WORKSHOP, Ng, W. (ed.), 79–82. Red Hook, NY: Curran Associates, Inc.

Jain, M. (2013). Perceived inflation persistence. Working Paper 2013–43, Bank of Canada.

Kozicki, S., P.A. Tinsley (2012). Effective use of survey information in estimating the evolution of expected inflation. *Journal of Money, Credit and Banking* 44, 145–169.

Krane, S.D. (2011). Professional forecasters' views of permanent and transitory shocks to GDP. *American Economic Journal: Macroeconomics* 3, 184–211

Kreps, D.M. (1998). Anticipated utility and dynamic choice. In FRONTIERS OF RESEARCH IN ECONOMIC THEORY: THE NANCY L. SCHWARTZ MEMORIAL LECTURES, 1983-1997, Jacobs, D. P., E. Kalai, M. I. Kamien (eds.), 242–274. Cambridge, MA: Cambridge University Press.

Leeper, E.M., T. Zha (2003). Modest policy interventions. *Journal of Monetary Economics* 50, 1673–1700.

Lindsten, F., P. Bunch, S. Särkkä, T.B. Schön, S.J. Godsill (2016). Rao-Blackwellized particle smoothers for conditionally linear Gaussian models. *IEEE Journal of Selected Topics in Signal Processing* 10, 353–365.

Lopes, H.F., R.S. Tsay (2011). Particle filters and Bayesian inference in financial econometrics. *Journal of Forecasting* 30, 168–209.

Mankiw, N.G., R. Reis (2002). Sticky information versus sticky prices: A proposal to replace the New Keynesian Phillips curve. *Quarterly Journal of Economics* 117, 1295–1328.

Meltzer, A.H. (2014). A History of the Federal Reserve: Volume 2, Book II, 1970–1986. Chicago, IL: The University of Chicago Press.

Mertens, E. (2016). Measuring the level and uncertainty of trend inflation. *The Review of Economics and Statistics* 98, 950–967.

Meyer, L. (1996). Monetary policy objectives and strategy. Remarks given at the National Association of Business Economists 38th Annual Meeting, Boston, MA (September 8). Available at `http://www.federalreserve.gov/boarddocs/speeches/1996/19960908.htm`.

Muth, J.F. (1960). Optimal properties of exponentially weighted forecasts. *Journal of the American Statistical Association* 55, 299–306.

Nason, J.M., G.W. Smith (2016a). Sticky professional forecasts and the unobserved components model of US inflation. Manuscript, Department of Economics, Queen's University.

Nason, J.M., G.W. Smith (2016b). Measuring the slowly evolving trend in US inflation with professional forecasts. Manuscript, Department of Economics, Queen's University.

Nelson, C.R. (2008). The Beveridge-Nelson decomposition in retrospect and prospect. *Journal of Econometrics* 146, 202–206.

Orphanides, A., D. Wilcox (2002). The opportunistic approach to disinflation. *International Finance* 5, 47–71.

Pitt M.K., N. Shephard, N. (2001). Auxiliary variable based particle filters. In Doucet, A., de Freitas, N., Gordon, N. (eds.) Sequential Monte Carlo Methods in Practice, New York: Springer-Verlag.

Pitt, M. K., N. Shephard (1999). Filtering via simulation: auxiliary particle filters. *Journal of the American Statistical Association* 94, 590–599.

Shephard, N. (2013). Martingale unobserved component models. Economics Series Working Papers 644, Department of Economics, University of Oxford.

Sims, C.A. (2003). Implications of rational inattention. *Journal of Monetary Economics* 50, 665–690.

Stock, J.H., M.W. Watson (2007). Why has US inflation become harder to forecast? *Journal of Money, Credit and Banking* 39(S1), 3–33.

Stock, J.H., M.W. Watson (2010). Modeling inflation after the crisis. In Macroeconomic Challenges: The Decade Ahead, Kansas City, MO: Federal Reserve Bank of Kansas City.

Storvik, G. (2002). Particle filters for state-space models with the presence of unknown static parameters. *IEEE Transactions on Signal Processing* 50, 281–289.

A1 Introduction

This appendix contains four sections. Section A2 builds state space models (SSMs) for the joint data generating process (DGP) of the sticky information (SI) prediction mechanism conditional on different Stock and Watson-unobserved components (SW-UC) models with stochastic volatility (SV). A joint DGP conditional on a SW-UC-SV model with static persistence in gap inflation is developed in section A2.1. Section A2.2 reviews the SSM of the SI-prediction mechanism and SW-UC-SV-TVP-AR(1) model, which is discussed in section 2.3 of the paper. Additional information about the Rao-Blackwellized auxiliary particle filter (RB-APF) of section (3.3) used to estimate the linear and nonlinear state variables of the joint DGP of the SI-prediction mechanism and the SW-UC-SV-TVP-AR(1) model is found in section A3. Estimates of the SSMs left out of the paper appear in section A4. Section A4.1 contains estimates of the SSM that consists of the SI-prediction mechanism and a SW-UC-SV model with no persistence in gap inflation, $\theta_t = 0$. When a static SI parameter, $\lambda_t = \lambda$ is part of the joint DGP, along with the SW-UC-SV-TVP-AR(1) model, the estimates are found in section A4.2.

A2 SSMs of the Joint DGP

The SSMs have several features in common. The features are h-step ahead rational expectations (RE) and SI forecasts, $\mathbf{E}_t\pi_{t+h}$ and $F_t\pi_{t+h}$, are integrated out of the state of the SSMs. Instead, the state vector consists in part of RE and SI inflation trends and gaps, τ_t, ε_t, $F_t\tau_t$, and $F_t\varepsilon_t$. The RE (SI) state variables drive $\mathbf{E}_t\pi_{t+h}$ $(F_t\pi_{t+h})$. Along with these state variables, the SSMs are constructed using the laws of motion of τ_t and ε_t defined by a SW-UC-SV model, and a conjecture for the laws of motion of $F_t\tau_t$ and $F_t\varepsilon_t$ that reflect the SI law of motion, which is equation (3.2) of the paper. Another implication of the SSM

is the RE and SI state variables, $\tau_t \;\; \varepsilon_t, \;\; F_t\tau_t$, and $F_t\varepsilon_t$, are linear conditional on nonlinear state variables. The nonlinear state variables are the SVs of trend and gap inflation, $\varsigma_{\eta,t}$ and $\varsigma_{\upsilon,t}$, drifting inflation gap persistence, θ_t, and the SI-TVP parameter, λ_t, where $\mathcal{V}_t = [\ln\varsigma^2_{\eta,t} \;\; \ln\varsigma^2_{\upsilon,t} \;\; \theta_t \;\; \lambda_t]'$. We gather the conditionally linear state variables together in $\mathcal{X}_t = [\tau_t \;\; \varepsilon_t]'$, $F_t\mathcal{X}_t = [F_t\tau_t \;\; F_t\varepsilon_t]'$, and $\mathcal{S}_t = [\mathcal{X}_t' \;\; F_t\mathcal{X}_t']'$. The SSM is completed by connecting the observables of realized inflation, π_t, and the average SPF participant's h-step ahead inflation predictions, $\pi^{SPF}_{t,t+h}$ to $\mathcal{S}_t$ plus the associated measurement errors, $\zeta_{\pi,t}$ and $\zeta_{h,t}$, $h = 1, \ldots, \mathcal{H}$. Hence, $\mathbf{E}_t\pi_{t+h}$ and $F_t\pi_{t+h}$ are replaced by the conditionally linear $\mathcal{S}_t$ in the observation equations of $\pi^{SPF}_{t,t+h}$ because these forecasts are linear functions of $\mathcal{X}_t$ and $F_t\mathcal{X}_t$.

A2.1 A SSM of π_t and $\pi^{SPF}_{t,t+h}$ when Persistence in ε_{t+1} Is Fixed

This section constructs a SSM for the joint DGP of the SI-prediction mechanism and a SW-UC-SV model with $\theta_t = \theta$. Our motivation is to study the joint DGP without the complication of specifying a TVP-AR(1) for gap inflation. The restriction is gap inflation evolves as a fixed coefficient AR(1) with SV, where $\varepsilon_{t+1} = \theta\varepsilon_t + \varsigma_{\upsilon,t+1}\upsilon_t$ and $\theta \in (-1, 1)$. In this case, the joint DGP maps into a SSM in which alone λ_t alters the transition dynamics of $F_t\mathcal{X}_t$.

The SSM of the joint DGP is built on RE and SI term structures of inflation. The SW-UC-SV model with fixed inflation gap persistence yields a SSM, which is the source of $\mathbf{E}_t\pi_{t+h}$. We compute $\mathbf{E}_t\pi_{t+h}$ using the observation and state equations of this SSM, which are equation (5.1)

$$\pi_t \;=\; \delta_{\mathcal{X}}\mathcal{X}_t \;+\; \sigma_{\zeta,\pi}\zeta_{\pi,t}, \tag{A2.1}$$

and equation (5.2) modified for fixed inflation gap persistence

$$\mathcal{X}_{t+1} \;=\; \boldsymbol{\Theta}\mathcal{X}_t \;+\; \boldsymbol{\Upsilon}_{t+1}\mathcal{W}_t, \tag{A2.2}$$

of the paper, where $\delta_{\mathcal{X}} = [1 \quad 1]$, $\mathbf{\Theta} = \begin{bmatrix} 1 & 0 \\ 0 & \theta \end{bmatrix}$, $\mathbf{\Upsilon}_{t+1} = \begin{bmatrix} \varsigma_{\eta,t+1} & 0 \\ 0 & \varsigma_{\upsilon,t+1} \end{bmatrix}$, and $\mathcal{W}_t = [\eta_t \;\; \upsilon_t]'$. The RE forecast of π_{t+h}, which is equation (6) of the paper (implied hereafter) is reproduced here

$$\mathbf{E}_t \pi_{t+h} = \delta_{\mathcal{X}} \mathbf{\Theta}^h \mathcal{X}_t, \quad h = 1, \ldots, \mathcal{H}, \tag{A2.3}$$

Equation (A2.3) is calculated by iterating the observation equation (A2.1) and state equations A2.2 forward h periods, substituting for $\mathcal{X}_{t+h}$ in the former equation using the latter, and applying the law of iterated expectations (LIE).

The SI term structure of inflation forecasts has a similar specification

$$F_t \pi_{t+h} = \delta_{\mathcal{X}} \mathbf{\Theta}^h F_t \mathcal{X}_t, \tag{A2.4}$$

which is equation (7). This specification is built on the SI-EWMA smoother (4), the RE term structure of inflation forecasts (A2.3), and the EWMA smoother of $F_t \mathcal{X}_t$. Construction of the latter begins by substituting $\delta_{\mathcal{X}} \mathbf{\Theta}^h \mathcal{X}_t$ for $\mathbf{E}_t \pi_{t+h}$ in the SI-EWMA smoother (4) to find

$$F_t \pi_{t+h} = \delta_{\mathcal{X}} \mathbf{\Theta}^h \sum_{j=0}^{\infty} \mu_{\lambda,t-j} \mathbf{\Theta}^j \left(\prod_{\ell=0}^{j} \lambda_{t-\ell} \right) \mathcal{X}_{t-j}. \tag{A2.5}$$

Next, a law of motion for the SI state vector, $F_{t+1}\mathcal{X}_{t+1}$, is needed to connect it to the RE state vector, $\mathcal{X}_t$. Remember the state variables $\mathcal{X}_t$ and $F_t \mathcal{X}_t$ contain all the information needed to construct the RE and SI term structures of inflation forecasts, which are equations (A2.3) and (A2.4). This information is useful for building a law of motion for the SI state variable. Since the SI law of motion (3.2) relates $F_t \pi_{t+h}$ to its own lag and $\mathbf{E}_t \pi_{t+h}$ weighted by λ_t and $(1 - \lambda_t)$, a law of motion for $F_t \mathcal{X}_{t+h}$ is found by swapping it, $F_{t-1}\mathcal{X}_{t+h}$, and $\mathbf{E}_t \mathcal{X}_{t+h}$ for $F_t \pi_{t+h}$, $F_{t-1}\pi_{t+h}$, and $\mathbf{E}_t \pi_{t+h}$ in the SI law of motion (3.2). The result is the law of motion

$$F_t\mathcal{X}_{t+h} \;=\; \lambda_t F_{t-1}\mathcal{X}_{t+h} \;+\; (1-\lambda_t)\mathbf{E}_t\mathcal{X}_{t+h}. \tag{A2.6}$$

Backward iteration of the SI law of motion (A2.6) yields the EWMA smoother of $F_t\mathcal{X}_{t+h}$

$$F_t\mathcal{X}_{t+h} \;=\; \sum_{j=0}^{\infty}\mu_{\lambda,t-j}\left(\prod_{\ell=0}^{j}\lambda_{t-\ell}\right)\boldsymbol{\Theta}^{h+j}\mathcal{X}_{t-j}, \tag{A2.7}$$

where $\mathbf{E}_{t-j}\mathcal{X}_{t+h} = \boldsymbol{\Theta}^{h+j}\mathcal{X}_{t-j}$. When $h = 0$,

$$F_t\mathcal{X}_{t} \;=\; \sum_{j=0}^{\infty}\mu_{\lambda,t-j}\left(\prod_{\ell=0}^{j}\lambda_{t-\ell}\right)\boldsymbol{\Theta}^{j}\mathcal{X}_{t-j}, \tag{A2.8}$$

which establishes the link between $F_t\pi_{t+h}$ and $F_t\mathcal{X}_t$ in the SI inflation term structure (A2.4).

We employ the state equations (A2.2) of $\mathcal{X}_{t+1}$ and the SI-EWMA smoother (A2.8) to build state equations for $F_{t+1}\mathcal{X}_{t+1}$. By pulling $\mathcal{X}_t$ out of the infinite sum of the SI-state equation EWMA smoother (A2.8), the result is

$$F_t\mathcal{X}_{t} \;=\; (1-\lambda_t)\mathcal{X}_t \;+\; \sum_{j=1}^{\infty}\mu_{\lambda,t-j}\left(\prod_{\ell=0}^{j}\lambda_{t-\ell}\right)\boldsymbol{\Theta}^{j}\mathcal{X}_{t-j}. \tag{A2.9}$$

The infinite sum of equation (A2.9) implies $F_{t-1}\mathcal{X}_{t-1} = \sum_{i=0}^{\infty}\mu_{\lambda,t-i-1}\left(\prod_{\ell=0}^{i}\lambda_{t-\ell}\right)\boldsymbol{\Theta}^{i+1}\mathcal{X}_{t-i-1}$ after a change of index, $j = i+1$. Substitute for the infinite sum in equation (A2.9) with $F_{t-1}\mathcal{X}_{t-1}$ to produce

$$F_t\mathcal{X}_{t} \;=\; (1-\lambda_t)\mathcal{X}_t \;+\; \lambda_t\boldsymbol{\Theta}F_{t-1}\mathcal{X}_{t-1}. \tag{A2.10}$$

The goal of finding the law of motion is almost complete. Subsequent to leading the law of motion (A2.10) forward one period and substituting for $\mathcal{X}_{t+1}$ using the state equations (A2.2), we have the SI state equations

$$F_{t+1}\mathcal{X}_{t+1} \;=\; \lambda_{t+1}\boldsymbol{\Theta}F_t\mathcal{X}_t \;+\; (1-\lambda_{t+1})\boldsymbol{\Theta}\mathcal{X}_t \;+\; (1-\lambda_{t+1})\boldsymbol{\Upsilon}_{t+1}\mathcal{W}_t, \tag{A2.11}$$

of the joint DGP of the SI prediction mechanism and the SW-UC-SV model with fixed inflation gap persistence. The state equations (A2.2) of $\mathcal{X}_{t+1}$ are stacked on top of the

state equations (A2.11) of $F_{t+1}\mathcal{X}_{t+1}$ to form

$$\mathcal{S}_{t+1} \;=\; \boldsymbol{\mathcal{A}}_{\boldsymbol{\Theta},t+1}\mathcal{S}_t \;+\; \boldsymbol{\mathcal{B}}_{t+1}\mathcal{W}_t, \tag{A2.12}$$

where $\boldsymbol{\mathcal{A}}_{\boldsymbol{\Theta},t+1} = \begin{bmatrix} \boldsymbol{\Theta} & \mathbf{0}_{2\times 2} \\ \big(1-\lambda_{t+1}\big)\boldsymbol{\Theta} & \lambda_{t+1}\boldsymbol{\Theta} \end{bmatrix}$, and $\boldsymbol{\mathcal{B}}_{t+1} = \begin{bmatrix} \boldsymbol{\Upsilon}_{t+1} \\ \big(1-\lambda_{t+1}\big)\boldsymbol{\Upsilon}_{t+1} \end{bmatrix}$. Thus, the system of state equations (A2.12) of the joint DGP reveal shocks to λ_{t+1} alone shift the transition dynamics of $F_{t+1}\mathcal{X}_{t+1}$ and its impulse dynamics react to λ_{t+1} and SVs.

The SSM of the joint DGP of the SI prediction mechanism and the SW-UC-SV model with fixed inflation gap persistence is finished by using equations (A2.1) and (3.1) to construct the system of observation equations

$$\mathcal{Y}_t \;=\; \boldsymbol{\mathcal{C}}_{\boldsymbol{\Theta}}\mathcal{S}_t \;+\; \boldsymbol{\mathcal{D}}\mathcal{U}_t, \tag{A2.13}$$

where $\mathcal{Y}_t = \begin{bmatrix} \pi_t \\ \pi^{SPF}_{1,t} \\ \vdots \\ \pi^{SPF}_{\mathcal{H},t} \end{bmatrix}$, $\boldsymbol{\mathcal{C}}_{\boldsymbol{\Theta}} = \begin{bmatrix} \delta_{\mathcal{X}} & \mathbf{0}_{1\times 2} \\ \mathbf{0}_{1\times 2} & \delta_{\mathcal{X}}\boldsymbol{\Theta} \\ \vdots & \vdots \\ \mathbf{0}_{1\times 2} & \delta_{\mathcal{X}}\boldsymbol{\Theta}^{\mathcal{H}} \end{bmatrix}$, $\boldsymbol{\mathcal{D}} = \begin{bmatrix} \sigma_{\zeta,\pi} & 0 & \dots & 0 \\ 0 & \sigma_{\zeta,1} & \dots & 0 \\ 0 & 0 & \ddots & 0 \\ 0 & 0 & \dots & \sigma_{\zeta,\mathcal{H}} \end{bmatrix}$, $\mathcal{U}_t = \begin{bmatrix} \zeta_{\pi,t} & \zeta_{1,t} & \dots & \zeta_{\mathcal{H},t} \end{bmatrix}'$, and $\boldsymbol{\Omega}_{\mathcal{U}} = \boldsymbol{\mathcal{D}}\boldsymbol{\mathcal{D}}'$. The SPF term structure of inflation predictions are the second through $\mathcal{H}+1$ rows of the observation equations (A2.13). These observation equations show $F_t\pi_{t+h}$ is integrated out of the SSM and that the factor loadings on $\mathcal{S}_t$ are time invariant.

A2.2 The Joint DGP with Drifting Persistence in Gap Inflation

The SSM of the SI-prediction mechanism and SW-UC-SV-TVP-AR(1) model is more difficult to construct compared with the SSM of the previous section. The difficulty stems from drifting persistence in gap inflation, which creates a nonlinearity in the transition dynamics of the state equations (5.2) of the SW-UC-SV-TVP-AR(1) model. This nonlin-

earity rule outs using the LIE to compute $\mathbf{E}_t \pi_{t+h}$. Instead, the anticipated utility model (AUM) is employed to solve the problem. Under the AUM assumptions stated in the paper, the average member of the SPF holds $\mathbf{\Theta}_{t+h}$ fixed at its date t realization when constructing h-step ahead inflation forecasts. For example, combine the AUM and procedures similar to ones used to construct the RE term structure of inflation (A2.3) under fixed inflation gap persistence generates the forecasts

$$\mathbf{E}_t \pi_{t+h} = \delta_{\mathcal{X}} \mathbf{\Theta}_{t|t}^{h} \mathcal{X}_t, \tag{A2.14}$$

where $\mathbf{\Theta}_t = \begin{bmatrix} 1 & 0 \\ 0 & \theta_t \end{bmatrix}$. The subscript on $\mathbf{\Theta}_{t|t}$ is held fixed in the RE term structure of inflation (A2.14) to reflect information available to evaluate the SW-UC-SV-TVP-AR(1) model at date t.

The SI term structure of inflation forecasts also has to be calculated to build the SSM of the joint DGP. Similar to the previous section, the process of computing these forecasts starts with the law of motion (A2.6) of $F_t \mathcal{X}_{t+h}$, $(1 - \lambda_t)\mathbf{E}_t \mathcal{X}_{t+h} + \lambda_t F_{t-1} \mathcal{X}_{t+h}$, and its EWMA smoother (A2.7), $\sum_{j=0}^{\infty} \mu_{\lambda,t-j} \left(\prod_{\ell=0}^{j} \lambda_{t-\ell} \right) \mathbf{E}_{t-j} \mathcal{X}_{t+h}$. Although this law of motion and smoother are unchanged from the case of $\theta_t = \theta$, drift in inflation gap persistence matters for constructing the map from $\mathbf{E}_{t-j} \mathcal{X}_{t+h}$ to $F_t \mathcal{X}_t$. Similar to the implication of AUM, which holds drifting inflation gap persistence fixed at $\theta_{t|t}$ to generate the h-step ahead RE inflation forecast (A2.14), we assume θ_t is fixed conditional on the information available to $F_t \mathcal{X}_{t+h}$. Thus, iterating the law of motion (A2.6) of $F_t \mathcal{X}_{t+h}$ backwards gives

$$F_t \mathcal{X}_{t+h} = \sum_{j=0}^{\infty} \mu_{\lambda,t-j} \left(\prod_{\ell=0}^{j} \lambda_{t-\ell} \right) \mathbf{\Theta}_{t|t}^{h+j} \mathcal{X}_{t-j}, \tag{A2.15}$$

which is implied by the RE term structure of inflation forecasts (A2.14), $\mathbf{E}_{t-j} \pi_{t+h} =$

$\boldsymbol{\Theta}_{t|t}^{h+j}\mathcal{X}_{t-j}$. Next, set $h = 0$ in the EWMA (A2.15) of $F_t\mathcal{X}_{t+h}$ to obtain

$$F_t\mathcal{X}_t = \sum_{j=0}^{\infty} \mu_{\lambda,t-j} \left(\prod_{\ell=0}^{j} \lambda_{t-\ell} \right) \boldsymbol{\Theta}_{t|t}^{j} \mathcal{X}_{t-j}. \tag{A2.16}$$

Apply the EWMA (A2.16) of $F_t\mathcal{X}_t$ to link the SI-EWMA smoother (4) to the h-step ahead RE inflation forecast (A2.14) yields

$$F_t\pi_{t+h} = \delta_{\mathcal{X}} \sum_{j=0}^{\infty} \mu_{\lambda,t-j} \left(\prod_{\ell=0}^{j} \lambda_{t-\ell} \right) \boldsymbol{\Theta}_{t|t}^{h+j} \mathcal{X}_{t-j}. \tag{A2.17}$$

The SI term structure of inflation forecasts

$$F_t\pi_{t+h} = \delta_{\mathcal{X}} \boldsymbol{\Theta}_{t|t}^{h} F_t\mathcal{X}_t, \tag{A2.18}$$

is an implication of the SI-EWMA smoothers (A2.16) of $F_t\pi_{t+h}$ and (A2.16) of $F_t\mathcal{X}_t$.

The SI-EWMA smoother (A2.16) of $F_t\mathcal{X}_t$ also contributes to the state equations of $F_{t+1}\mathcal{X}_{t+1}$. Unwinding the infinite sum of (A2.16) gives the recursion

$$F_t\mathcal{X}_t = (1 - \lambda_t)\mathcal{X}_t + \lambda_t \boldsymbol{\Theta}_{t|t} F_{t-1}\mathcal{X}_{t-1}. \tag{A2.19}$$

Lead the law of motion (A2.19) of $F_t\mathcal{X}_t$ by one period and substitute for $\mathcal{X}_{t+1}$ using the state equations (5.2) to produce

$$F_{t+1}\mathcal{X}_{t+1} = (1 - \lambda_{t+1})\boldsymbol{\Theta}_{t+1}\mathcal{X}_t + \lambda_{t+1}\boldsymbol{\Theta}_{t+1}F_t\mathcal{X}_t + (1 - \lambda_{t+1})\boldsymbol{\Upsilon}_{t+1}\mathcal{W}_t, \tag{A2.20}$$

where we drop the conditioning time subscript on $\boldsymbol{\Theta}_{t+1}$. Equations (A2.20) duplicate the bottom two rows of the state equations (8.1). The timing of the conditionally linear and nonlinear state variables on the right hand side of the state equations (A2.20) appear nonstandard. However, the timing conventions of these state equations are consistent with the specification of the hierarchical conditional linear Gaussian (CLG) model studied by Lindsten, Bunch, Särkkä, Schön, and Godsill (2016). They develop a

particle smoother for the CLG model that we employ to generate smoothed estimates of the linear and nonlinear state variables of the SSMs of this and the previous section. Thus, our use of the Lindsten et al particle smoother is supported by the AUM assumptions and the assumption that θ_{t+1} is held fixed at its current realization when iterating backwards to construct SI-EWMA smoothers.

A3 Econometric Methods

We estimate the SSM (8.1) and (8.2) using Bayesian sequential Monte Carlo (SMC) methods. The methods combine Rao-Blackwellization (RB) of the SSM with the auxiliary particle filter (APF) of Pitt and Shephard (1999, 2001) to estimate the linear and nonlinear state variables. Our RB-APF algorithm is adapted from a version outlined by Creal (2012) and algorithm 2 Lopes and Tsay (2011, p. 173). Estimates of the static scale volatility coefficients are produced with the particle learning estimator (PLE) of Storvik (2002); also see Carvalho, Johannes, Lopes, and Polson (2010). The next section gives details about running the RB-APF that is sketched in section 3.3 of our paper.

A3.1 The RB-APF Algorithm

The RB-APF of section (3.3) produces M filtered estimates of the linear states, $\mathcal{S}_t$, its mean square error (MSE), $\boldsymbol{\Sigma}_t$, and the nonlinear states, $\mathcal{V}_{t+1}$. The Kalman filter (KF) is the source of estimates of $\mathcal{S}_t$ and $\boldsymbol{\Sigma}_t$ particle by particle while M synthetic samples of $\mathcal{V}_{t+1}$ are generated by simulating the multivariate random walk (9). The predictive step of the KF yields M estimates of the likelihood that are the source of the weights used to resample the M particles of $\mathcal{S}_t$, $\boldsymbol{\Sigma}_t$, and $\mathcal{V}_{t+1}$. Conditioning on the resampled $\mathcal{S}_t$, $\boldsymbol{\Sigma}_t$, and $\mathcal{V}_{t+1}$, running the KF produces updates of the linear states.

We carry out the RB-APF algorithm in the following steps.

1. Initialize the filter with $i = 1, \ldots, M$ particle draws of $\mathcal{V}_0^{(i)}$ sampled from the priors

$$\begin{aligned}
\ln \varsigma_{\eta,0}^{2\,(i)} &\sim \ln \mathcal{N}\left(\ln\left(\overline{\varsigma}_{\eta,0}^2\right) - \frac{\sigma_{\varsigma_\eta,0}^2}{2},\, \sigma_{\varsigma_\eta,0}^2\right), \\
\ln \varsigma_{\upsilon,0}^{2\,(i)} &\sim \ln \mathcal{N}\left(\ln\left(\overline{\varsigma}_{\upsilon,0}^2\right) - \frac{\sigma_{\varsigma_\upsilon,0}^2}{2},\, \sigma_{\varsigma_\upsilon,0}^2\right), \\
\theta_0^{(i)} &\sim \mathcal{TN}\left(\overline{\theta}_0,\, \sigma_{\phi,0}^2,\, -1.0,\, 1.0\right),
\end{aligned}$$

   and

$$\lambda_0^{(i)} \sim \mathcal{TN}\left(\overline{\lambda}_0,\, \sigma_{\kappa,0}^2,\, 0.0,\, 1.0\right),$$

   where $\mathcal{TN}$ denotes the truncated normal distribution, the prior means $\overline{\varsigma}_{\eta,0}^2 = 0.2$, $\overline{\varsigma}_{\upsilon,0}^2 = 0.4$, $\overline{\theta}_0 = 0$, $\overline{\lambda}_0 = 0.5$ and prior variances $\sigma_{\varsigma_\eta,0}^2 = \sigma_{\varsigma_\upsilon,0}^2 = 10.0$ and $\sigma_{\phi,0}^2 = \sigma_{\kappa,0}^2 = 1.0$ are listed in table 2 and conditional on $\mathcal{V}_0^{(i)}$ draw $\mathcal{S}_0 \sim \mathcal{N}\left(\mathcal{S}_{0|0}^{(i)}, \boldsymbol{\Sigma}_{0|0}^{(i)}\right)$.

2. Next, the multivariate random walk (12), priors on θ_0 and λ_0, and priors on the scale volatility coefficients are employed to draw proposals of $\mathcal{V}_1^{(i)}$ from $\mathcal{V}_0^{(i)}$ using $\ln \varsigma_{\eta,1}^{2\,(i)} = \ln \varsigma_{\eta,0}^{2\,(i)} + \sigma_{\eta,1}^{(i)} \eta_1^{(i)}$, $\ln \varsigma_{\upsilon,1}^{2\,(i)} = \ln \varsigma_{\upsilon,0}^{2\,(i)} + \sigma_{\upsilon,1}^{(i)} \upsilon_1^{(i)}$, $\theta_1^{(i)} \sim \mathcal{TN}\left(\theta_0^{(i)}, \sigma_{\phi,1}^{(i)}, -1.0, 1.0\right)$, and $\lambda_1^{(i)} \sim \mathcal{TN}\left(\lambda_0^{(i)}, \sigma_{\kappa,1}^{(i)}, 0.0, 1.0\right)$, where $\eta_1^{(i)}$ and $\upsilon_1^{(i)}$ represent draws from standard normal distributions, $\sigma_{\ell,1}^{(i)} = \sqrt{\frac{\beta_\ell}{\sum_{k=1}^{t_\nu} Z'_{M,k} Z_{M,k}}}$, $\ell = \eta,\ \upsilon,\ \phi$, and κ, $t_\nu = \alpha_\ell$ is a degrees of freedom correction, α_ℓ and β_ℓ are scale and shape parameters of the inverse gamma ($\mathcal{IG}$) priors displayed in table 1, $Z_{M \times t_\nu} \sim \mathcal{N}(\mathbf{0}, \mathbf{I})$, and $i = 1, \ldots, M$.

3. Repeat the following steps for $t = 2, \ldots, T$, where each step uses the particles $\mathcal{V}_t^{(i)}$, $\mathcal{S}_{t-1|t-1}^{(i)}$, and $\boldsymbol{\Sigma}_{t-1|t-1}^{(i)}$, which are the outcomes of applying the KF, resampling, and transition equations implied by the priors on the scale volatility coefficients.

(a) For $i = 1, 2, \ldots, M$, draw new particles $\mathcal{V}_t^{(i)}$ conditional on resampled $\mathcal{V}_{t-1}^{(i)}$ and its law of motion (12) by updating step 2 with $\sigma_{\ell,t}^{(i)} = \sqrt{\frac{\beta_{\ell,t}^{(i)}}{\sum_{k=1}^{t_\nu} Z'_{M,k} Z_{M,k}}}$ and $\beta_{\ell,t}^{(i)} = \beta_{\ell,t-1}^{(i)} + \left(\Delta_{\ell,t}^{(i)}\right)^2$, where $\Delta_{\eta,t}^{(i)} = \sigma_{\eta,t}^{(i)} \eta_t^{(i)}$, $\Delta_{\eta,t}^{(i)} = \sigma_{\upsilon,t}^{(i)} \upsilon_t^{(i)}$, $\Delta_{\phi,t}^{(i)} = d\mathcal{IN}_{\phi,t}^{(i)}$, and $\Delta_{\kappa,t}^{(i)} = d\mathcal{IN}_{\kappa,t}^{(i)}$, the increments $d\mathcal{IN}_{\phi,t}^{(i)}$ and $d\mathcal{IN}_{\kappa,t}^{(i)}$ are associated with updating $\theta_{t-1}^{(i)}$ and $\lambda_{t-1}^{(i)}$ in step 2, $\beta_{\ell,t-1}^{(i)}$ and $\Delta_{\ell,t}^{(i)}$ have been resampled, and $t_\nu = t - 1 + \alpha_\ell$ (for $t \geq 2$).

(b) At date t, engage the KF predictive step to compute

$$
\begin{aligned}
\mathcal{S}_{t|t-1}^{(i)} &= \mathcal{A}_t^{(i)} \mathcal{S}_{t-1|t-1}^{(i)}, \\
\boldsymbol{\Sigma}_{t|t-1}^{(i)} &= \mathcal{A}_t^{(i)} \boldsymbol{\Sigma}_{t-1|t-1}^{(i)} \left(\mathcal{A}_t^{(i)}\right)' + \mathcal{B}_t^{(i)} \left(\mathcal{B}_t^{(i)}\right)', \\
\boldsymbol{\Omega}_{t|t-1}^{(i)} &= \mathcal{C}_t^{(i)} \boldsymbol{\Sigma}_{t|t-1}^{(i)} \left(\mathcal{C}_t^{(i)}\right)' + \boldsymbol{\Omega}_{\mathcal{U}}^{(i)}, \\
\tilde{\mathcal{Y}}_t^{(i)} &= \mathcal{Y}_t - \mathcal{C}_t^{(i)} \mathcal{S}_{t|t-1}^{(i)}, \\
\ell_t^{(i)} &= -\frac{1}{2}\left[\ln\left|\boldsymbol{\Omega}_{t|t-1}^{(i)}\right| + \left(\tilde{\mathcal{Y}}_t^{(i)}\right)' \left(\boldsymbol{\Omega}_{t|t-1}^{(i)}\right)^{-1} \tilde{\mathcal{Y}}_t^{(i)}\right],
\end{aligned}
$$

across the M particles, $i = 1, 2, \ldots, M$.[A.1]

(c) Compute particle weights $\widehat{\omega}_t^{(i)} = \frac{\exp\left\{\ell_t^{(i)}\right\}}{\sum_{i=1}^{M} \exp\left\{\ell_t^{(i)}\right\}}$.

(d) Shuffle the index i=1, …, M by drawing from a multinominal distribution using the *pdf* of $\widehat{\omega}_t^{(i)}$, which is stratified resampling of the particles $\mathcal{V}_t^{(i)}$, $\beta_{\ell,t}^{(i)}$, $\Delta_{\ell,t}^{(i)}$, $\mathcal{S}_{t-1|t-1}^{(i)}$, and $\boldsymbol{\Sigma}_{t-1|t-1}^{(i)}$, where $\ell = \eta, \upsilon, \phi$, and κ; see Hol, Schön, and Gustafsson (2006) for details. Also, resample from the ensemble $\left\{\widehat{\omega}_t^{(i)}\right\}_{i=1}^{N}$ to create $\left\{\widetilde{\omega}_t^{(i)}\right\}_{i=1}^{N}$.

[A.1] There are missing observations in the SPF inflation data that the KF handles using standard methods.

(e) Given resampled particles $\left\{\mathcal{V}_t^{(i)},\ \beta_{\ell,t}^{(i)},\ \Delta_{\ell,t}^{(i)},\ \mathcal{S}_{t-1|t-1}^{(i)},\ \boldsymbol{\Sigma}_{t-1|t-1}^{(i)}\right\}_{i=1}^{M}$, run the KF

$$
\begin{aligned}
\mathcal{S}_{t|t-1}^{(i)} &= \boldsymbol{\mathcal{A}}_t^{(i)}\mathcal{S}_{t-1|t-1}^{(i)},\\
\boldsymbol{\Sigma}_{t|t-1}^{(i)} &= \boldsymbol{\mathcal{A}}_t^{(i)}\boldsymbol{\Sigma}_{t-1|t-1}^{(i)}\left(\boldsymbol{\mathcal{A}}_t^{(i)}\right)' + \boldsymbol{\mathcal{B}}_t^{(i)}\left(\boldsymbol{\mathcal{B}}_t^{(i)}\right)',\\
\boldsymbol{\Omega}_{t|t-1}^{(i)} &= \mathfrak{C}_t^{(i)}\boldsymbol{\Sigma}_{t|t-1}^{(i)}\left(\mathfrak{C}_t^{(i)}\right)' + \boldsymbol{\Omega}_{\mathcal{U}}^{(i)},\\
\widetilde{\mathcal{Y}}_t^{(i)} &= \mathcal{Y}_t - \mathfrak{C}_t^{(i)}\mathcal{S}_{t|t-1}^{(i)},\\
\mathcal{K}_t^{(i)} &= \boldsymbol{\Sigma}_{t|t-1}^{(i)}\left(\mathfrak{C}_t^{(i)}\right)'\left(\boldsymbol{\Omega}_{t|t-1}^{(i)}\right)^{-1},\\
\mathcal{S}_{t|t}^{(i)} &= \boldsymbol{\mathcal{A}}_t^{(i)}\mathcal{S}_{t|t-1}^{(i)} + \mathcal{K}_t^{(i)}\widetilde{\mathcal{Y}}_t^{(i)},\\
\boldsymbol{\Sigma}_{t|t}^{(i)} &= \boldsymbol{\Sigma}_{t|t-1}^{(i)} - \boldsymbol{\Sigma}_{t|t-1}^{(i)}\left(\mathfrak{C}_t^{(i)}\right)'\left(\boldsymbol{\Omega}_{t|t-1}^{(i)}\right)^{-1}\mathfrak{C}_t^{(i)}\boldsymbol{\Sigma}_{t|t-1}^{(i)},\\
\ell_t^{(i)} &= -\frac{1}{2}\left[\ln\left|\boldsymbol{\Omega}_{t|t-1}^{(i)}\right| + \left(\widetilde{\mathcal{Y}}_t^{(i)}\right)'\left(\boldsymbol{\Omega}_{t|t-1}^{(i)}\right)^{-1}\widetilde{\mathcal{Y}}_t^{(i)}\right],\\
\omega_t^{(i)} &= \frac{\exp\left\{\ell_t^{(i)}\right\}}{\sum_{i=1}^{M}\exp\left\{\ell_t^{(i)}\right\}},
\end{aligned}
$$

particle by particle to create updates of $\mathcal{S}_{t|t}^{(i)}$, $\boldsymbol{\Sigma}_{t|t}^{(i)}$, and $\ell_t^{(i)}$, and new weights $\omega_t^{(i)}$, which are used to resample $\left\{\mathcal{V}_t^{(i)}\right\}_{i=1}^{M}$.

(f) Update the nonlinear states, $\left\{\mathcal{V}_{t+1}^{(i)}\right\}_{i=1}^{M}$, using the multivariate random walk (12) conditional on the previous period's resampled nonlinear states, $\left\{\mathcal{V}_t^{(i)}\right\}_{i=1}^{M}$, the static scale volatility parameters σ_η^2, σ_υ^2, σ_ϕ^2, and σ_κ^2, and draws from the standard normal distribution for the innovations $\xi_{\eta,t+1}$, $\xi_{\upsilon,t+1}$, ϕ_{t+1}, and κ_{t+1}.

4. Conditional on $\mathcal{V}_t$, $\mathcal{Y}_{1:t}$, and Ψ, the filtered distribution of $\mathcal{V}_{t+1}$ is approximated by the discrete distribution of particles $\mathcal{V}_{t+1}^{(i)}$ using the *pdf* of $\omega_t^{(i)}$, where $\omega_t^{(i)} = \dfrac{\omega_t^{(i)}}{\widetilde{\omega}_t^{(i)}}$, and the associated filtered distribution of $\mathcal{S}_t$ is approximated by a mixture of normals $\mathcal{N}\left(\mathcal{S}_{t|t}^{(i)}, \boldsymbol{\Sigma}_{t|t}^{(i)}\right)$. Thus, the filtered means of $\mathcal{S}_t$ and $\mathcal{V}_{t+1}$ are approximated by $\mathcal{S}_{t|t} = \sum_{i=1}^{M}\omega_t^{(i)}\mathcal{S}_{t|t}^{(i)}$ and $\mathcal{V}_{t+1|t+1} = \sum_{i=1}^{M}\omega_t^{(i)}\mathcal{V}_{t+1}^{(i)}$ while for the mean square error of $\mathcal{S}_{t|t}$ the approximation is $\boldsymbol{\Sigma}_{t|t} = \sum_{i=1}^{M}\omega_t^{(i)}\boldsymbol{\Sigma}_{t|t}^{(i)}$.

5. Store conditional moments $\mathcal{S}_{t|t}^{(i)}$ and $\boldsymbol{\Sigma}_{t|t}^{(i)}$ and particle draws $\mathcal{V}_{t+1}^{(i)}$ to report estimates of the joint DGP of the SI-prediction mechanism and SW-UC-SV-TVP-AR(1) model.

The RB-APF algorithm is straightforward to adapt to gap inflation lacking persistence or to a fixed SI parameter. In the former case, the nonlinear state vector $\mathcal{V}_{t+1}$ drops θ_t and σ_ϕ^2 is deleted from Ψ. Otherwise, the algorithm described above is unchanged. Fixing the SI parameter, $\lambda_t = \lambda$, has a larger impact on the RB-APF algorithm. Besides cutting λ_t out of $\mathcal{V}_{t+1}$ and σ_κ^2 from Ψ, a prior is needed for λ. The posterior for λ has to be analytic for the prior to satisfy the demands of the particle learning estimator (PLE). Another restriction to satisfy is $\lambda \in (0, 1)$. A beta distribution fulfills the requirements of the PLE and the restriction on λ, given the shape parameters equal one (*i.e.*, a uniform distribution on the open unit interval). The RB-APF algorithm is further adjusted by including λ in Ψ, given the beta prior attached to λ.

A4 Additional Results

This section presents estimates of the joint DGPs not discussed in the paper. The estimates are displayed in figures that are similar to ones contained in the paper. However, figure 1 is not reproduced here because it depicts realized inflation, the SPF nowcast and 1-, 2-, and 4-quarter ahead SPF inflation predictions.

A4.1 Estimates of the Joint DGP when $\theta_t = 0$

Estimates of the joint DGP of the SI-prediction mechanism and SW-UC-SV model with zero or no gap inflation persistence, $\theta_t = 0$, appear in figures A2–No Gap Persistence, A3–No Gap Persistence, A4–No Gap Persistence, and A7–No Gap Persistence. This numbering matches figures 2, 3, 4, and 7 of the paper. Hence, conditional on $\theta_t = 0$, this

section presents estimates of the scale volatility parameters σ_η^2, σ_υ^2, and σ_κ^2 in figure A2–No Gap Persistence, filtered RE and SI trend and gap inflation, $\tau_{t|t}$, $F_{t|t}\tau_t$, $\varepsilon_{t|t}$, and $F_{t|t}\varepsilon_t$, in figure A3–No Gap Persistence, filtered and smoothed trend and gap inflation SVs, $\varsigma_{\eta,t|t}$, $F_{t|t}\varsigma_{\eta,t}$, $\varsigma_{\upsilon,t|t}$, and $F_{t|t}\varsigma_{\upsilon,t}$, in figure A4–No Gap Persistence, and the volatility of RE and SI trend inflation, τ_t and $F_t\tau_t$, conditional on different information sets in figure A7–No Gap Persistence.

Restricting ε_t to have zero persistence in the joint DGP produces four key differences compared with estimates of the joint DGP when there is drifting persistence in gap inflation. First, estimates of σ_η^2, σ_υ^2, and σ_κ^2 in figure A2–No Gap Persistence are smooth compared with the estimates found in figures 2(a), 2(b), and 2(d). Second, figures A3(a) and A3(b)–No Gap Persistence plot $\tau_{t|t}$ and $F_{t|t}\tau_t$ that are closer to $\pi_{t,t+1}^{SPF}$ and $\pi_{t,t+5}^{SPF}$ than produced by the joint DGP of the SI-prediction mechanism and SW-UC-SV-TVP-AR(1) model, which are plotted in figures 3(a) and 3(b). The implication is $\varepsilon_{t|t}$ and $F_{t|t}\varepsilon_t$, which are seldom greater than two percent and are displayed in figure A3(d)-No Gap Persistence, are less than a third as volatile compared with the estimates of RE and SI gap inflation shown in figure A3(d). Next, when $\theta_t = 0$, $\varsigma_{\eta,t|t}$ and $F_{t|t}\varsigma_{\eta,t}$ have similar peaks around the 1973–1975 and 1981–1982 recessions figures A4(a) and A4(b)–No Gap Persistence. This differs from the peaks in $\varsigma_{\eta,t|t}$ and $F_{t|t}\varsigma_{\eta,t}$ that occur during the latter recession in figures 4(a) and 4(b). Subsequently, $\varsigma_{\eta,t|t}$ and $F_{t|t}\varsigma_{\eta,t}$ decline through the restr of the sample period, except for a small spike around the 2007–2009 recession, in figures A4(a) and A4(b)–No Gap Persistence. Figures 4(c) and (d) and A4(c) and A4(d)–No Gap Persistence have qualitatively similar estimates of $\varsigma_{\upsilon,t|t}$ and $F_{t|t}\varsigma_{\upsilon,t}$ in that all these plots show a peak during the 1973–1975 recession. Lastly, estimates of the volatility of τ_t and $F_t\tau_t$ are qualitatively similar in figures 7 and A7–No Gap Persistence. However, conditioning only on realized inflation, π_t, yields lower estimates of the volatility of τ_t and $F_t\tau_t$, given $\theta_t = 0$, compared with the corresponding estimates in figure 7.

Figure A2–No Gap Persistence: Estimates of Static Volatility Parameters, 1968$Q4$ to 2017$Q2$

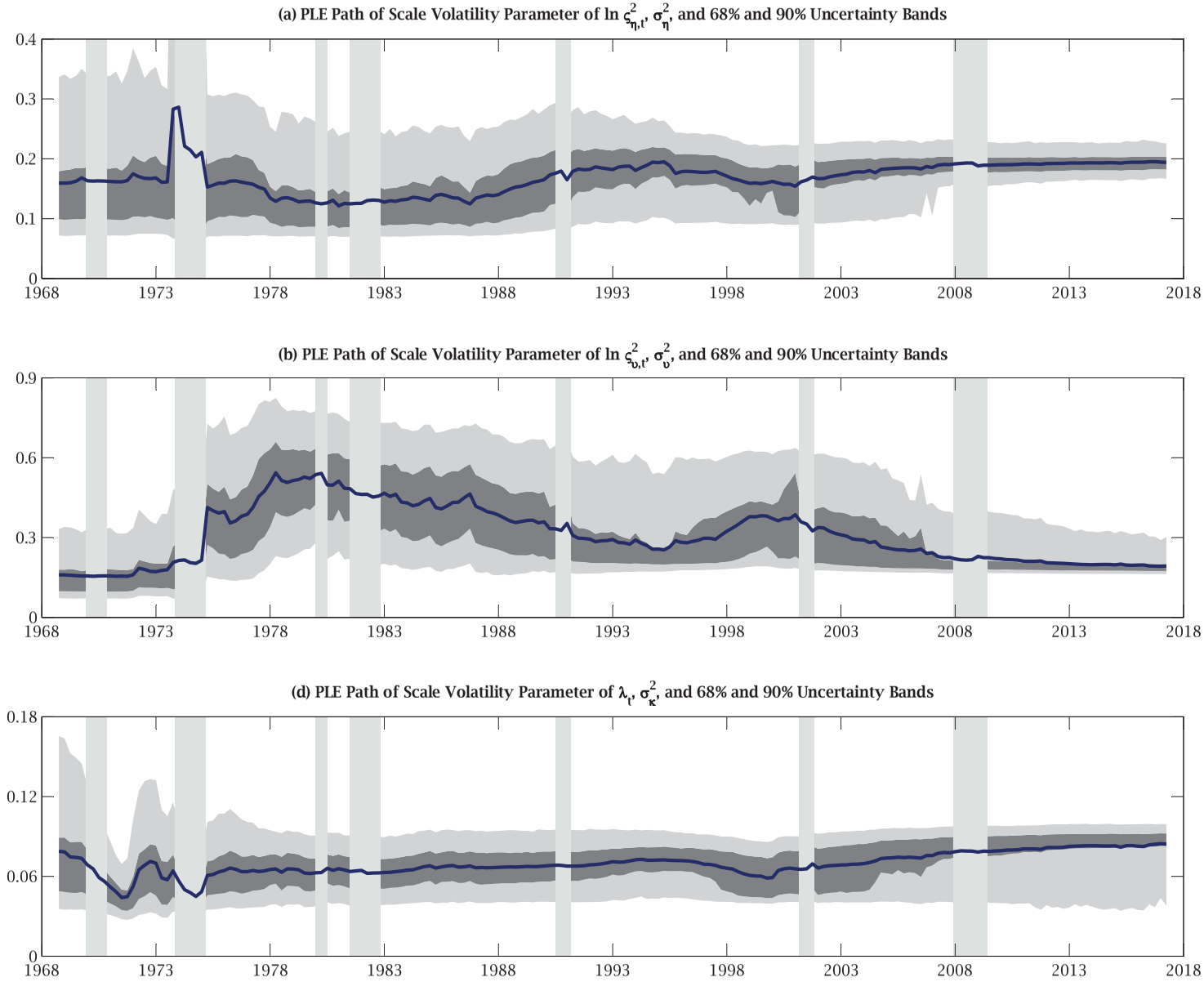

Note: The static volatility parameters are estimated in a joint DGP in which gap inflation, ε_t, has no persistence. The dark (light) gray areas surrounding estimates of the static scale volatility parameters, σ^2_η, σ^2_υ, and σ^2_κ cover 68 (90) percent uncertainty bands. The four plots contain vertical gray bands that denote NBER dated recessions.

Figure A3–No Gap Persistence: Realized Inflation, SPF Inflation Predictions, and Estimates of Trend and Gap Inflation, 1968$Q4$ to 2017$Q2$

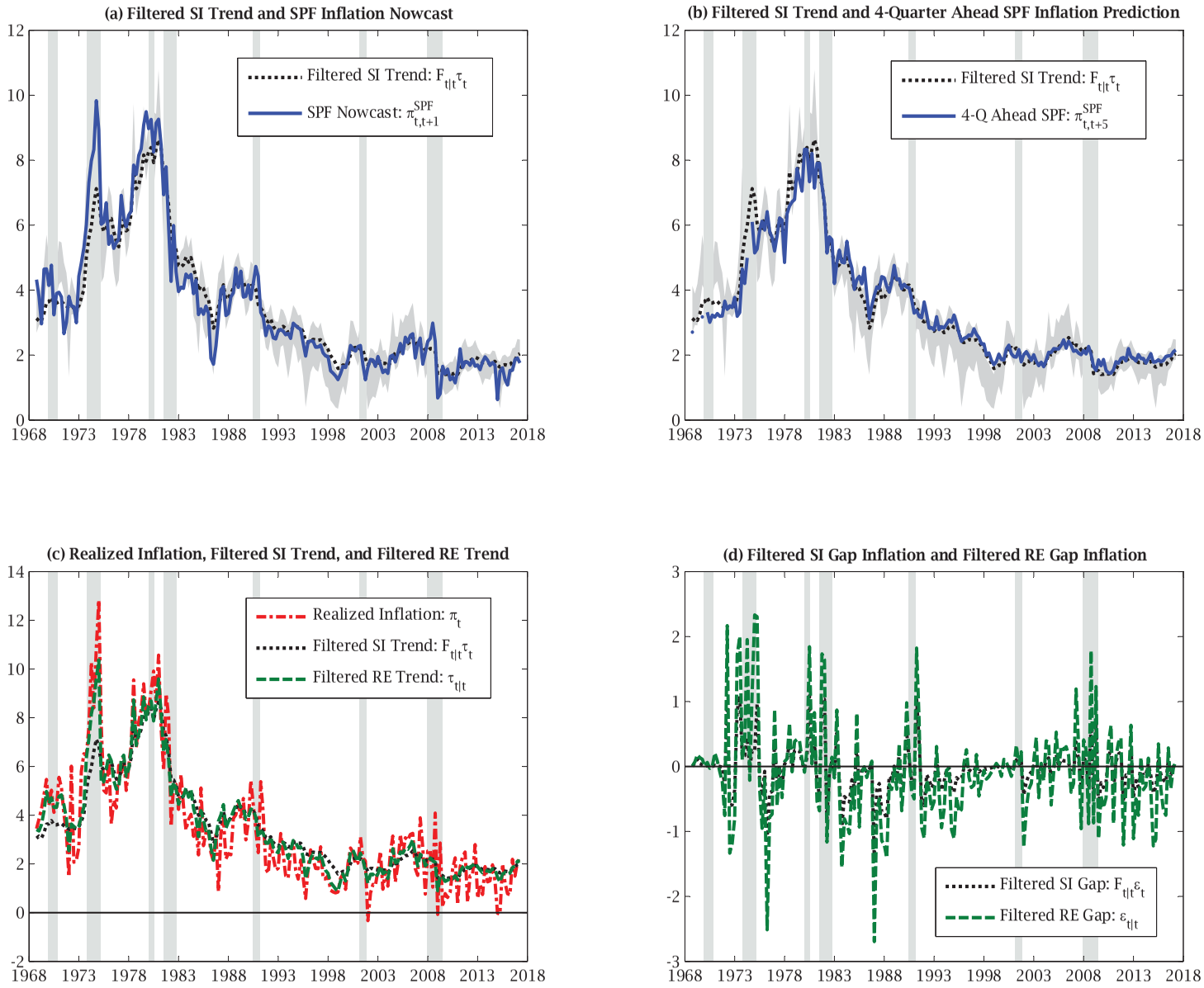

Note: The filtered RE and SI inflation trends and gaps are estimated in a joint DGP in which gap inflation, ε_t, has no persistence. The top row of charts contains light gray shaded areas that represent 68 percent uncertain bands around estimates of filtered SI trend inflation, $F_{t|t}\tau_t$. The vertical gray bands denote NBER dated recessions in the four charts.

Figure A4–No Gap Persistence: Estimates of the Stochastic Volatility of Trend and Gap Inflation, 1968$Q4$ to 2017$Q2$

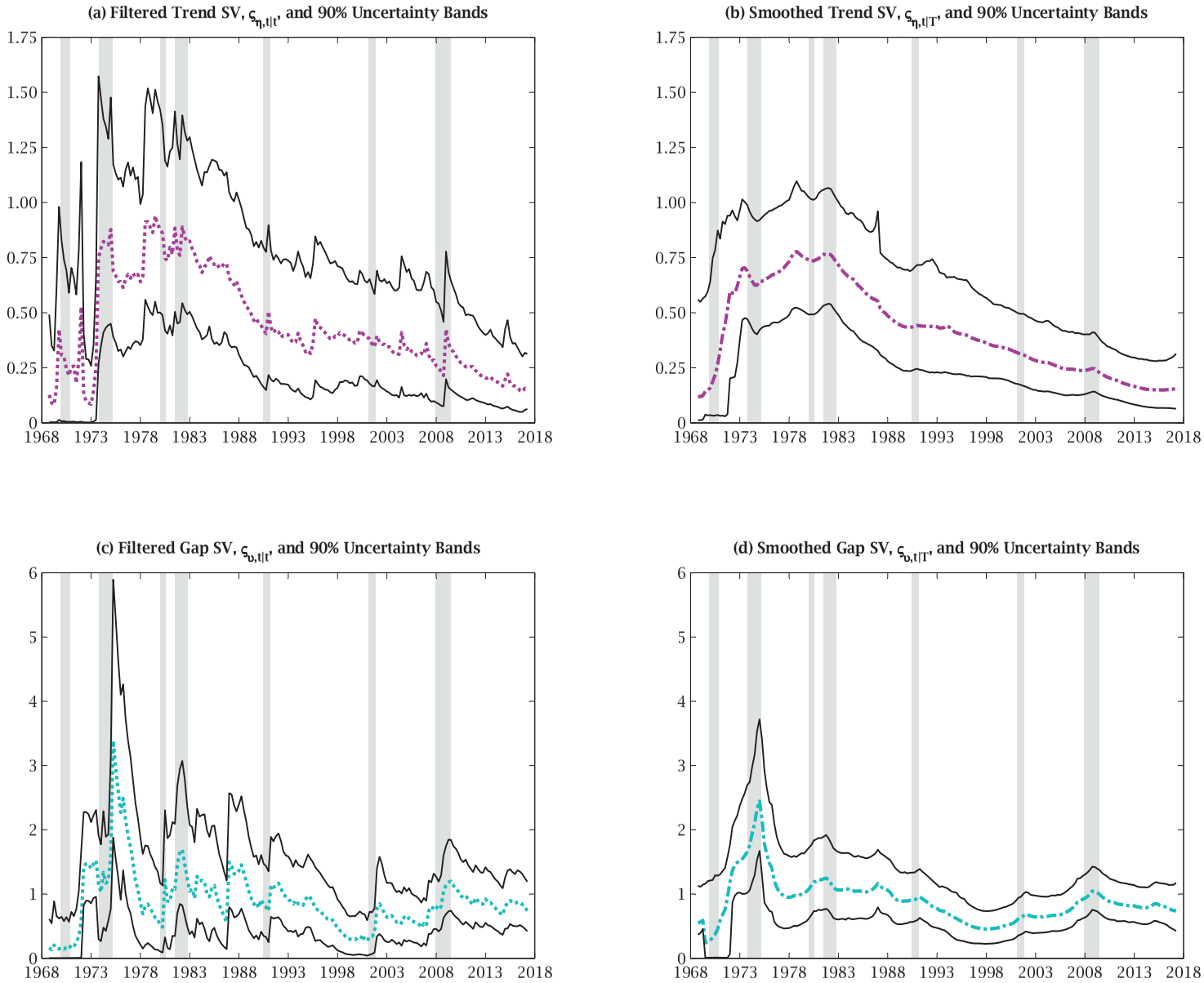

Note: The filtered and smoothed SVs of trend and gap inflation, $\varsigma_{\eta,t|t}$ and $\varsigma_{\eta,t|T}$, are estimated in a joint DGP in which gap inflation, ε_t, has no persistence. The solid thin (black) lines around $\varsigma_{\eta,t|t}$ and $\varsigma_{\eta,t|T}$ are lower and upper bounds on 90 percent uncertainty bands. The four plots display vertical gray bands that denote NBER dated recessions.

Figure A7–No Gap Persistence: Uncertainty Measure of Trend Inflation Conditional on Different Information Sets, 1968$Q4$ to 2017$Q2$

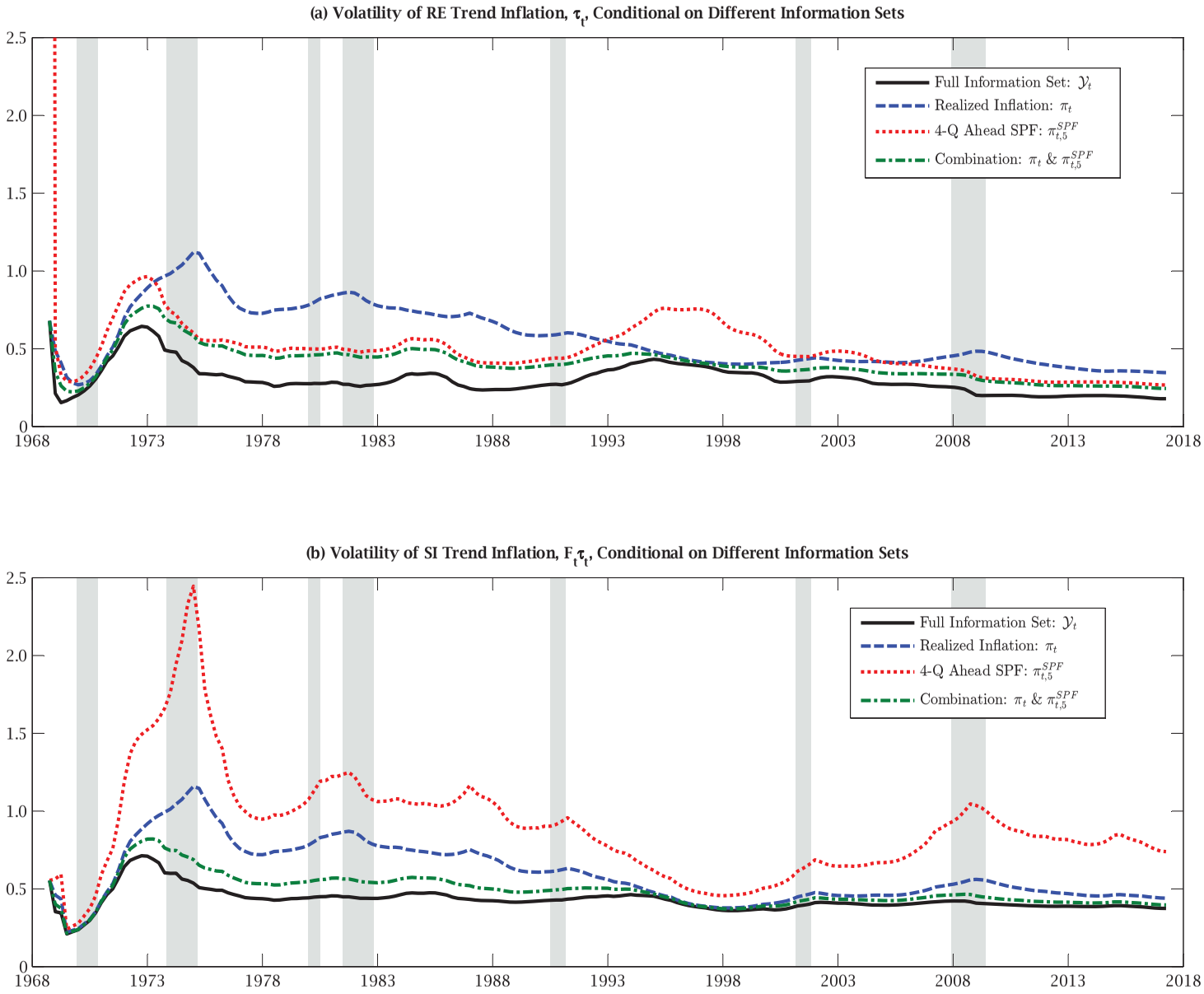

Note: The volatilities of RE and SI inflation trend are estimated in a joint DGP in which gap inflation, ε_t, has no persistence. The two plots contain vertical gray bands that denote NBER dated recessions.

A4.2 Estimates of the Joint DGP when $\lambda_t = \lambda$

Fixing the SI parameter generates estimates of the joint DGP that differ only along one dimension compared with the joint DGP of the SI-prediction mechanism and SW-UC-SV-TVP-AR(1) model. The difference is the minimal fluctuations of σ_η^2, σ_υ^2, and σ_ϕ^2 displayed in figure A2–$\widehat{\lambda}$, which repeats the theme of the plots presented in figure A2-No Gap Persistence. Otherwise, the joint DGP with $\lambda_t = \lambda$ is responsible for $\tau_{t|t}$, $F_{t|t}\tau_t$, $\varepsilon_{t|t}$, and $F_{t|t}\varepsilon_t$ (see figure A3–$\widehat{\lambda}$), of $\varsigma_{\eta,t|t}$, $\varsigma_{\eta,t|T}$, $\varsigma_{\upsilon,t|t}$, and $\varsigma_{\upsilon,t|T}$ (see figure A4–$\widehat{\lambda}$), of $\theta_{t|t}$, $\theta_{t|T}$, $|\theta_{t|T}|$, and $|\theta_{t|T}| - |\theta_{1|T}|$ (see figure A5–$\widehat{\lambda}$), and of the volatility of τ_t and $F_t\tau_t$ against disparate information sets (see figure A7–$\widehat{\lambda}$) that give evidence about the stickiness, persistence, and volatility of π_t and $\pi_{t,t+h}^{SPF}$ that support the results and interpretation reported by the paper.

This section concludes with a figure that plots the PLE path of $\widehat{\lambda}$. The PLE path of $\widehat{\lambda}$, 68 percent uncertainty bands, and 90 percent uncertainty bands appear in Figure–$\widehat{\lambda}$. This figure shows that by the end of the 1973–1975 recession the PLE path of $\widehat{\lambda}$ displays smaller fluctuations and from 1988 to the end of the sample exhibits almost no movement settling around 0.30 with 95 percent uncertainty bands ranging from 0.25 to 0.36. The dearth of movement in the PLE path of $\widehat{\lambda}$, especially after 1988, is a reason the data prefer the joint DGP of the SI prediction mechanism and SW-UC-SV-TVP-AR(1) model.

Figure A2–$\widehat{\lambda}$: Estimates of Static Volatility Parameters, 1968$Q4$ to 2017$Q2$

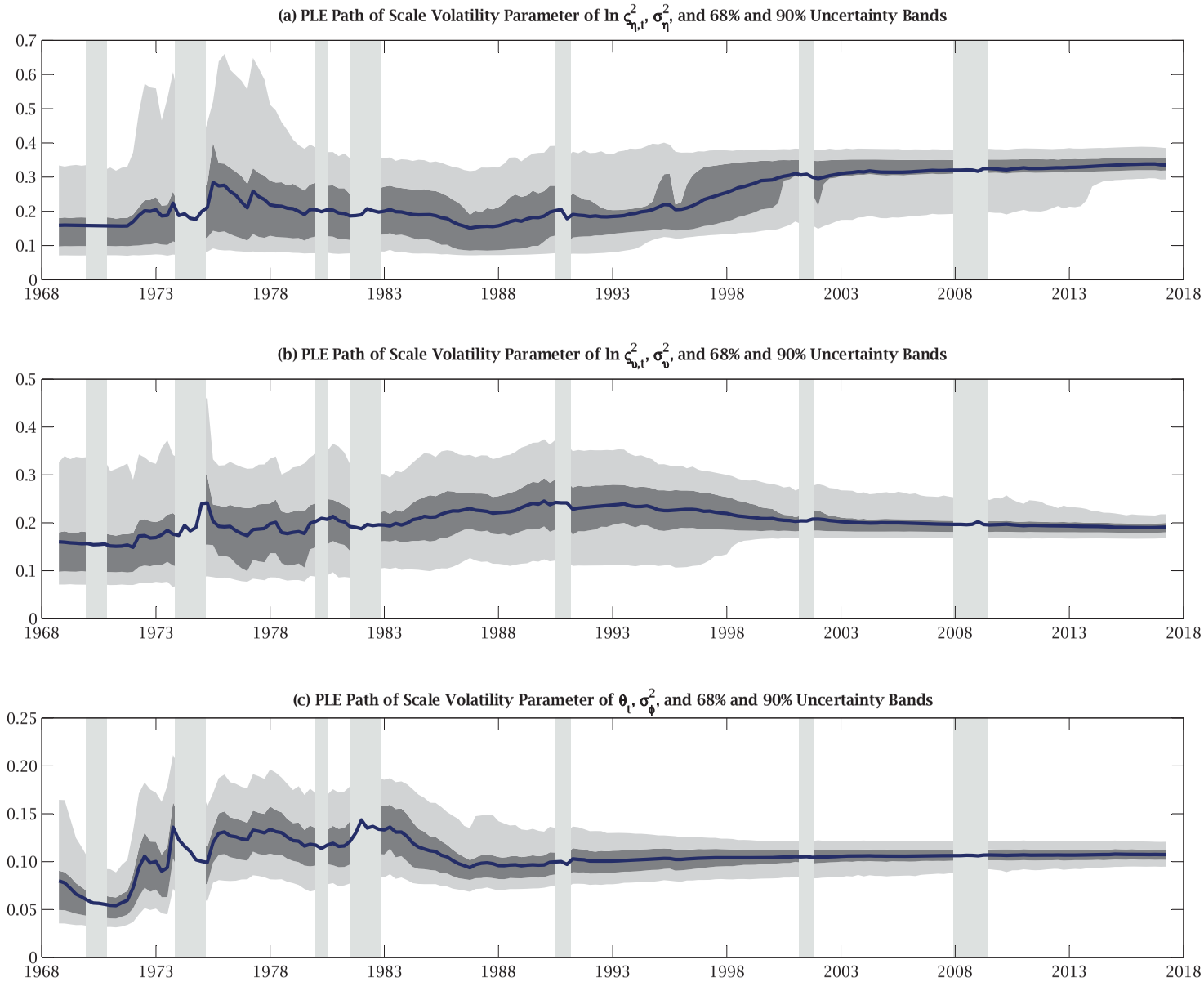

Note: The static volatility parameters are estimated in a joint DGP that has a static SI parameter, $\lambda_t = \lambda$. The dark (light) gray areas surrounding estimates of the static scale volatility parameters, σ^2_{η}, σ^2_{υ}, and σ^2_{ϕ} cover 68 (90) percent uncertainty bands. The four plots contain vertical gray bands that denote NBER dated recessions.

Figure A3-$\hat{\lambda}$: Realized Inflation, SPF Inflation Predictions, and Estimates of Trend and Gap Inflation, 1968$Q4$ to 2017$Q2$

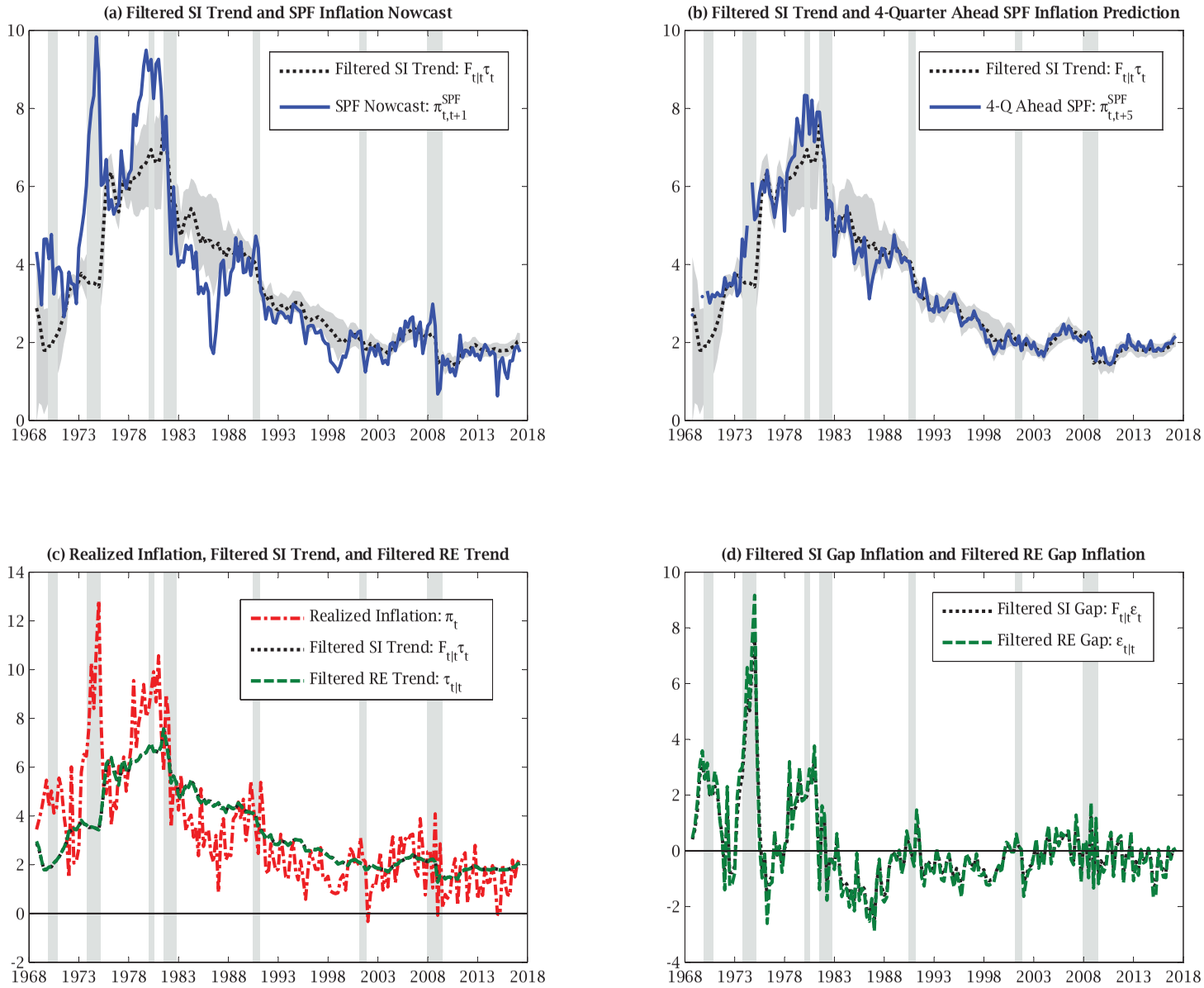

Note: The filtered RE and SI inflation trends and gaps are estimated in a joint DGP that has a static SI parameter, $\lambda_t = \lambda$. The top row of charts contains light gray shaded areas that represent 68 percent uncertain bands around estimates of filtered SI trend inflation, $F_{t|t}\tau_t$. The vertical gray bands denote NBER dated recessions in the four charts.

Figure A4-$\widehat{\lambda}$: Estimates of the Stochastic Volatility of Trend and Gap Inflation, 1968$Q4$ to 2017$Q2$

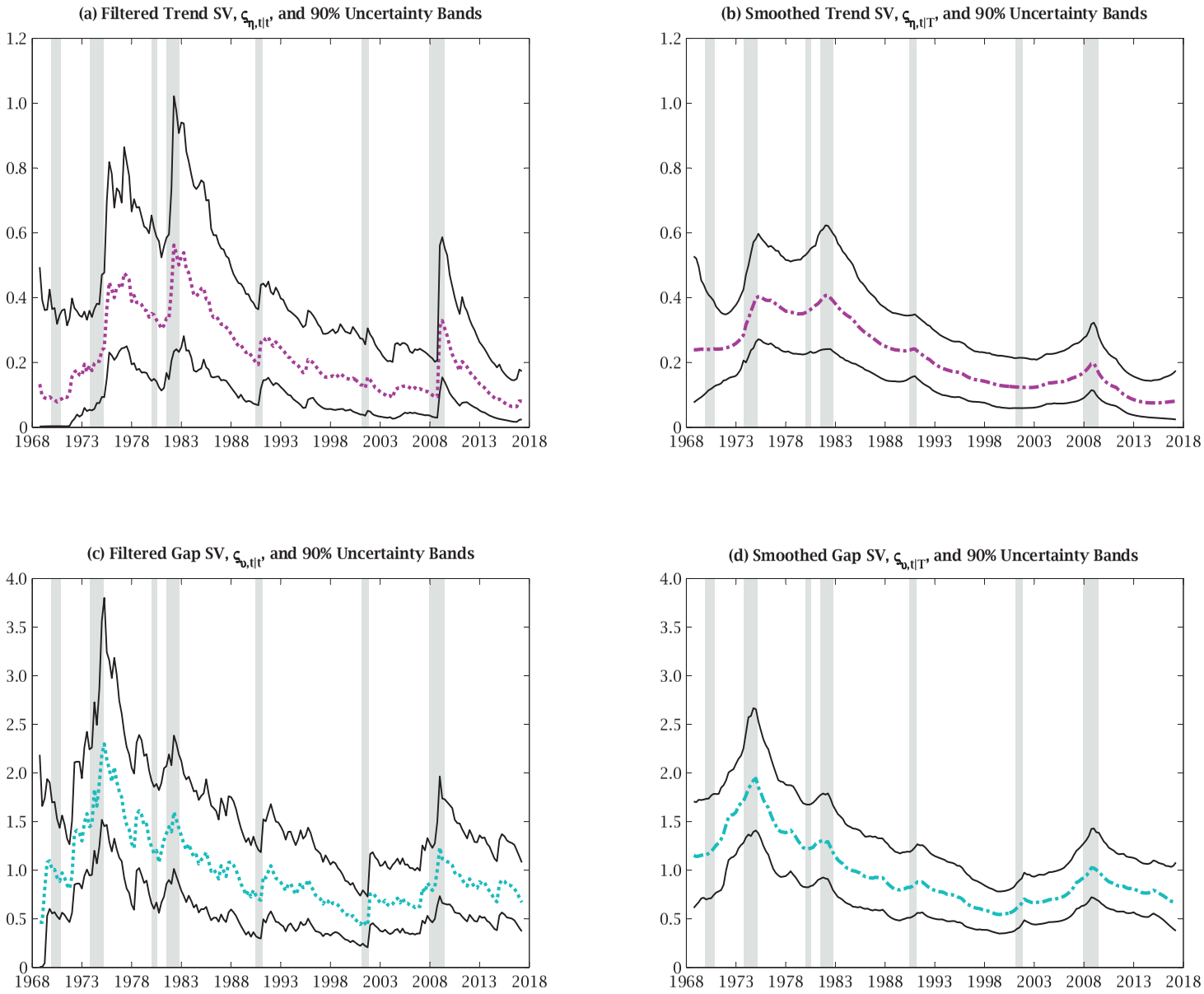

Note: The filtered and smoothed SVs of trend and gap inflation, $\varsigma_{\eta,t|t}$ and $\varsigma_{\eta,t|T}$, are estimated in a joint DGP that has a static SI parameter, $\lambda_t = \lambda$. The solid thin (black) lines around estimates of $\varsigma_{\eta,t|t}$ and $\varsigma_{\eta,t|T}$ are lower and upper bounds on 90 percent uncertainty bands. The four plots contain vertical gray bands that denote NBER dated recessions.

Figure A5–$\hat{\lambda}$: Estimates of Time-Varying Inflation Gap Persistence, 1968Q4 to 2017Q2

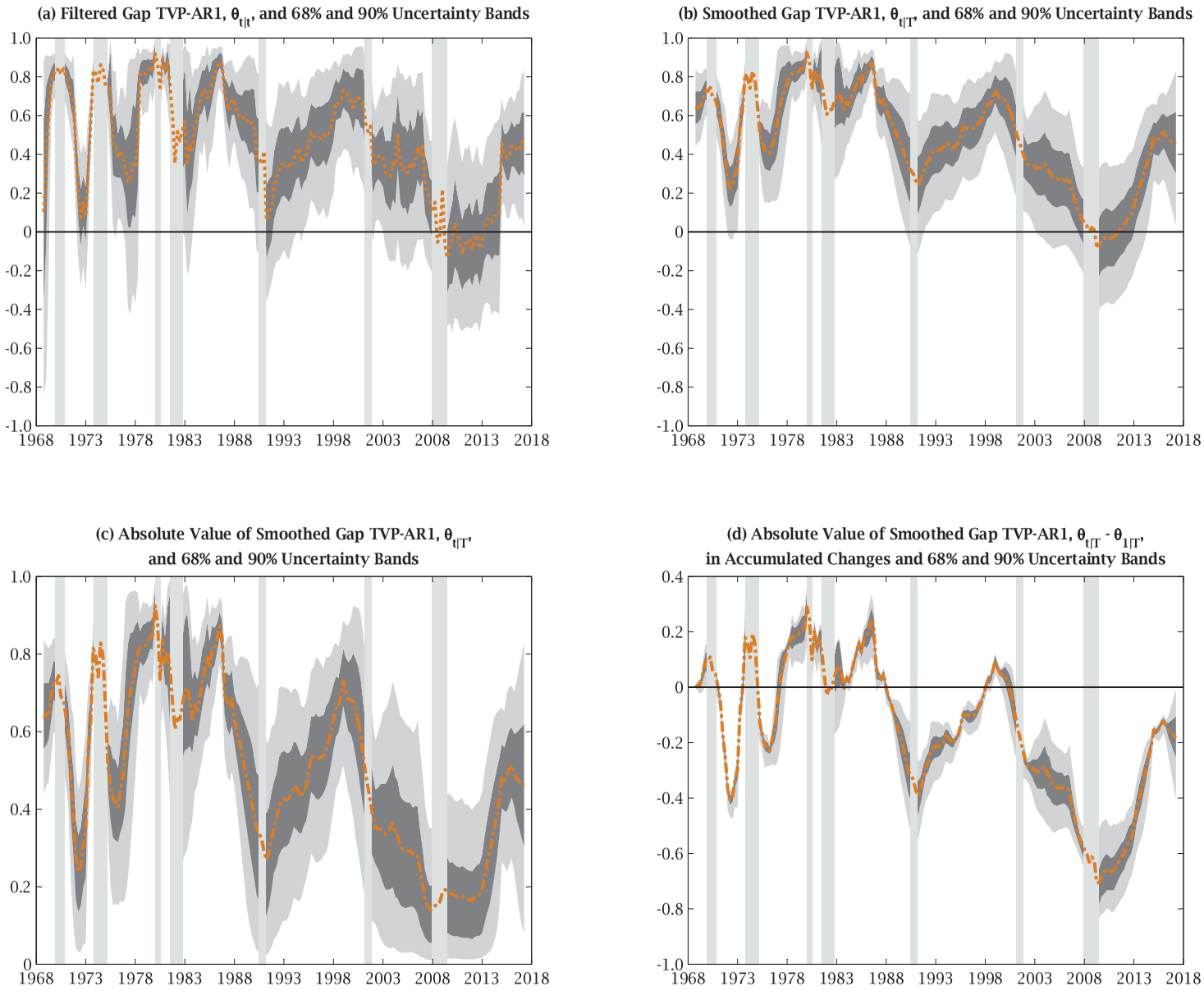

Note: The filtered and smoothed TVP-AR1 parameter of gap inflation is estimated in a joint DGP that has a static SI parameter, $\lambda_t = \lambda$. The dark (light) gray areas surrounding estimates of the TVP-AR1 of gap inflation cover 68 (90) percent uncertainty bands. The four plots contain vertical gray bands that denote NBER dated recessions.

Figure A7-$\widehat{\lambda}$: Uncertainty Measure of Trend Inflation Conditional on Different Information Sets, 1968$Q4$ to 2017$Q2$

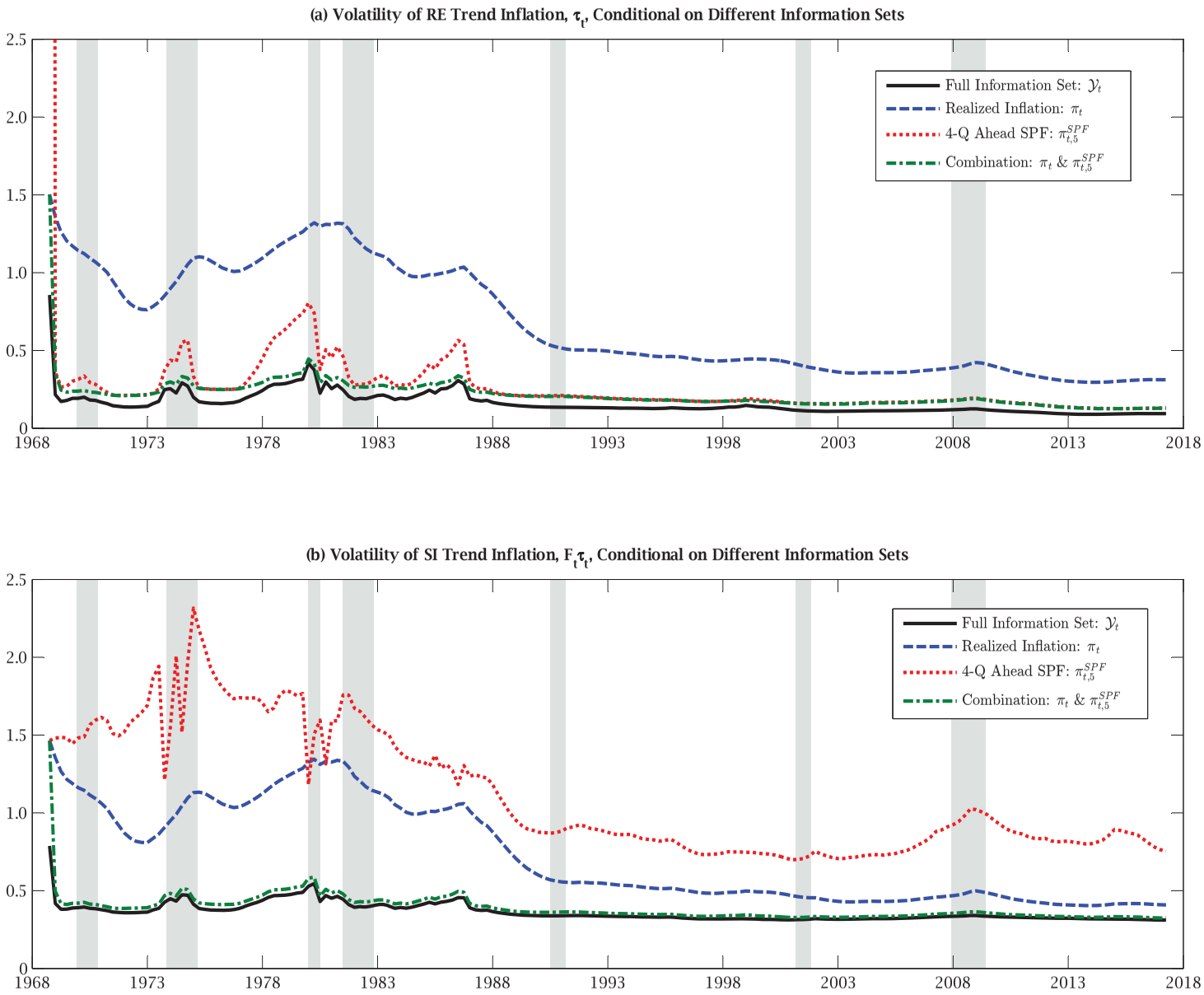

Note: The volatilities of RE and SI inflation trend are estimated in a SW-UC-SV model in which the SI parameter is static, $\lambda_t = \lambda$. The two plots contain vertical gray bands that denote NBER dated recessions.

Figure-$\widehat{\lambda}$: Particle Learning Estimates of the Static SI Parameter, λ, $1968Q4$ to $2017Q2$

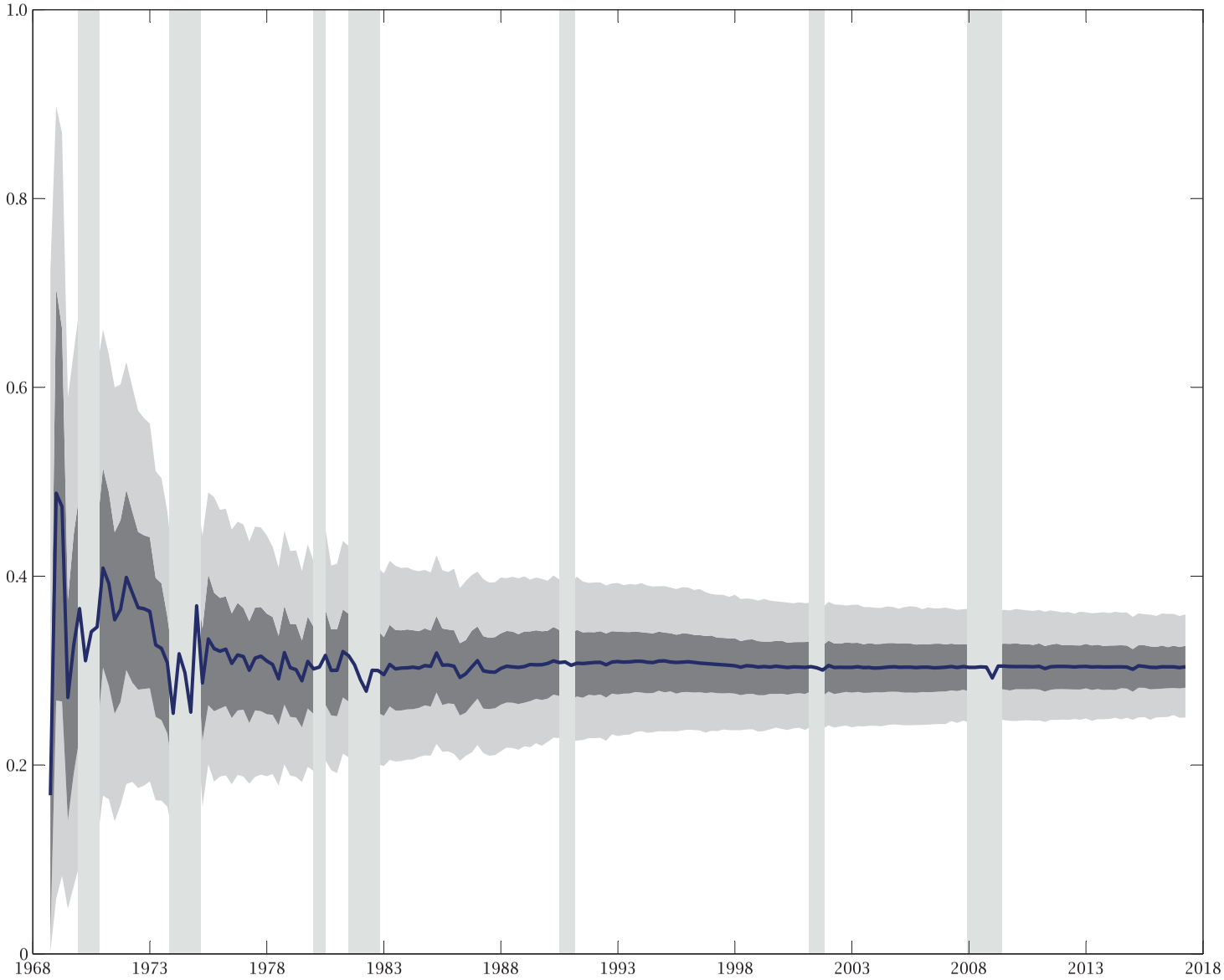

Note: The PLE estimates of λ are the solid blue line. The dark (light) gray areas surrounding estimates of λ cover 68 (90) percent uncertainty bands. The figure also has vertical gray bands that denote NBER dated recessions.